1-1-2008

Self-consistent field theory for polyelectrolytes and its applications.

Rajeev Kumar
University of Massachusetts Amherst

SELF-CONSISTENT FIELD THEORY FOR POLYELECTROLYTES AND ITS APPLICATIONS

A Dissertation Presented

by

RAJEEV KUMAR

Submitted to the Graduate School of the
University of Massachusetts Amherst in partial fulfillment
of the requirements for the degree of

DOCTOR OF PHILOSOPHY

September 2008

Polymer Science and Engineering Department

SELF-CONSISTENT FIELD THEORY FOR POLYELECTROLYTES AND ITS APPLICATIONS

A Dissertation Presented

by

RAJEEV KUMAR

Approved as to style and content by:

Murugappan Muthukumar, Chair

Jonathan Machta, Member

Anthony D. Dinsmore, Member

Gregory M. Grason, Member

Shaw Ling Hsu, Department Chair
Polymer Science and Engineering Department

SELF-CONSISTENT FIELD THEORY FOR POLYELECTROLYTES AND ITS APPLICATIONS

A Dissertation Presented

by

RAJEEV KUMAR

Approved as to style and content by:

Murugappan Muthukumar, Chair

Jonathan Machta, Member

Anthony D. Dinsmore, Member

Gregory M. Grason, Member

Shaw Ling Hsu, Department Chair
Polymer Science and Engineering Department

DEDICATION

To my parents and my wife.

ACKNOWLEDGMENTS

This work would have been impossible without the motivation, help and the guidance provided by many individuals. I would like to express my sincere gratitude to all of them here. I am sincerely indebted to my advisor, Prof. M. Muthukumar, for his continuous guidance and support during the course of my graduate studies. He has always amazed me with his intuition and the physical insights about different problems in almost all areas of polymer physics. His drive for simplicity and looking at the "big picture" has been a great source of inspiration to me. I am very thankful to him for giving me an opportunity to learn how to think physically and the freedom to choose the problems of my own interest.

I would like to thank Prof. Jonathan Machta, Prof. Anthony Dinsmore and Prof. Greg Grason for being on my committee. I am grateful to them for their patience and critical remarks they have given me regarding the research work. In particular, I am thankful to Prof. Grason for the discussions regarding some of the ongoing problems.

I am completely oblivious of the extensive paperwork involved during my graduate studies. This has been possible due to the sincere efforts of a number of people. I would like to thank all of them. In particular, I would like to thank Eileen for a warm welcome to the department and Vivien for taking care of the important deadlines and the paperwork.

I am lucky to be a part of the research group, where I got to interact with people with vastly different backgrounds ranging from Mathematicians working with abstract field theories to experimentalists, who sometimes don't want to see Mathematics at all. I got to learn a great deal about how different people think about the same problem.

I would like to thank all the present and past group members. In particular, I would like to thank Dr. Chilun Lee, who helped me in learning the necessary statistical mechanics and answered all of my questions even when they were plain stupid. Also, I have learned a lot from Dr. Vladimir Belyi. He has taught me how to use fundamental concepts in physics to get an idea (which may or may not be right) about complicated problems in general. It was a pleasure for me to have many discussions with him on topics unrelated to science also. He has been a source of enthusiasm and energy for me. I am surely going to miss the hiking trips with the group and non-scientific discussions we had in the campus cafeteria after the group meetings. Many thanks are due to Dr. C.Y. Kong and Dr. Arindam Kundagrami for helping me out with the numerical work essential for my graduate studies.

Of course, the stay at University of Massachusetts, Amherst would not have been so pleasant without many friends I made over the period of this research. I would like to take this opportunity to thank a couple of my friends : Harish Venkataramani, Rakesh Kothari, Niranjan, Saurav Singh, Vidit Jain and Dr. Ajay Panwar.

I don't have words to explain my gratitude to my parents for the continuous emotional support and belief in me. Thanks to my father, Sh. Madan Lal and my mother, Smt. Krishna Devi, without whose efforts I would not have been what I am today. Because of their efforts, I have the honor of being the first person in my family to attain this level of academic qualification. Also, I want to thank my wife, Pooja, for the love and support she has provided me in my stressful times. I sincerely appreciate and acknowledge her efforts in making me a better person.

Finally, I would like to gratefully acknowledge funding provided to this research by the National Science Foundation (NSF), National Institute of Health (NIH) and Materials Research Science and Engineering Center (MRSEC) at University of Massachusetts, Amherst.

ABSTRACT

SELF-CONSISTENT FIELD THEORY FOR POLYELECTROLYTES AND ITS APPLICATIONS

SEPTEMBER 2008

RAJEEV KUMAR,B.Tech., INDIAN INSTITUTE OF TECHNOLOGY DELHI

M.S., UNIVERSITY OF MASSACHUSETTS AMHERST

Ph.D., UNIVERSITY OF MASSACHUSETTS AMHERST

Directed by: Professor Murugappan Muthukumar

In this work, we have developed a self-consistent field theory (SCFT) for polyelectrolytic systems and studied four important problems of contemporary interest : microphase separation in the melts of charged-neutral diblock copolymers, confinement effects on flexible polyelectrolytes, counterion adsorption on single flexible polyelectrolyte chain and the origin of translocation barriers in polyelectrolytic systems. Using the theory, we have been able to capture the effects of the degree of ionization, salt concentration, electrostatic and the excluded volume interaction strengths, degree of polymerization, role of architecture and solvent quality on these polyelectrolytic systems. Within saddle-point approximation, the polyelectrolyte chain configuration is described as a walk in the presence of fields coming from the excluded volume interactions and the other effects such as incompressibility in addition to the electrostatic potential. The electrostatic potential, on the other hand, is obtained from Poisson-Boltzmann like equation. So, in contrast to the SCFT for neutral polymers,

there are two coupled non-linear equations namely modified diffusion equation describing the walk in the fields and the Poisson-Boltzmann equation, which have to be solved self-consistently. In this work, we have developed various numerical schemes to solve these coupled non-linear sets of equations. Furthermore, comparison of the SCFT results with a previous developed variational theory for polyelectrolytes has been carried out. Also, systematic expansions around the saddle-point results have been carried out to capture the effects of the density fluctuations of the small ions in the systems.

TABLE OF CONTENTS

LIST OF TABLES

LIST OF FIGURES

Figure Page

CHAPTER 1

INTRODUCTION

For decades, polyelectrolytes have presented a challenge to the scientific community due to the presence of both short and long range interactions. This leads to an interplay of many length scales, while describing their behavior in different sets of conditions. The aim of this research work is to investigate and comprehend the characteristic properties of flexible polyelectrolytes using coarse-grained models, which capture the essential physics while satisfying thermodynamic laws.

To achieve this aim, the field theory first proposed by Sam Edwards[1, 2, 3, 4] in the context of neutral polymers presents a nice computational framework. The theory captures the essential thermodynamics and presents opportunities for carrying out systematic analysis to assess and improve upon certain approximations used to analyze many complicated systems such as polyelectrolytes. In this theory, conformational entropy of a phantom chain (a chain whose connected segments don't interact with each other) is described by mapping different configurations of the chain, while keeping its ends fixed at two particular locations, on to a path integral with the limits of the integral as the positions of the ends of the chain. Integrand of this path integral represents the probability distribution function for finding the ends of the chain at particular locations, which is a continuous version of the Wiener measure for a phantom chain. In the presence of interactions between the connected segments, different chain configurations can be described by random walks in the presence of fields, which arise solely due to the fact that there are interactions present in the system. This physical argument can be proven rigorously using certain field the-

oretical transformations such as Hubbard-Stratonovich[5] transformation, which is well-known in field theory. So, the behavior of a polymer chain in the presence of different kinds of intra-chain interactions can be described once the fields are known. In general, an exact computation of these fields is almost an impossible task. That's the reason, theoretical developments resort to certain approximations for computing these fields, which work well for most of the practical purposes. Once these fields are known, the physical properties can be described in terms of these fields. It was shown by Edwards[2, 3] that the similar analysis can be carried out for systems with many chains, where inter-chain interactions also affect the properties in addition to intra-chain interactions.

In this work, we have extended the field theory developed for neutral polymers to the polymers having charges on the backbone and in the presence of externally added salt ions. We have used this theory for problems involving a single chain as well as many chains. Due to the general nature of the field theoretical formalism, we have used this tool to investigate four different problems, which appear even in the case of neutral polymers and have a long history in polymer literature. Specifically, we have investigated the following systems :

1. Theoretical studies of the microphase separation in the melts of charged-neutral diblock copolymers. In this study, we have paid particular attention to the length scale to be appeared when the system is on the verge of going from the homogeneous phase to the inhomogeneous phase.

2. Confinement effects on a single flexible polyelectrolyte chain are studied by considering a polyelectrolyte chain in a non-adsorbing spherical cavity. Nowadays, it is widely appreciated that spherical confinement is different from confinement in one (polymer between infinitely long parallel plates) or two (polymer inside an infinitely long cylindrical cavity) dimensions. We have computed the free energy of confinement and investigated the role of energy and entropy in the free energy. Osmotic pressure

and mean activity coefficients for the salt ions are computed. Also, the effects of density fluctuations of the small ions and the monomers on the free energy, osmotic pressure and mean activity coefficients are studied.

3. Counterion adsorption on a single flexible polyelectrolyte chain in a spherical cavity is studied using SCFT. Comparison of these results with the variational calculations carried out by Muthukumar are presented.

4. Free energy barriers for the arrival of a polyelectrolyte chain end at a specified location on the surface of the confining spherical cavity are computed and the origin of these barriers is investigated. Comparison of these free energy barriers with that for a neutral chain is carried out.

This thesis is organized as follows : in Chapter 2, a general background on the field theoretical formalism for polyelectrolytes is presented. In Chapter 3, we study microphase separation in the melts of charged-neutral diblock copolymers. Chapters 4,5 and 6 present the results for the above mentioned three single chain problems namely, confinement effects on a single flexible polyelectrolyte chain in spherical cavities, counterion adsorption and the free energy barriers for the arrival of the chain end at a specified location on the surface of a confining spherical cavity. Conclusions and the future work are discussed at the end of individual chapters.

CHAPTER 2

SELF-CONSISTENT FIELD THEORY

In this Chapter, we present a general outline of the self-consistent field theory (SCFT) for multiblock polyelectrolyte solutions containing externally added salt ions. The theory is a generalization of the SCFT developed by Sam Edwards[1, 2, 3, 4, 6, 7, 8, 9] for neutral polymers to polyelectrolytes. For neutral polymers, SCFT has been used extensively for many different kinds of polymeric systems near surfaces[8] and in solutions[9]: many chain systems such as concentrated solutions and melts of block copolymers, polymer blends, mixtures of homopolymers and block copolymers etc., and problems involving single chain in solutions as well as near different kind of interfaces such as membranes, adsorbing, non-adsorbing and patterned surfaces. Extensive use of the theory to get an insight into problems of different kinds arises due to the general nature of the approach and a reasonable computational demand of the theory in comparison with the simulations.

Besides the general nature of the theory, it presents an avenue for a systematic study to include or remove certain effects while analyzing the problems. In this Chapter, we present the general approach for studying polymeric problems starting from the path integral representation of a polymer chain. Also, we present the details of certain approximations, which allow us to carry out some analytical calculations.

2.1 Partition Function - Extension of Edward's Formulation

We consider the computation of the free energy of a system containing n_p monodisperse multiblock polyelectrolytic chains, each containing a total of N segments with

the same sequence and the number of blocks (= m), where each block is made up of different monomers. $m = 1, 2, \cdots$ represent homopolymer, diblock and so on. In addition to this, there are small ions due to the added salt (in total volume Ω) along with the counterions coming from the polyelectrolyte chains so that the whole system is globally electroneutral. Let Z_j and n_j be the valency and number of the j^{th} species. Subscripts $p, m, c, +$ and $-$ are used to represent polymer, monomer in the m^{th} block, counterions from the polyelectrolyte, positive and negative salt ions, respectively. Using the path integral formulation[1], we represent a polyelectrolyte chain as a continuous curve of length Nb, where b is the Kuhn segment length. For the treatment shown below, we assume that the volume occupied by each monomer is the same ($= b^3 \equiv 1/\rho_o, \rho_o$ being the bulk density) and that the system is incompressible. We use an arc length variable t_β to represent any segment along the backbone of β^{th} chain. Also, the position vector for a particular segment is represented by $R_\beta(t_\beta)$. For this system, partition function Z can be written within Edward's formalism by:

$$Z = \frac{1}{n_p!}\int d\mathbf{r}\int d\mathbf{r}'\int_{\mathbf{r}}^{\mathbf{r}'}\prod_{\beta=1}^{n_p} D[\mathbf{R}_\beta(t_\beta)]\sum_{\{g_{t_\beta}\}}\int\prod_j \frac{1}{n_j!}\prod_{\lambda=1}^{n_j} d\mathbf{r}_\lambda \exp\left(-H[\mathbf{R}_\beta(t_\beta), \mathbf{r}_\lambda]\right)$$
$$\prod_{\mathbf{r}}\delta\left(\sum_\gamma \hat{\rho}_\gamma(\mathbf{r}) - \rho_0\right), \tag{2.1}$$

where $\gamma = m, s$ represents monomers and solvent molecules and $j = s, c, +, -$ depicts all the small molecules such as solvent, counterions from polymer and salt ions. In the above equation, g_{t_β} is a parameter describing charge distribution on the monomer t_β. In writing the partition function, we have summed over all possible locations of the small molecules in the volume under investigation (represented by volume integrals over $\mathbf{r}_m$) and the sum over all possible conformations of an individual chain is represented by functional integrals over all the possible paths originating from one end and finishing at the other (written as functional integral over $\mathbf{R}_\beta(t_\beta)$, $\mathbf{R}_\beta(t_\beta)$ being the position vector of t^{th} segment on β^{th} chain). Depending on the problem of

interest, the ends of the chains ($\mathbf{r}$ and $\mathbf{r}'$ in Eq. 2.1) can be fixed (as in the case of polymer brushes) or free to enjoy the translational degrees of freedom. In the latter case, integrals over positions of ends needs to be carried out to compute the partition function. In Eq. 2.1, it is assumed that the ends can be anywhere in space and hence. the integrals are the possible locations of the ends of chains has been carried out. We don't distinguish between two molecules of the same species. That is the reason, the partition function has to be divided by $n_j!$ to avoid double counting. Polyelectrolytes can have different kinds of charge distributions depending on different situations and that is the origin of the summation over charge parameter g_{t_β}. In order to simplify the mathematics, incompressibility condition is used by assuming small ions to be point charges (represented by the delta function in the above equation). Incompressibility condition works pretty well due to very small compressibility of the polymeric systems. The effect of the finite size of the small ions can be included trivially through the incompressibility condition. However, we will not follow that approach here due to the fact that for the problems involving monovalent ions. the results are almost indistinguishable from point charge case. Origin of this agreement between the finite size and point-like ions lies in the fact that typical radii of monovalent ions are very small in comparison with the size of monomers (in terms of Kuhn step length).

Hamiltonian, H, in Eq. (2.1) can be split into the connectivity and interaction terms, so that

$$H[\mathbf{R}_\beta(t_\beta), \mathbf{r}_\lambda] = \sum_{\beta=1}^{n_p} H_0[\mathbf{R}_\beta(t_\beta)] + \sum_{\beta=1}^{n_p}\sum_{\lambda=1}^{n_p} H_{pp}[\mathbf{R}_\beta(t_\beta), \mathbf{R}_\lambda(t_\lambda)]$$
$$+ \sum_{j}\sum_{\beta=1}^{n_p}\sum_{\lambda=1}^{n_j} H_{pj}[\mathbf{R}_\beta(t_\beta), \mathbf{r}_\lambda] + \sum_{j}\sum_{a}\sum_{\beta=1}^{n_j}\sum_{\lambda=1}^{n_a} H_{ja}[\mathbf{r}_\beta, \mathbf{r}_\lambda], \qquad (2.2)$$

where $j, a = s, c, +, -$ and represent all the small molecular species in the system. Also, $H_0[\mathbf{R}_\beta]$ is the chain connectivity part, which comes from the fact that in the absence of interactions, the probability distribution function for the chains must be

a Wiener measure. In the continuum representation[3], this term is written explicitly as

$$H_0[\mathbf{R}_\beta(t_\beta)] = \frac{3}{2b}\int_0^{Nb} dt_\beta \left(\frac{\partial R_\beta(t_\beta)}{\partial t_\beta}\right)^2. \tag{2.3}$$

We must stress here that the connectivity part represented by the functional integrals over the possible paths in Eq. (2.1) are not properly normalized. This leads to some unknown constants in the computation of absolute free energy of the system. However, for most of the practical purposes, we are interested in either the relative free energy or the derivatives of the free energy such as osmotic pressure etc. In other words, the normalization factor can be taken care of by choosing an appropriate reference system. In the polymeric problems, where we are interested in studying the effect of different kinds of interactions, the reference system for each chain can be taken as the chain of the same number of segments *without* any interactions (i.e. a phantom chain of the same length) in free space (or vacuum). For a single phantom chain in free space, the partition function, Z_0, can be written as

$$Z_0 = \int D[\mathbf{R}] \exp\left[-H_0[\mathbf{R}],\right] \tag{2.4}$$

which is divergent.

Second term, $H_{pp}[\mathbf{R}_\beta(t_\beta), \mathbf{R}_\lambda(t_\lambda)]$, in Eq. (2.2) is the polymer-polymer interaction term, which includes inter as well as intra chain monomer-monomer interactions arising from the excluded volume and electrostatic effects. To compute the polymer-polymer interaction energy, we have to include the interactions among all monomeric species. If the excluded volume interaction terms are written by using delta functional form for the potential as used by Edwards for neutral polymers then

$$H_{pp}[\mathbf{R}_\beta(t_\beta), \mathbf{R}_\lambda(t_\lambda)] = \sum_{m,m'} h_{mm'} \int dt_\beta \int dt_\lambda \left[w_{mm'}\delta(\mathbf{R}_\beta(t_\beta) - \mathbf{R}_\lambda(t_\lambda)\right)$$

$$+\frac{Z_m Z_{m'} e^2 g_{t_\beta} g_{t_\lambda}}{k_B T} \frac{\epsilon^{-1}(\mathbf{R}_\beta(t_\beta), \mathbf{R}_\lambda(t_\lambda))}{|\mathbf{R}_\beta(t_\beta) - \mathbf{R}_\lambda(t_\lambda)|}\Bigg], \tag{2.5}$$

where $h_{mm'} = \Theta(-\delta_{mm'}) + 1/2$, $\Theta(x)$ and $\delta_{mm'}$ being the Heaviside step function and Kronecker delta function, respectively. Also, $\delta(x)$ represents the Dirac delta function in this work. Unless specified in this Chapter, the limits of integrals for t_β and t_λ integrals are the values of the contour variable t over which β^{th} and λ^{th} chain has monomers of type m and m', respectively.

Some comments regarding the delta functional form for the excluded volume interaction energy are in order here. In Eq. (2.5), $w_{mm'}$ is a parameter to assess the strength of excluded volume interactions and has the dimensions of volume. This form for the excluded volume term was suggested by Edwards by realizing that for large length scales, properties of the system should not depend upon the specific details of interactions, which may be due to steric effects, van der Waals attraction etc. As far as the interaction term is written in terms of a short range function, the predictions of the theory should not change. However, we must point out here that the delta functional form for the interaction potential leads to divergences when $\mathbf{R}_\beta(t_\beta) = \mathbf{R}_\lambda(t_\lambda)$. However, these divergences don't affect any physically measurable quantity. But these short range divergences cause the absolute free energy of the system to diverge. However,the free energy differences, which are important experimentally, remain well behaved. Also, it should be noted that $w_{mm'}$ is dependent on temperature[3] through the relation

$$w_{mm'} = \int d\mathbf{r} \left[1 - \exp\left(-\frac{V_{mm'}(\mathbf{r})}{k_B T}\right)\right] = A - \frac{B}{T}, \tag{2.6}$$

where $V_{mm'}(\mathbf{r})$ is the potential energy of interaction between a monomer of species m with another monomer of species m'. The latter form for $w_{mm'}$ is obtained by splitting $V_{mm'}$ into strong hard-core repulsive part and a weak attractive part. A and B are constants, which are independent of temperature T. Using the definition

of Flory or Θ temperature[6] as the temperature at which $w_{mm'}$ vanishes, it can be written in the form

$$w_{mm'} = w^0_{mm'}\left(1 - \frac{\Theta}{T}\right). \tag{2.7}$$

The rightmost term in Eq. (2.5) is the electrostatic interaction energy, which is written after describing the response of the inhomogeneous systems to an applied electric field by a non-local response function (also known as the inverse dielectric function[10, 11]), $\epsilon^{-1}(\mathbf{r}, \mathbf{r}')$) defined by

$$\int d\mathbf{r}'\epsilon^{-1}(\mathbf{r}, \mathbf{r}')\epsilon(\mathbf{r}', \mathbf{r}'') = \delta(\mathbf{r} - \mathbf{r}''), \tag{2.8}$$

where $\epsilon(\mathbf{r}, \mathbf{r}')$ is the dielectric function in real space. In general, the inverse dielectric function can be obtained by solving Eq. (2.8) and can be written in terms of molecular polarizabilities of the charged species. Computations of the inverse dielectric function add another set of complexity in assessing the effect of long-range electrostatic interactions. For the length scales explored in this work, we have taken the dielectric function in real space to be local in nature so that $\epsilon(\mathbf{r}, \mathbf{r}')$ is replaced by $\epsilon(\mathbf{r})$ and $\epsilon^{-1}(\mathbf{r}, \mathbf{r}')$ by $1/\epsilon(\mathbf{r})$ in Eq. (2.5). Also, note the similarity in divergences arising from this term when $\mathbf{R}_\beta(t_\beta) = \mathbf{R}_\lambda(t_\lambda)$ and the divergences in excluded volume interaction terms. Both of these divergences set the length scale below which this coarse-grained model fail to describe the system properly.

Furthermore, g_{t_β} is a random variable used to specify the charge distribution on the β^{th} polyelectrolyte chain. The sum over this variable in Eq. (2.1) is defined by

$$\sum_{\{g_{t_\beta}\}} [\cdots] = \int \prod_{\beta=1}^{n_p} dg_{t_\beta} [\cdots] \prod_{\beta=1}^{n_p} P(g_{t_\beta}), \tag{2.9}$$

where $P(g_{t_\beta})$ is the probability distribution function for g_{t_β} and defines different kinds of charge distributions on the chain. For example, for the so-called *smeared*

and *annealed* charge distributions[12] on all the chains, $P(g_{t_\beta}) = \prod_m \delta(g_{t_\beta} - \alpha_m)$ and $P(g_{t_\beta}) = \prod_m \{\alpha_m \delta(g_{t_\beta} - 1) + (1 - \alpha_m)\delta(g_{t_\beta})\}$, respectively. Here, α_m is the degree of ionization of the part of the chain containing monomers of type m. In writing the charge distribution, it is understood that the values of t appearing in g_{t_β} correspond to contour length describing monomer of type m on the backbone. Physically, this means that in smeared charge distribution each monomer of type m on the chain has a charge equal to $Z_m \alpha_m e$, where e is the electronic charge and in annealed charge distribution, charged and uncharged sites on the chain are randomly distributed with the probability of finding a charged site as α_m and uncharged site as $(1 - \alpha_m)$.

Third term, $H_{pj}[\mathbf{R}_\beta(t_\beta), \mathbf{r}_\lambda]$, in Eq. (2.2) is the monomer-small molecule interaction term, which depends on the small molecular species. For polymer-solvent interactions, polarization effects are ignored and the interactions are modelled by delta functional form for the excluded volume interactions so that

$$H_{ps}[\mathbf{R}_\beta(t_\beta), \mathbf{r}_\lambda] = \sum_m \int dt_\beta w_{ms} \delta(\mathbf{R}_\beta(t_\beta) - \mathbf{r}_\lambda). \tag{2.10}$$

w_{ms} being the monomer-solvent excluded volume parameter. As the small ions (counterions and coions) are taken to be point like in this study, so their interactions with the monomers are taken to be purely electrostatic in nature, written by

$$H_{pj}[\mathbf{R}_\beta, \mathbf{r}_\lambda] = \sum_m \int dt_\beta \left[\frac{Z_m Z_j e^2 g_{t_\beta}}{k_B T} \frac{\epsilon^{-1}(\mathbf{R}_\beta(t_\beta), \mathbf{r}_\lambda)}{|\mathbf{R}_\beta(t_\beta) - \mathbf{r}_\lambda|} \right]. \tag{2.11}$$

where $j = c, +, -$.

Last term on the right hand side in Eq. (2.2) takes care of interactions among small molecules. Similar to monomer-monomer excluded volume interactions, we model solvent-solvent interaction energy as

$$H_{ss}[\mathbf{r}_\beta, \mathbf{r}_\lambda] = \frac{1}{2} w_{ss} \delta(\mathbf{r}_\beta - \mathbf{r}_\lambda), \tag{2.12}$$

w_{ss} being the solvent-solvent excluded volume parameter. Like monomer-solvent electrostatic interactions, we ignore the solvent-ion electrostatic interactions so that $H_{sj} = 0$ for $j = c, +, -$ due to the point like sizes of the ions, which exhibit zero excluded volume. Also, taking ion-ion interactions to be purely electrostatic in nature, we can write

$$H_{ja}[\mathbf{r}_\beta, \mathbf{r}_\lambda] = h_{ja}\frac{Z_j Z_a e^2}{k_B T}\frac{\epsilon^{-1}(\mathbf{r}_\beta, \mathbf{r}_\lambda)}{|\mathbf{r}_\beta - \mathbf{r}_\lambda|}, \tag{2.13}$$

where $j, a = c, +, -$.

The complicated partition function as presented in Eq. (2.1) can be written in a simplified form using microscopic densities for different species in the system, defined as

$$\hat{\rho}_m(\mathbf{r}) = \frac{1}{b}\sum_{\beta=1}^{n_p}\int dt_\beta\, \delta(\mathbf{r} - R_\beta(t_\beta)) \tag{2.14}$$

$$\hat{\rho}_j(\mathbf{r}) = \sum_{\beta=1}^{n_j}\delta(\mathbf{r} - \mathbf{r}_\beta) \tag{2.15}$$

for monomers and small-molecular species, respectively. Using these definitions of number densities and using identity

$$\delta(\mathbf{R} - \mathbf{R}') = \int d\mathbf{r}\delta(\mathbf{r} - \mathbf{R})\delta(\mathbf{r} - \mathbf{R}'). \tag{2.16}$$

Eq. (2.2) can be written as

$$H[\mathbf{R}_\beta(t_\beta), \mathbf{r}_\lambda] = \sum_{\beta=1}^{n_p} H_0[\mathbf{R}_\beta(t_\beta)] + H_w + H_\epsilon, \tag{2.17}$$

where H_w and H_ϵ are the contributions coming from the excluded volume and the electrostatic interactions among different components, respectively. Explicitly,

$$H_w = \frac{1}{2}\sum_\gamma\sum_{\gamma'\neq\gamma}\chi_{\gamma\gamma'}b^3\int d\mathbf{r}\hat{\rho}_\gamma(\mathbf{r})\hat{\rho}_{\gamma'}(\mathbf{r}) + \frac{\rho_0}{2}\sum_\gamma w_{\gamma\gamma}n_\gamma \tag{2.18}$$

for $\gamma, \gamma' =$ m,s and

$$H_e = \frac{1}{2}\int d\mathbf{r}\int d\mathbf{r}'\frac{\hat{\rho}_e(\mathbf{r})\hat{\rho}_e(\mathbf{r}')}{\epsilon(\mathbf{r})k_BT|\mathbf{r}-\mathbf{r}'|}. \tag{2.19}$$

In these equations, $\chi_{\gamma\gamma'} = \chi_{\gamma'\gamma}$ is the dimensionless Flory's chi parameter defined as

$$\frac{w_{\gamma\gamma}+w_{\gamma'\gamma'}}{2} - w_{\gamma\gamma'} = -\chi_{\gamma\gamma'}b^3 \tag{2.20}$$

and $\hat{\rho}_e(\mathbf{r})$ is the microscopic charge density at $\mathbf{r}$ defined as

$$\hat{\rho}_e(\mathbf{r}) = e\left[\sum_m \frac{Z_m}{b}\sum_{\beta=1}^{n_p}\int dt_\beta\, g_{t_\beta}\delta(\mathbf{r}-\mathbf{R}_\beta(t_\beta)) + \sum_{j=c,+,-} Z_j\hat{\rho}_j(\mathbf{r})\right]. \tag{2.21}$$

2.2 Transformation from Particles to Fields

So far, we have written the partition function in terms of the microscopic density variables starting from a microscopic description of the interactions among different components in the system. However, level of the complexity of the problem is still the same due to intricate coupling of these densities. In order to make some progress, these couplings need to be decoupled. This can be done using two different transformation schemes, both of which give the same results within normalization constants. Here, we present the details of these two methods. First scheme is based on some functional integral identities[4]. The second scheme is based on a well-known identity for Gaussian functional integrals known as Hubbard-Stratonovich[5] transformation, which we present here for the sake of completeness.

2.2.1 Transformation using Functional Integral Identities

For any arbitrary functional, f , of microscopic variables $\hat{\rho}$

$$f[\hat{\rho}] = \int D[\rho]\delta(\rho-\hat{\rho})f[\rho], \tag{2.22}$$

$$\delta(\rho - \hat{\rho}) = \mu \int D[w] \exp\left[i \int d\mathbf{r} w(\mathbf{r})(\rho(\mathbf{r}) - \hat{\rho}(\mathbf{r}))\right] \quad (2.23)$$

$$\Rightarrow f[\hat{\rho}] = \mu \int D[\rho] \int D[w] \exp\left[i \int d\mathbf{r} w(\mathbf{r})(\rho(\mathbf{r}) - \hat{\rho}(\mathbf{r}))\right] f[\rho], \quad (2.24)$$

where μ is the appropriate normalization factor. Using this transformation, any functional of microscopic variable $\hat{\rho}(\mathbf{r})$ can be written as functional integrals over a collective density variable $\rho(\mathbf{r})$ and a field variable $w(\mathbf{r})$. Introducing a density and field variable for the charge density variable, $\hat{\rho}_e(\mathbf{r})$, each microscopic number density variable involved in the incompressibility constraint, $\hat{\rho}_\gamma(\mathbf{r})$, and replacing the incompressibility constraint on the microscopic densities using the functional integral identity for delta function as in Eq. (2.23), the partition function in Eq. (2.1) can be written as

$$Z = \Lambda \int \prod_\gamma D[\rho_\gamma] \int D[w_\gamma] \int D[\eta] \int D[\rho_e] \int D[v] \sum_{\{g_{t_3}\}} \exp[-H], \quad (2.25)$$

where $\gamma = m.s$ and $\eta(\mathbf{r})$ is the field variable corresponding to the incompressibility constraint. $\rho_e(\mathbf{r})$ and $v(\mathbf{r})$ are the collective charge density and field variables. In this equation, Λ is the normalization factor and functional dependence of H on $\rho_j, \rho_\gamma, w_j, w_\gamma, \eta$ and g_{t_3} has been suppressed for notational convenience. Note here that all the collective field and density variables are real. It should also be kept in mind that the functional integrals over density variables (ρ's) can be carried out exactly for the two body interaction model used in this work and only functional integrals over field variables need to be approximated by some appropriate approximation scheme to make a progress. An alternate way is to introduce two collective variables for each microscopic density variable along with collective charge variables $\rho_e(\mathbf{r}), v(\mathbf{r})$ and $\eta(\mathbf{r})$. We don't follow that approach in this chapter due to redundant collective variables used in the formulation. However, the approach is particularly useful in making connections with the density functional theories as described in Chapter 3.

2.2.2 Hubbard-Stratonovich Transformation

This transformation is a generalization of a result for multivariate Gaussian integrals to functionals so that for any real, symmetric, positive-definite operator $A(\mathbf{r},\mathbf{r}')$,

$$\exp\left[-\frac{1}{2}\int d\mathbf{r}\int d\mathbf{r}' J(\mathbf{r})A^{-1}(\mathbf{r},\mathbf{r}')J(\mathbf{r}')\right] = \frac{\int D[f]\,\exp\left[-(1/2)\int d\mathbf{r}\int d\mathbf{r}' f(\mathbf{r})A(\mathbf{r},\mathbf{r}')f(\mathbf{r}') + i\int d\mathbf{r} J(\mathbf{r})f(\mathbf{r})\right]}{\int D[f]\exp\left[-(1/2)\int d\mathbf{r}\int d\mathbf{r}' f(\mathbf{r})A(\mathbf{r},\mathbf{r}')f(\mathbf{r}')\right]}. \quad (2.26)$$

where $J(\mathbf{r})$ and $f(\mathbf{r})$ are arbitrary functions and $i=\sqrt{-1}$. Similarly, another functional integral identity can be written for exponents of Gaussian quantities with positive sign as

$$\exp\left[\frac{1}{2}\int d\mathbf{r}\int d\mathbf{r}' J(\mathbf{r})A^{-1}(\mathbf{r},\mathbf{r}')J(\mathbf{r}')\right] = \frac{\int D[f]\,\exp\left[-(1/2)\int d\mathbf{r}\int d\mathbf{r}' f(\mathbf{r})A(\mathbf{r},\mathbf{r}')f(\mathbf{r}') + \int d\mathbf{r} J(\mathbf{r})f(\mathbf{r})\right]}{\int D[f]\exp\left[-(1/2)\int d\mathbf{r}\int d\mathbf{r}' f(\mathbf{r})A(\mathbf{r},\mathbf{r}')f(\mathbf{r}')\right]}. \quad (2.27)$$

Note that both of these identities are also valid when positive sign in front of linear $J(\mathbf{r})$ term is replaced by a negative sign. This is a generalization of the fact that for simple Gaussian integrals

$$\int_{-\infty}^{\infty} dx \quad \exp\left[-\frac{ax^2}{2}\pm iJx\right] = \sqrt{\frac{2\pi}{a}} \quad \exp\left[-\frac{J^2}{2a}\right] \quad (2.28)$$

Furthermore, in these equations, inverse operator $A^{-1}(\mathbf{r},\mathbf{r}')$ is defined through the relation

$$\int d\mathbf{r}' A^{-1}(\mathbf{r},\mathbf{r}')A(\mathbf{r}',\mathbf{r}'') \;=\; \delta(\mathbf{r}-\mathbf{r}''). \quad (2.29)$$

For simple operators such as $A(\mathbf{r},\mathbf{r}')=1/|\mathbf{r}-\mathbf{r}'|$, it can be shown that inverse operator is $A^{-1}(\mathbf{r},\mathbf{r}')=-\delta(\mathbf{r}-\mathbf{r}')\nabla^2_{\mathbf{r}}/4\pi$ using the property $\nabla^2_{\mathbf{r}}\left[\frac{1}{4\pi|\mathbf{r}-\mathbf{r}'|}\right]=-\delta(\mathbf{r}-\mathbf{r}')$.

Similarly, taking into account the fact that the Poisson's equation must be satisfied even for position dependent dielectric constant, it can be shown that inverse operator for $A(\mathbf{r},\mathbf{r}') = 1/\epsilon(\mathbf{r})|\mathbf{r}-\mathbf{r}'|$ is $A^{-1}(\mathbf{r},\mathbf{r}') = -\delta(\mathbf{r}-\mathbf{r}')\,\nabla_{\mathbf{r}'}\,\epsilon(\mathbf{r}')\,\nabla_{\mathbf{r}''}/4\pi$.

In order to use this transformation for the Hamiltonian as represented by Eq. (2.17), microscopic density terms which are quadratic in nature needs to be written in the form given by the left hand side in Eqs. (2.26) and (2.27). Electrostatic terms in H_ϵ are already in the appropriate form. It is only the terms in H_w that needs to be rewritten. This can be achieved by rewriting H_w in terms of order parameters and total density. For a n component system, all the microscopic densities can be described by $n-1$ independent order parameters (due to the incompressibility constraint serving as the n^{th} relation among the densities). There are many different ways of defining these order parameters. One convenient definition, which makes Mathematics simple, is the deviation of densities of solutes from the solvent density i.e., defining $\phi_j(\mathbf{r}) = \hat{\rho}_j(\mathbf{r}) - \hat{\rho}_s(\mathbf{r})$ for $j = 1, 2, \cdots (n-1)$, where j is the index for different solutes (monomers, counterions and the salt ions). Using the transformation for each quadratic term in the Hamiltonian (cf. Eq. (2.17)), the partition function becomes

$$Z = \frac{1}{\Lambda_\eta \Lambda_\psi \prod_j \Lambda_j} \int \prod_j D[\zeta_j] \int D[\eta] \int D[\psi] \sum_{\{g_{t\beta}\}} \exp\left[-H'\right], \qquad (2.30)$$

where ζ_j is the field variable introduced for the quadratic term involving $\phi_j(\mathbf{r})$ and Λ_j is the corresponding normalization factor. Similarly, ψ is the field variable introduced for the quadractic electrostatic energy term and Λ_ψ is the normalization factor arising as a result. As mentioned earlier, η is the field variable introduced for the incompressibility constraint and Λ_η is the *unknown* normalization constant.

Sometimes, it is advantageous to use this technique rather than the method using functional integral identities as presented in previous section due to the fact that the functional integrals over density variables don't appear in the formulation and one has to deal with only the functional integrals over the fields with appropriate normalization factors. On the other hand, this technique is plagued with two main shortcomings. One is the fact that in general, it is not easy to find the inverse operator A^{-1} for any given A. Second, the technique can only be used for quadratic terms in Hamiltonian. In case, there are higher order terms such as in the problems considering polymers in poor solvent conditions, the method presented in the previous section should come handy. For quadratic functionals, after carrying out Gaussian integrals over collective density variables such as in Eq. (2.25), it can be shown that the method presented in the previous section is the same as the one using Hubbard-Stratonovich transformation. Specific details for using any of the above methods will be presented in the context of specific problem under investigation in latter chapters. For the discussion in this chapter, let's use the transformation using functional integral identities (cf. Eq. (2.25)).

2.3 Sum over Charge Distributions

In order to carry out the sum over charge distributions in Eq. (2.25), we need to compute the sum

$$S = \sum_{\{g_{t_\beta}\}} \exp\left[-\sum_{\beta=1}^{n_p}\sum_{m}\frac{eZ_m}{b}\int dt_\beta\, g_{t_\beta}\psi(\mathbf{R}_\beta)\right]. \tag{2.31}$$

Using Eq. (2.9), it can be shown that for the smeared charge distribution

$$S = \exp\left[-\sum_{\beta=1}^{n_p}\sum_{m}\frac{eZ_m\alpha_m}{b}\int dt_\beta\,\psi(\mathbf{R}_\beta)\right] \tag{2.32}$$

and for the annealed distribution

$$S = \exp\left[\sum_m \ln\left\{\alpha_m \exp\left(-\sum_{\beta=1}^{n_p} \frac{eZ_m}{b}\int dt_\beta\, v(\mathbf{R}_\beta)\right) + (1-\alpha_m)\right\}\right]. \quad (2.33)$$

2.4 Saddle Point Approximation

For the sake of discussion, we consider the smeared charge distribution so that Eq. (2.25) can be written as

$$Z = \Lambda \int \prod_\gamma D[\rho_\gamma] \int D[w_\gamma] \int D[\eta] \int D[\rho_e] \int D[v] \exp[-f]\,. \quad (2.34)$$

where f is given by

$$\begin{aligned}\exp(-f) = \frac{Q_p^{n_p} Q_s^{n_s} \prod_j Q_j^{n_j}}{n_p! n_s! \prod_j n_j!} \exp\Bigg[&-\frac{\rho_0}{2}\sum_\gamma w_{\gamma\gamma} n_\gamma - \frac{1}{2}\sum_\gamma \sum_{\gamma'\neq\gamma} \chi_{\gamma\gamma'} b^3 \int d\mathbf{r}\rho_\gamma(\mathbf{r})\rho_{\gamma'}(\mathbf{r}) \\ &-\frac{1}{2}\int d\mathbf{r}\int d\mathbf{r}'\frac{\rho_e(\mathbf{r})\rho_e(\mathbf{r}')}{\epsilon(\mathbf{r})k_B T|\mathbf{r}-\mathbf{r}'|} + i\int d\mathbf{r}\rho_e(\mathbf{r})v(\mathbf{r}) \\ &+i\int d\mathbf{r}\sum_\gamma w_\gamma(\mathbf{r})\rho_\gamma(\mathbf{r}) + i\int d\mathbf{r}\,\eta(\mathbf{r})\{\sum_\gamma \rho_\gamma(\mathbf{r}) - \rho_0\}\Bigg]. \end{aligned} \quad (2.35)$$

In Eq. (2.35), the Q's are the partition functions of individual components in the presence of a field. Explicitly, for the polyelectrolyte chain with smeared charge distribution along the backbone, single chain partition function is given by

$$Q_p = \int D[\mathbf{R}] \exp\left[-\frac{3}{2b}\int_0^{Nb} dt \left(\frac{\partial \mathbf{R}}{\partial t}\right)^2 - \frac{i}{b}\sum_m \int dt\ \{eZ_m\alpha_m v(\mathbf{R}) + w_m(\mathbf{R})\}\right]. \quad (2.36)$$

Similarly, the partition function for a solvent molecule is written as

$$Q_s = \int d\mathbf{r} \exp[-i w_s(\mathbf{r})] \quad (2.37)$$

and the partition function for the small ions of type $j = c, +, -$ is given by

$$Q_j = \int d\mathbf{r} \exp\left[-ieZ_j\psi(\mathbf{r})\right]. \tag{2.38}$$

As mentioned earlier, all the functional integrals over collective variables can not be carried out exactly. One of the approximations used extensively in the literature to evaluate these functional integrals is called saddle point approximation. In this approximation, functional integrals over collective variables are approximated by the value of the integrand at the saddle point i.e. free energy is approximated to be

$$\frac{F}{k_BT} = -\ln Z \simeq f\left\{\rho_\gamma^\star, w_\gamma^\star, \eta^\star, \rho_e^\star, \psi^\star\right\}. \tag{2.39}$$

where $\rho_\gamma^\star, w_\gamma^\star, \eta^\star, \rho_e^\star$ and $\psi^\star$ are to be obtained by solving the set of equations

$$\frac{\delta f}{\delta \rho_\gamma}_{|_{\rho_\gamma=\rho_\gamma^\star}} = 0, \quad \frac{\delta f}{\delta w_\gamma}_{|_{w_\gamma=w_\gamma^\star}} = 0, \quad \frac{\delta f}{\delta \eta}_{|_{\eta=\eta^\star}} = 0, \quad \frac{\delta f}{\delta \rho_e}_{|_{\rho_e=\rho_e^\star}} = 0, \quad \frac{\delta f}{\delta \psi}_{|_{\psi=\psi^\star}} = 0. \tag{2.40}$$

Details of carrying out the functional derivatives are presented in Appendix A. The equations obtained after taking functional derivatives are presented here in the order presented in Eq. (2.40).

$$iw_\gamma^\star(\mathbf{r}) = b^3 \sum_{\gamma' \neq \gamma} \chi_{\gamma\gamma'} \rho_{\gamma'}^\star(\mathbf{r}) + i\eta^\star(\mathbf{r}) \tag{2.41}$$

$$\rho_s^\star(\mathbf{r}) = \frac{n_s \exp\left[-iw_s^\star(\mathbf{r})\right]}{\int d\mathbf{r} \exp\left[-iw_s^\star(\mathbf{r})\right]} \tag{2.42}$$

$$\rho_m^\star(\mathbf{r}) = \frac{n_p \int dt q(\mathbf{r}, t) q^*(\mathbf{r}, N-t)}{\int d\mathbf{r} q(\mathbf{r}, N)} \tag{2.43}$$

$$\sum_\gamma \rho_\gamma^\star(\mathbf{r}) = \rho_0 \tag{2.44}$$

$$i\psi^\star(\mathbf{r}) = \int d\mathbf{r}' \frac{\rho_e^\star(\mathbf{r}')}{\epsilon(\mathbf{r}) k_B T |\mathbf{r} - \mathbf{r}'|} \tag{2.45}$$

$$\rho_e^*(\mathbf{r}) = \epsilon \left[\sum_m Z_m \alpha_m \rho_m^*(\mathbf{r}) + \sum_{j=+,-,c} \frac{n_j Z_j \exp\left[-ieZ_j \psi^*(\mathbf{r})\right]}{\int d\mathbf{r} \exp\left[-ieZ_j \psi^*(\mathbf{r})\right]} \right]. \quad (2.46)$$

In these equations, $q(\mathbf{r}, t)$ satisfies the modified diffusion equation

$$\frac{\partial q(\mathbf{r}, t)}{\partial t} = \left[\frac{b^2}{6} \nabla_{\mathbf{r}}^2 - i \left\{ eZ_m \alpha_m \psi^*(\mathbf{r}) + w_m^*(\mathbf{r}) \right\} \right] q(\mathbf{r}, t) \quad (2.47)$$

for the values of t encompassing monomer of type m along the backbone with the initial condition $q(\mathbf{r}, 0) = 1$. Similarly, $q^*(\mathbf{r}, N - t)$ satisfies

$$\frac{\partial q^*(\mathbf{r}, N - t)}{\partial t} = - \left[\frac{b^2}{6} \nabla_{\mathbf{r}}^2 - i \left\{ eZ_m \alpha_m \psi^*(\mathbf{r}) + w_m^*(\mathbf{r}) \right\} \right] q^*(\mathbf{r}, N - t) \quad (2.48)$$

with initial condition $q^*(\mathbf{r}, 0) = 1$. Also, note that for computational purposes, Eq. (2.45) can be written in the differential form as

$$\nabla_{\mathbf{r}} \epsilon(\mathbf{r}) \nabla_{\mathbf{r}} ie\psi^*(\mathbf{r}) = -\frac{4\pi e^2}{k_B T} \left[\sum_m Z_m \alpha_m \rho_m^*(\mathbf{r}) + \sum_{j=+,-,c} \frac{n_j Z_j \exp\left[-ieZ_j \psi^*(\mathbf{r})\right]}{\int d\mathbf{r} \exp\left[-ieZ_j \psi^*(\mathbf{r})\right]} \right]. \quad (2.49)$$

Different numerical techniques, which are useful for solving the modified diffusion and the Poisson-Boltzmann equations are presented in Appendix B.

2.5 Fluctuations around the Saddle Point

To go beyond the saddle point approximation described in the previous section, it is advantageous to use Hubbard-Stratonovich transformation to get rid of redundant functional integrals over collective density variables (ρ's in Eq. (2.34)) and use Eq. (2.30) as the starting point for the partition function with the explicitly known normalization constants except Λ_η. Saddle point approximation within this formalism now requires taking functional derivatives with respect to fields only. It can be

shown rigorously that the saddle point equations obtained in these two formalisms are equivalent and the free energies at the saddle point differ by a constant.

Let's say after summing over charge distributions, the partition function becomes (cf. Eq. (2.30))

$$Z = \frac{1}{\Lambda_\eta \Lambda_\psi \prod_j \Lambda_j} \int \prod_j D[\zeta_j] \int D[\eta] \int D[\psi] \exp\left[-f'\right]. \tag{2.50}$$

Within saddle point approximation, the partition function is approximated by $Z \simeq f'\left\{\zeta_j^\star, \eta^\star, \psi^\star\right\}$, where saddle point values for the fields are to be obtained by extremizing f' with respect to the fields. For n component system, there are $n+1$ field variables designated by ζ_j, η and ψ, for $j = 1, 2, \cdots, (n-1)$. For notational convenience, let's write them as ζ_j, where $j = 1, 2, \cdots (n+1)$ and $j = n, n+1$ represent η and ψ, respectively. To go beyond the saddle point approximation, we use the functional Taylor expansion[13] of the integrand and neglect all the terms beyond quadratic terms i.e., we write

$$f'\left\{\zeta_j\right\} = f'\left\{\zeta_j^\star\right\} + \frac{1}{2} \int d\mathbf{r} \int d\mathbf{r}' \sum_{jk} K_{jk}(\mathbf{r}, \mathbf{r}') \left(\zeta_j(\mathbf{r}) - \zeta_j^\star(\mathbf{r})\right) \left(\zeta_k(\mathbf{r}') - \zeta_k^\star(\mathbf{r}')\right), \tag{2.51}$$

where the linear terms in ζ_j don't appear due to the saddle-point conditions and

$$K_{jk}(\mathbf{r}, \mathbf{r}') = \frac{\delta^2 f'\left\{\zeta_j\right\}}{\delta\zeta_j(\mathbf{r})\delta\zeta_k(\mathbf{r}')} \Big|_{\zeta_j = \zeta_j^\star}. \tag{2.52}$$

for $j, k = 1, 2, \cdots, (n+1)$. Plugging the functional Taylor expansion for f' in Eq. (2.50), the functional integrals to be carried out are Gaussian in nature and can be carried out. Formally, the result is the one-loop approximation[7] for the free energy in terms of a ratio of determinants of continuous block matrices i.e.,

$$\frac{F}{k_B T} \simeq f'\left\{\zeta_j^\star\right\} + \frac{1}{2} \ln \frac{\det K}{\det K_0}, \tag{2.53}$$

where K is the square block matrix of order $n+1$ with its block elements represented by K_{jk} and K_0 is the diagonal square block matrix of order $n+1$ (which appear because of the normalization factors and unknown normalization constant Λ_η has been used to define K_0). It turns out that the individual determinants appearing in Eq. 2.53 are divergent due to the presence of divergent terms on the principal diagonal, which in turn highlights the fact that the model is ill-defined at very small length scales. This is similar to the familiar ultraviolet divergences appearing in one-loop calculations in field theory. The unknown Λ_η can be estimated by identifying the divergent terms in $\det K$, which should cancel out exactly at one-loop level. Specific details of this technique are presented in Chapter 4, while studying a single polyelectrolyte chain in spherical cavities.

CHAPTER 3

MICROPHASE SEPARATION IN POLYELECTROLYTIC DIBLOCK COPOLYMERS MELTS : WEAK SEGREGATION LIMIT

3.1 Introduction

The science behind the complex behavior of amphiphilic systems continues to be of interest to scientific community. A great deal of theoretical[14, 15, 16, 17, 18, 19, 20, 21] and experimental effort[22, 23, 24, 25, 26, 27] has been made to study this behavior. Especially, self-assembly of amphiphiles[24] is of significant importance in understanding many biological systems. An amphiphilic diblock copolymer system has applications such as encapsulation[25, 26] and drug delivery[27], which are dependent on self-assembly of macromolecules.

Self-assembly of neutral block copolymers in concentrated regimes, has already been studied extensively in the last three decades. Seminal work in developing theory for microdomains in diblock copolymer melt was done by Helfand[4, 28] *et al.*, where the unit cell approximation was used to calculate the properties for sharp interfaces (strong segregation limit (SSL)). Later on, Leibler [29] calculated morphology diagrams in weak segregation limit (WSL) using the random phase approximation (RPA), when the system is on the verge of transformation from disordered to ordered phases and interfaces between the ordered domains are diffuse. Few years later, Semenov [30] and Ohta [31]*et al.* calculated morphology diagrams in SSL taking into account a sharp interface between the domains. Semenov used ground state dominance and Ohta *et al.* extended the RPA method developed by Leibler to SSL.

Afterwards, Muthukumar [32, 33] *et al.* and Matsen[34]*et al.* bridged the gap between WSL and SSL theories by using density functional theory (DFT) and SCFT respectively. As a result of these theories, equilibrium morphology diagram for neutral diblock copolymer melt was chalked out and verified experimentally (Fig. 3.1). To go beyond mean field, fluctuations of the order parameter were included by Fredrickson and Helfand[35], Olvera de la cruz[36] and Muthukumar[37].

Although we have a sound understanding of neutral copolymers, our understanding of charged copolymers is inadequate. A number of researchers have tried to explore charged diblock systems. Some of these efforts are invested in studying dilute solutions (micelle regime)[38, 39, 40, 41] and others have been carried out in the concentrated regime[16, 17, 18, 42, 43]. The fundamental question is how Coulomb interactions affect the relative stabilities of ordered morphologies. First work in this direction was carried out by Marko and Rabin [16] who explored charged copolymers in both the melts and solutions. In their study, they presented the effect of degree of ionization and salt on critical parameters for weak segregation in melt and studied micelle behaviour also. But they did not consider any ordered microstructures for melts. Recently, SCFT for polyelectrolytic systems has been developed by Shi and Noolandi[44] and Wang[45] *et al.*

In this work, we have considered microphase separation in diblock copolymer melts, formed out of polyelectrolyte (A) block and neutral (B) block. RPA is presented in Sec. 3.2.1 and SCFT equations are briefly presented in Sec. 3.2.2. Calculated results and conclusions are presented in Sec. 3.3 and 3.4, respectively.

3.2 Theory

We consider diblock copolymer melts containing n_p charged-neutral diblock copolymer chains, each containing a total of N segments of two species (A and B) with f as the fraction of the charged block A. Number of segments in blocks A and B is repre-

sented by N_A and N_B, respectively, so that ($f = N_A/N, N = N_A + N_B$). Block A is taken to be negatively charged and we assume that there are n_c counterions released by the block. In addition to this, there are $n_\pm$ ions of species $\pm$ coming from the added salt (in total volume Ω) so that the whole system is globally electroneutral. Let Z_j be the valency of the j^{th} charged species. Subscripts $A, B, s, c, +$ and $-$ are used to represent monomer A, B, solvent, counterion from block A, positive and negative salt ions, respectively. We consider smeared charge distribution for the charged block (A) so that the degree of ionization of the block (per chain) is taken to be α. In other words, each of the fN segments of A type carry a charge of $eZ_A\alpha$, where e is the electronic charge. To use the field theory, we represent a copolymer chain as a continuous curve of length Nb, where b is the Kuhn segment length. For the treatment shown below, we assume that volume occupied by each A and B monomer is the same ($= b^3 \equiv 1/\rho_o, \rho_o$ being the bulk density) and small ions are taken to be point like. We consider the diblock copolymer solution in the incompressibility limit so that $\Omega = nNb^3$. We use the arc length variable t_β to represent any segment along the backbone of β^{th} chain. In this notation, A block in β^{th} chain is represented by $t_\beta (0 \leq t_\beta \leq N_A b)$. Also, the position vector for a particular segment is represented by $\mathbf{R}_\beta(t_\beta)$. Furthermore, the permittivity of the medium,ϵ, is taken to be independent of the position (in units of $4\pi\epsilon_o$, where ϵ_o is the permittivity of vacuum). Using the field theoretical technique as described in section 2.2.1 of Chapter 2, Helmholtz free energy F can be written as

$$\exp\left[-\frac{F}{k_B T}\right] = \Lambda \int \prod_j D[\rho_j] \int D[w_j] \int \prod_\gamma D[\rho_\gamma] \int D[w_\gamma] \int D[\eta] \exp[-H]\,. \tag{3.1}$$

where $j = c, +, -$ and $\gamma = A, B$. Here, $\eta(\mathbf{r})$ is the field variable corresponding to the incompressibility constraint. Λ is the normalization factor and H is a functional of

ρ_j, w_j and η. Note here that only for the smeared charge distribution, microscopic charge density can be written as a linear combination of microscopic densities of all the charged species in the system. That's the reason, instead of introducing collective variables corresponding to the microscopic charge density, we have introduced collective variables for each species (i.e., ρ_ϵ and ψ don't appear in this formulation). This approach is quite useful in making connection with density functional theories, which deal with number densities rather than charge densities.

3.2.1 WSL - Random Phase Approximation

3.2.1.1 Stability Limit

Near the stability limit of the melt, densities of all components in the inhomogeneous phase deviate slightly from their average values in the homogeneous phase. So, the free energy of the inhomogenous phase can be obtained by expanding the corresponding free energy expression for the homogeneous phase about the average densities. Neglecting cubic and higher order terms in densities, the free energy of the inhomogeneous phase is obtained in terms of the order parameter $\phi(\mathbf{r})$ (see Appendix C) and has the form:

$$F = F_0 + \delta F(\phi) + O(\phi^3), \tag{3.2}$$

where the order parameter ϕ is the same as that used for neutral block copolymer melts, given by

$$\phi(\mathbf{r}) = \delta\rho_A(\mathbf{r}) = \rho_A(\mathbf{r}) - f\,\rho_0. \tag{3.3}$$

F_0 is the free energy of the homogeneous phase and is given by a Flory-type equation:

$$\frac{F_0}{k_B T} = \sum_{j=c,+,-} n_j \ln(n_j) - \frac{\kappa^3}{12\pi} + \chi_{AB} f(1-f) \tag{3.4}$$

In writing F_0, linear and constant terms have been ignored. In Eq. (3.4), χ_{AB} and $\kappa^{-1} = r_D$ are Flory's chi parameter and the Debye screening length, respectively. κ

is given by

$$\kappa^2 = 4\pi l_B \sum_{j=c,+,-} \frac{n_j}{\Omega} Z_j^2 \tag{3.5}$$

and $l_B = e^2/\epsilon k_B T$ stands for the Bjerrum length (in units of $4\pi\epsilon_o$). In Eq. (3.4), the first term corresponds to the translational entropy of small ions, κ^3 term accounts for counterions and coions correlation effect and χ_{AB} term gives the contribution of chemical mismatch between blocks.

The second degree term in ϕ defines the structure factor ($S(k)$) and is given by:

$$\delta F(\phi) = \frac{1}{2}\int \frac{d^3k}{(2\pi)^3} S^{-1}(k)\phi(k)\phi(-k) \tag{3.6}$$

$$S^{-1}(k) = S_0^{-1}(k) + S_1^{-1}(k) \tag{3.7}$$

$$S_0^{-1}(k) = Q(x) - 2\chi_{AB}b^3 \tag{3.8}$$

$$Q(x) = \frac{g(1,x)}{\rho_0 N\left\{g(f,x)g(1-f,x) - [g(1,x) - g(f,x) - g(1-f,x)]^2/4\right\}} \tag{3.9}$$

$$S_1^{-1}(k) = \frac{4\pi l_B Z_A^2 \alpha^2 N b^2}{6x + \kappa^2 N b^2} \tag{3.10}$$

In Eq. (3.7), $S_0^{-1}(k)$ is the contribution due to short range excluded volume interactions and $S_1^{-1}(k)$ is due to the long range Coulomb interactions present in the system. $g(f,x)$ is the Debye function given by

$$g(f,x) = \frac{2(fx + e^{-fx} - 1)}{x^2}, \quad x = \frac{k^2 N b^2}{6} = k^2 R_g^2 \tag{3.11}$$

Note that Eqs. (3.6 - 3.10) are the same as in Ref.[16].

3.2.1.2 Limiting Laws

To understand the qualitative behavior of the system at the stability limit, a scaling analysis is presented here for two limiting cases. In order to carry out the scaling

analysis, the complicated equation for $S_0^{-1}(k)$ is approximated by an expression, used previously for neutral block copolymers[31], which reproduces $S_0^{-1}(k)$ with about 5 % accuracy. Using the approximate expression, Eq. (3.6) becomes:

$$\delta F\{\phi\} = \frac{1}{2\rho_0 N}\int \frac{d^3k}{(2\pi)^3}\left\{B(f)k^2 + \frac{A(f)}{k^2} + \frac{C(l_B)}{k^2+\kappa^2} - \bar{\chi}\right\}\phi(k)\phi(-k) \quad (3.12)$$

$$B(f) = \frac{Nb^2}{12f(1-f)} \quad (3.13)$$

$$A(f) = \frac{9}{Nb^2 f^2(1-f)^2} \quad (3.14)$$

$$C(l_B) = 4\pi l_B Z_A^2 \alpha^2 \rho_0 N \quad (3.15)$$

$$\bar{\chi} = 2\chi_{AB}N\rho_0 b^3 - \frac{s(f)}{2f^2(1-f)^2} \quad (3.16)$$

Here, $s(f)$ is a parameter used to reproduce $S_0^{-1}(k)$. At the stability limit, $S(k)$ diverges at the wave-vector $k = k^\star$ and the second degree term δF in free energy vanishes at $k = k^\star$ and $\chi_{AB}N = \chi^\star_{AB}N$. In the case of neutral block copolymers (i.e. $C(l_B) = 0$), the divergence corresponds to $k^\star = (A/B)^{1/4} \sim N^{-1/2}$ so that the period $D = 2\pi/k^\star \sim N^{1/2}$. Hence, δF vanishes at $\bar{\chi}^\star = 2\sqrt{AB}$ so that $\chi^\star_{AB}N$ is given by expression

$$(\chi^\star_{AB}N)_{neutral} = \frac{1}{\rho_0 b^3}\left[\frac{s(f)}{4f^2(1-f)^2} + \sqrt{\frac{3}{4f^3(1-f)^3}}\right] \quad (3.17)$$

Now, for charged block copolymers, consider the two limiting cases: (i) $k^2 \ll \kappa^2$ and (ii) $k^2 \gg \kappa^2$. In terms of the Debye screening length , these cases correspond to $r_D \ll D$ and $r_D \gg D$, respectively.

Case (i): Strong Screening - $r_D \ll D$

In this regime, the structure factor becomes

$$S^{-1}(k) \simeq Bk^2 + \frac{A}{k^2} - \left(\bar{\chi} - \frac{C}{\kappa^2}\right) \quad (3.18)$$

The maxima of the structure factor corresponds to $k^\star = (A/B)^{1/4} \sim N^{-1/2}$ so that the period $D = 2\pi/k^\star \sim N^{1/2}$ and is *independent* of degree of ionization of charged

block. So,charged block copolymer behaves like neutral copolymer. This is because the electrostatic interactions are short ranged in this regime. But there is a remarkable effect of small ions on $\chi^{\star}_{AB}N$ and in fact, it is found that charged block copolymers have to have higher $\chi^{\star}_{AB}N$ as compared to its neutral analog for undergoing the microphase separation. For salty systems,

$$(\chi^{\star}_{AB}N)_{charged} = (\chi^{\star}_{AB}N)_{neutral} + \frac{2\pi l_B Z_A^2 \alpha^2 \rho_0 N}{\kappa^2} \tag{3.19}$$

For salt-free incompressible system where $\kappa^2 = 4\pi l_B f \alpha Z_c^2/b^3$, this expression simplifies to

$$(\chi^{\star}_{AB}N)_{charged} = (\chi^{\star}_{AB}N)_{neutral} + \frac{1}{2}\left(\frac{Z_A}{Z_c}\right)^2 \frac{\alpha N}{f} \tag{3.20}$$

Physically, this means that homogeneous phase in charged copolymer enjoys larger parameter space as compared to its neutral analog.

Case (ii): Weak Screening - $r_D \gg D$

In this regime, the structure factor becomes

$$S^{-1}(k) = Bk^2 + \frac{A+C}{k^2} - \bar{\chi} \tag{3.21}$$

The maxima of the structure factor corresponds to

$$k^{\star} = \left(\frac{A+C}{B}\right)^{1/4} \Rightarrow D = 2\pi\left(\frac{A+C}{B}\right)^{-1/4} \tag{3.22}$$

so that $\bar{\chi}^{\star} = 2\sqrt{(A+C)B}$. Plugging in expressions for A, B and C

$$D = \frac{2\pi N^{1/2} f^{1/4}(1-f)^{1/4} b}{\left[108 + 48\pi Z_A^2 (1-f)^2 (f\alpha N)^2 l_B b^2 \rho_0\right]^{1/4}} \tag{3.23}$$

$$(\chi^{\star}_{AB}N)_{charged} = \frac{1}{\rho_0 b^3}\left[\frac{s(f)}{4f^2(1-f)^2} + \sqrt{\frac{3}{4f^3(1-f)^3} + \frac{(4\pi l_B b^2 \rho_0)(\alpha N)^2 Z_A^2}{12 f(1-f)}}\right]$$

(3.24)

From the expression for D, it is clear that *the period decreases with an increase in the degree of ionization* in this limiting case. Comparing $\chi^{*}_{AB}N$ for charged and neutral block copolymer cases (Eq. (3.24) and Eq. (3.17)), it can be inferred that in this limiting regime also, $(\chi^{*}_{AB}N)_{charged} > (\chi^{*}_{AB}N)_{neutral}$ and increases with an increase in α.

Further, it can be shown that the correlation effect of ions (Debye-Hückel theory) is weak as long as $\kappa l_B \ll 1$. This means that all of the above limiting laws for salt-free systems are valid as long as $\kappa l_B \ll 1$.

3.2.1.3 Numerical Calculations for Stability Limit

From here onwards, we consider the salt-free melt. To calculate the stability limit for salt-free melts, inverse temperature dependence of χ_{AB} and l_B is clubbed together by the introduction of a parameter (called reduced temperature[46]) defined as

$$t = \frac{b}{4\pi\alpha l_B} \quad \text{and} \quad \chi_{AB} = \frac{1}{20\pi t} \tag{3.25}$$

Having written structure factors in terms of t, the stability limit is calculated using

$$\frac{\delta S^{-1}(k)}{\delta k}\,|_{k=k^{*},t=t^{*}} = 0 \tag{3.26}$$

$$S^{-1}(k)\,|_{k=k^{*},t=t^{*}} = 0 \tag{3.27}$$

where $S^{-1}(k)$ is given in Eqs. (3.7 - 3.10). Solving these equations for t^{*}

$$t^{*} = \frac{-L + \sqrt{L^2 - 4PR}}{2P} > 0. \tag{3.28}$$

where

$$P = 60\pi x^\star A(x^\star) \tag{3.29}$$

$$L = 10\pi f N Z_c^2 A(x^\star) - 6x^\star + 10\pi Z_A^2 \alpha N \tag{3.30}$$

$$R = -f N Z_c^2 \tag{3.31}$$

$$A(x^\star) = Q(x^\star) \tag{3.32}$$

In writing these equations, we have taken $b = 1$. Function Q appearing in these equations has already been defined in Eq. (3.9). Using Eq. (3.26), the wavevector at the stability limit is given by solving the equation

$$\frac{\delta Q(x)}{\delta x} \mid_{x=x^\star} = \frac{6 Z_A^2 \alpha N t^\star}{(6x^\star t^\star + f N Z_c^2)^2}. \tag{3.33}$$

First, Eq. (3.33) is solved for $x^\star$ and then $t^\star$ is calculated using Eq. (3.28). Effect of α and N on the stability limit is shown in Figs. 3.2 - 3.3. $x^\star$ obtained by using Eq. (3.33) for different values of N is shown in Fig. 3.4.

3.2.1.4 Ordered Structures

To derive free energy expressions for different ordered structures, we employ the method used by Leibler[29]. Following Leibler, we expand the free energy expression in terms of the order parameter up to fourth order. Taking advantage of the fact that in WSL (near stability limit), important fluctuations in polymer densities are those with the wavevector $k = k^\star$, we approximate the order parameter by a sum of plane waves, each having the wavevector $k = k^\star$. Using this expression for the order parameter, free energy density becomes

$$\delta F_n = \frac{N(F - F_0)}{\Omega k_B T} = 2Nb^3(\chi_s - \chi)\phi_n^2 - \zeta_n \phi_n^3 + \eta_n \phi_n^4 \tag{3.34}$$

Morphology	ζ_n	η_n
Lamellar	$\zeta_1 = 0$	$\eta_1 = \frac{N}{4}\Gamma_4(0,0)$
Cylinder	$\zeta_3 = -(2/3\sqrt{3})N\Gamma_3$	$\eta_3 = \frac{N}{12}[\Gamma_4(0,0) + 4\Gamma_4(0,1)]$
Sphere	$\zeta_6 = -(4/3\sqrt{6})N[\Gamma_3 + 2\Gamma_4(0,2) + 4\Gamma_4(1,2)]$	$\eta_6 = \frac{N}{24}[\Gamma_4(0,0) + 8\Gamma_4(0,1)]$

Table 3.1. Coefficients ζ_n and η_n calculated by Leibler[29]

$$2\chi_s b^3 = Q(x^\star) + \frac{Z_A^2 \alpha N b^3}{6x^\star t + fNZ_c^2} \quad \text{and} \quad \chi = \chi_{AB} \tag{3.35}$$

where the value of n corresponds to the morphology being studied. To be specific, $n = 1, 3$ and 6 correspond to lamellar, hexagonally close packed (HCP) cylinder and body centred cubic (BCC) spherical morphology, respectively. Functions Γ_3, Γ_4 and coefficients ζ_n, η_n were calculated by Leibler[29, 47] (summarized in Table 3.1). Further, we have adopted the notation used in Ref.[29] for the arguments of the function Γ_4. The coefficients have the property that $\eta_1 < \eta_3 < \eta_6$ for all f and specifically, for $f = 1/2$, $\zeta_n = 0$. For all the calculations presented in this paper, these coefficients are evaluated at $k = k^\star$.

3.2.1.5 Transition Boundaries

By following the Leibler's procedure[29], the disorder-order transition (DOT) and the order-order transitions (OOT) are studied. Minimizing the free energy density (Eq. (3.34)) with respect to the order parameter, equilibrium order parameter and free energy densities are obtained. Results of these minimizations are presented in Table 3.2 where γ_n is given by

Morphology	Order Parameter ($\bar{\phi}_n$)	Free Energy Density (δF_n)
DOT	$\zeta_n/(2\eta_n)$	0
Lamellar	$\sqrt{(\chi-\chi_s)N/\eta_1}$	$-N^2(\chi_s-\chi)^2/\eta_1$
Sphere, Cylinder	$3\zeta_n(1+\gamma_n)/(8\eta_n)$	$27\zeta_n^4(1+\gamma_n)^3(1-3\gamma_n)/(4096\eta_n^3)$

Table 3.2. Equilibrium order parameters and free energy densities

$$\gamma_n = \left[1 - \frac{64\eta_n}{9\zeta_n^2}(\chi_s - \chi)N\right]^{1/2} \tag{3.36}$$

In order to determine the morphology that evolves at DOT, the free energy density is equated to zero so that $\chi_n N$ at DOT is found to be

$$\chi_n N = \chi_s N - \frac{\zeta_n^2}{8\eta_n} \tag{3.37}$$

Using the coefficients ζ_n and η_n, it can be shown that BCC ($n = 6$) gives the lowest value for $\chi_n N$ (or highest value of t). So, the morphology that appears first is BCC. Writing Eq. (3.37) for DOT in terms of the reduced temperature t, the DOT boundary is given by Eq. (3.28) where $A(x^\star)$ is now given by

$$A(x^\star) = Q(x^\star) - \frac{\zeta_6^2}{4N\eta_6} \tag{3.38}$$

Subscript 6 implies that the morphology is sphere ($n = 6$). Similarly, order-order transition boundaries are calculated by equating free energy densities for different morphologies. In general, all the transition boundaries (stability limit, DOT and order-order transitions) are calculated using Eq. (3.28), where only $A(x^\star)$ varies.

Transition Boundary	Mathematical Conditions	$A(x^*)$
Stability Limit	$\frac{\delta S^{-1}(k)}{\delta k} \mid_{k=k^*,t=t^*} = 0$ $S^{-1}(k) \mid_{k=k^*,t=t^*} = 0$	$Q(x^*)$
Disorder - Order	$\frac{\partial(\delta F_n)}{\partial \phi_n} \mid_{\phi_n=\bar{\phi}_n} = 0$ $\frac{\partial^2(\delta F_n)}{\partial \phi_n^2} \mid_{\phi_n=\bar{\phi}_n} > 0$ $\delta F_n(\bar{\phi}_n, t_n) = 0$	$Q(x^*) - \zeta_6^2/(4N\eta_6)$
Sphere - Cylinder	$\delta F_6 = \delta F_3$	$Q(x^*) + 2y/N$
Cylinder - Lamellar	$\delta F_3 = \delta F_1$	$Q(x^*) + 9\zeta_3^2(\gamma_3^2 - 1)/(32N\eta_3)$

Table 3.3. Description of different transition boundaries

Mathematical conditions and values of $A(x^*)$ for different transition boundaries are summarized in Table 3.3. Function y appearing in Table 3.3 is the solution of Eq. (V-35) in Leibler's work [29]. Solving these sets of equations, the morphology diagram can be constructed as discussed in Sec. 3.3.

3.2.2 Self-Consistent Field Theory (SCFT)

Although RPA gives a valuable insight into the physics of the problem, it is only a linear response treatment. Strictly, this treatment is valid close to the stability limit of homogeneous phase but far from the limit, RPA calculations are not quantitatively correct[32, 33, 34]. To go far away from the stability limit, SCFT has been used extensively in the literature[9, 34, 45]. Using standard methods as described in Chapter 2, the following self-consistent equations are obtained using the saddle point approximation for the *salt-free melt* after taking $b = 1$:

$$\chi_{AB}N\rho_B(\mathbf{r}) = w_A(\mathbf{r}) + \eta(\mathbf{r}) \tag{3.39}$$

$$\chi_{AB}N\rho_A(\mathbf{r}) = w_B(\mathbf{r}) + \eta(\mathbf{r}) \tag{3.40}$$

$$\rho_A(\mathbf{r}) + \rho_B(\mathbf{r}) = 1 \tag{3.41}$$

$$\rho_c(\mathbf{r}) = \frac{n_c \exp\left[-Z_c\psi(\mathbf{r})\right]}{\int d\mathbf{r} \exp\left[-Z_c\psi(\mathbf{r})\right]} \tag{3.42}$$

$$\rho_A(\mathbf{r}) = \frac{\Omega \int_0^f dt\, q(\mathbf{r},t)q^\star(\mathbf{r},1-t)}{\int d\mathbf{r}\, q(\mathbf{r},1)} \tag{3.43}$$

$$\rho_B(\mathbf{r}) = \frac{\Omega \int_f^1 dt\, q(\mathbf{r},t)q^\star(\mathbf{r},1-t)}{\int d\mathbf{r}\, q(\mathbf{r},1)} \tag{3.44}$$

$$\nabla^2_{\mathbf{r}}\psi(\mathbf{r}) = -4\pi l_B \left[Z_c\rho_c(\mathbf{r}) + Z_A\alpha\rho_A(\mathbf{r})\right] \tag{3.45}$$

$$\frac{\partial q(\mathbf{r},s)}{\partial t} = \begin{cases} \left[\frac{N}{6}\nabla^2_{\mathbf{r}} - \left\{Z_A\alpha N\psi(\mathbf{r}) + w_A(\mathbf{r})\right\}\right] q(\mathbf{r},t) & t \le f \\ \left[\frac{N}{6}\nabla^2_{\mathbf{r}} - w_B(\mathbf{r})\right] q(\mathbf{r},t) & t \ge f \end{cases} \tag{3.46}$$

$$\frac{\partial q^\star(\mathbf{r},t)}{\partial t} = \begin{cases} \left[\frac{N}{6}\nabla^2_{\mathbf{r}} - \left\{Z_A\alpha N\psi(\mathbf{r}) + w_A(\mathbf{r})\right\}\right] q^\star(r,t) & t \ge (1-f) \\ \left[\frac{N}{6}\nabla^2_{\mathbf{r}} - w_B(\mathbf{r})\right] q^\star(\mathbf{r},t) & t \le (1-f) \end{cases} \tag{3.47}$$

These equations are to be solved with initial conditions $q(\mathbf{r},0) = 1, q^\star(\mathbf{r},0) = 1$ and the free energy expression for the salt-free melt (per chain) becomes

$$\begin{aligned} \frac{F}{n_p k_B T} = & -\frac{1}{\Omega}\int d\mathbf{r}\chi_{AB}N\rho_A(\mathbf{r})\rho_B(\mathbf{r}) - \frac{N}{8\pi l_B\Omega}\int d\mathbf{r}|\nabla_{\mathbf{r}}\psi(\mathbf{r})|^2 + \frac{1}{\Omega}\int d\mathbf{r}\,\eta(\mathbf{r}) \\ & + \ln\left[\frac{n_p}{\int d\mathbf{r} q(\mathbf{r},1)}\right] - \frac{Z_A f\alpha N}{Z_c}\ln\left[\frac{n_c}{\int d\mathbf{r}\exp\left[-Z_c\psi(\mathbf{r})\right]}\right] + \frac{Z_A f\alpha N}{Z_c} - 1 \end{aligned} \tag{3.48}$$

Here, we have used the notation $ie\psi(\mathbf{r}) \to \psi(\mathbf{r}), iNw_{A/B}(\mathbf{r}) \to w_{A/B}(\mathbf{r}), iN\eta(\mathbf{r}) \to \eta(\mathbf{r}), n_c = -Z_A f\alpha/Z_c$ for all the purely imaginary fields. The free energy of the homogeneous phase (where all the densities and fields are constant) is given by

$$\frac{F}{n_p k_B T} = \chi_{AB} N f(1-f) + \left(-\frac{Z_A}{Z_c} f\alpha N\right)\left\{\ln\left[-\frac{Z_A}{Z_c} f\alpha\right] - 1\right\} \quad (3.49)$$

This numerical technique leads to coupling of full non-linear Poisson-Boltzmann equation with standard modified diffusion equation for the polymer chains. We have solved these sets of equations using an efficient spectral technique[34]. While solving these equations, experimentally found inverse dependence of Flory's χ parameter has been exploited by using reduced temperature t (Eq. (3.25)). We have studied the effect of α on $\chi^*_{AB}N$ and compared with the corresponding RPA calculations. Also, the effect of degree of segregation on the period of lamellar morphology is studied (Fig. 3.5). Monomer densities, counterion densities and electrostatic potential obtained from SCFT calculations are shown in Figs. 3.6 - 3.8, respectively..

3.3 Results

In the previous section , we have provided the necessary equations to describe the microphase separation. Here, we present results for salt-free charged-neutral diblock melts, by solving the above equations.

3.3.1 Stability Limit - RPA Results

In Figs. 3.2 and 3.3, we have drawn the stability limits for charge/neutral block copolymer salt-free melt at different degrees of ionizations for $N = 1000$ and $N = 10,000$, respectively. The critical value of the reduced temperature required to induce microphase separation decreases with an increase in the degree of ionization. This is in qualitative agreement with limiting laws presented in Sec. 3.2.1 and the already established concept that the effective Flory's χ parameter decreases with an increase in degree of ionization for polyelectrolytes[46]. Unlike the neutral copolymers, χ and N for polyelectrolytic diblock copolymers are independent parameters that govern the phase behaviour. Also, the stability limit depends on fraction of charged

block (f) in an unsymmetric fashion. It is to be noted that these results are in agreement with the results reported by Marko and Rabin[16]. In Ref.[16], temperature dependence of χ parameter was not taken into account and critical parameters were calculated by choosing a fixed value of l_B/l. The method of calculations used by Marko and Rabin was similar to the one presented in Appendix C.

3.3.2 Period of Lamellar Phase ($f = 1/2$)

In RPA, near the stability limit, the period of an ordered structure is approximated by $D = 2\pi/k \simeq 2\pi/k^\star$. It is well known that the mean field theory[29] for neutral block copolymer predicts $\chi^\star_{AB}N = 10.495$ and $x^\star = 3.7852$ at $f = 1/2$. Also, the period shows 1/2 power law dependence on N in WSL (i.e. x = constant) as long as the wavevector dependence of higher order terms in free energy expression is suppressed[32, 33, 34]. Physically, this means that block copolymer chains are obeying the Gaussian statistics for chain conformations. Experimentally, there are deviations from this power law because of chain stretching[48]. As shown in Fig. 3.4, same power law dependence is obtained using RPA for polyelectrolytic block copolymers when N is large, but the period ($D \sim \sqrt{N/x^\star}$) for a given N is smaller than that for an equivalent neutral copolymer system. This effect has been seen by other researchers also[16]. The decrease in period with increase in degree of ionization, is explained in Ref.[16] by an argument that counterions need to be rearranged on microphase segregation and entropy loss is lower if the length scale of fluctuations for these counterions is smaller. It is to be stressed that lowering of D with α is *not* purely entropic effect. This effect is an outcome of electrostatic screening due to counterions and hence, includes both energetic as well as entropic contributions.

At present, we are not aware of any experimental data on the period of charged-neutral block copolymer. Nevertheless we expect the polyelectrolyte chains to be non-Gaussian and D to deviate strongly from $N^{1/2}$ power law in the case of charged

systems. SCFT has been quite successful in predicting the period of ordered structures for neutral copolymers. Expecting that SCFT results are valid for weakly charged polyelectrolyte copolymers, results obtained from SCFT calculations are plotted in Fig. 3.5 for lamellar phase ($f = 1/2, N = 1000$). Lowermost point in the plots of Fig. 3.5 corresponds to $\chi^*_{AB}N$. By comparing Fig. 3.5 with Figs. 3.2 and 3.4, it is clear that the RPA calculations for $\chi^*_{AB}N$ and x^*, are in good agreement with the corresponding SCFT calculations. Analogous to neutral copolymers, it is found that $N^{1/2}$ power law is not valid for ordered microstructures. In addition the qualitative feature that the period of ordered structures is lower than its neutral analog, is clearly seen in these plots.

3.3.3 Counterion Distribution

The RPA calculations do not provide counterion distributions. On the other hand, SCFT allows calculations of counterion densities and potential self-consistently. Figs. 3.6 - 3.8 show monomer densities for charged block (A), counterion densities, and the electrostatic potential, respectively. The onset of microphase separation leads to creation of monomer and counterion density waves (Figs. 3.6 and 3.7) because of the incompatibility between the blocks and coupling between charged monomer (A) and counterions, respectively. From these plots, it can be inferred that in the strong segregation limit ($\chi N \to \infty$), all the counterions are confined to the charged domains. One of the effects of these density waves in the lamellar phases, is the presence of a potential difference between the charged and neutral domains (Fig. 3.8) whose magnitude increases with the degree of segregation. For the weakly charged diblock copolymer system studied here, total local charge density is close to zero and it is hard to determine the shape of the charge density wave for the system due to the possible numerical errors. To verify the observation that the effective degree of segregation is reduced because of the electrostatic interactions (RPA calculations),

we have plotted monomer densities for neutral and charged block copolymer at the same χN (Fig. 3.9). These plots clearly confirm that effective degree of segregation is lower for charged copolymer melt and counterions have a tendency to drive the system towards homogeneous phase.

3.3.4 Morphology Diagram for Charged-Neutral Diblock Copolymer

The calculation of morphology diagrams using SCFT is a computationally intensive task because of the vast parameter space for polyelectrolytic systems. To get an idea about transition boundaries, we have used RPA calculations presented in section 3.2.1, assuming that only the classical morphologies[29] compete in charged-neutral diblock copolymer systems. Figs. 3.10 and 3.11 show the calculated morphology diagrams for different α and N. We observe that DOT and OOT boundaries are strongly dependent on α and N. The temperature of occurrence of DOT decreases with an increase in α and increases with an increase in N (analogous to the shift of stability limit - Figs. 3.2, 3.3) . Furthermore, these transition boundaries for DOT and OOT are highly asymmetric with respect to f.

3.4 Conclusions & Future Work

We have addressed the microphase separation in charged-neutral diblock copolymer melts in the weak segregation limit, by using the RPA and SCFT methods. We have shown in Sections 3.2.1 and 3.3 that the critical value of the χ parameter for microphase separation is higher for charged copolymers and of concentration modulation is smaller in comparison with neutral copolymers. From morphology diagrams, it can be seen that the parameter space for ordered microstructures is reduced when degree of ionization of charged block is increased. In other words, charging a block stabilizes the homogeneous phase.

The SCFT results show that the counterions partition themselves preferentially within the charged domains. This leads to creation of a potential difference between charged and neutral domains. This process of partitioning is unfavorable both entropically and energetically. Hence, the length scale of these partitioning is lower when there are more number of counterions to be partitioned for the same number of monomers.

Finally, we summarize the assumptions in obtaining the above results. We have taken the counterions to be point charges. Our treatment can be readily extended to counterions with finite size by modifying the incompressibility condition and incorporating excluded volume interactions. The Kuhn segment lengths for the neutral and charged blocks are taken to be same. It has been shown that conformational asymmetry has an effect on the order-order transition boundaries for neutral copolymers[49]. Analogously, there will be an effect on our system as well. In the case of polyelectrolytes, electrostatic interactions cause stiffening of the chain so that the effective segment length[50] depends on various factors such as κ, α etc. in a complicated manner. By assuming that the segment length for charged and neutral blocks to be the same, we implicitly assume that the charged block copolymer under consideration is conformationally symmetric and is weakly charged, so that the difference between the effective and bare segment lengths is negligible . Another important assumption in the present theory is that the position/concentration dependence of the dielectric constant ϵ is suppressed . Recently, the effect of dielectric constants of individual components in a multi-component polyelectrolyte[45] solution has been presented. In the work, dielectric constant of a component was taken to be linearly dependent on the concentration of the component. In principle, dielectric constant depends on the concentration of ions in a complex manner[51]. At present, there is no satisfactory well-established model for the dependence of microscopic dielectric constant on macroscopic density. So, we model dielectric constant (ϵ) appearing in the expression

for the Bjerrum length as the effective dielectric constant for the mixture of A, B monomers and counterions. Position dependence of dielectric constant will definitely play an important role in the strong segregation limit. However, for melts in WSL, the average value of dielectric constant can be taken as a constant. Further, we have considered only the lamellar, cylindrical and spherical morphologies as the competing structures. Extensions of the present theory for other morphologies are in progress.

At present we are unaware of any systematic experimental study on charged-neutral copolymers. We hope that the present theoretical work will instigate experimental work on charged block copolymers in the concentrated regime. Future extensions of the current work include the study of sharp polymeric interfaces encountered in the strong segregation limit. In particular, the effect of dielectric mismatch between the charged and neutral domains on the period of the morphologies is one of the studies, which is of utmost importance for many industrial applications and fundamental understanding. Extensions of the current work to triblock copolymers, effect of solvent, conformational asymmetry of the charged and neutral blocks, and most important, the effect of concentration fluctuations on the microphase separation characteristics are some of the directions of future research.

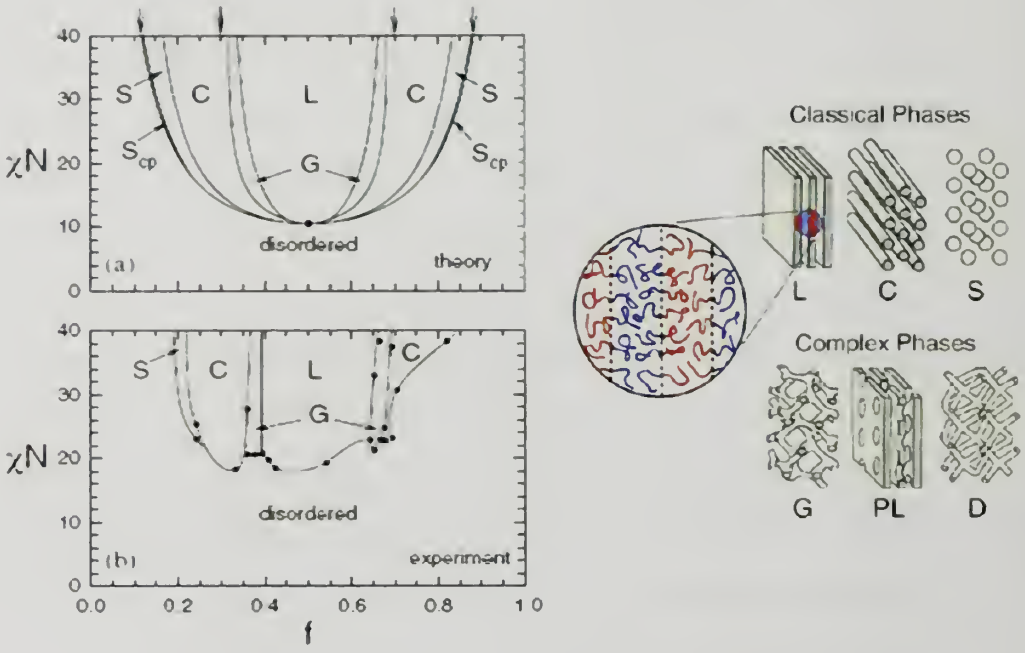

Figure 3.1. (a) Theoretical and (b) experimental equilibrium morphology diagrams calculated using SCFT and measured using polystyrene – polyisoprene (neutral-neutral) diblock copolymers. On the right, schematic illustrations of the domains occupied by the smaller minority blocks into the classical lamellar (L), cylindrical (C), spherical (S) phases, and the complex gyroid (G), perforated-lamellar (PL) and double-diamond (D) phases is shown. The expanded view of the L phase demonstrates the self-assembly of individual molecules within the morphology. In (a), the solid dot denotes the mean-field critical point and the vertical arrows indicate the L/C and C/S phase boundaries as predicted by strong segregation theory[30]. In (b), the solid dots denote the experimental data points, while the curves serve only as a guide to the eye. Figures are adapted from ref. [34].

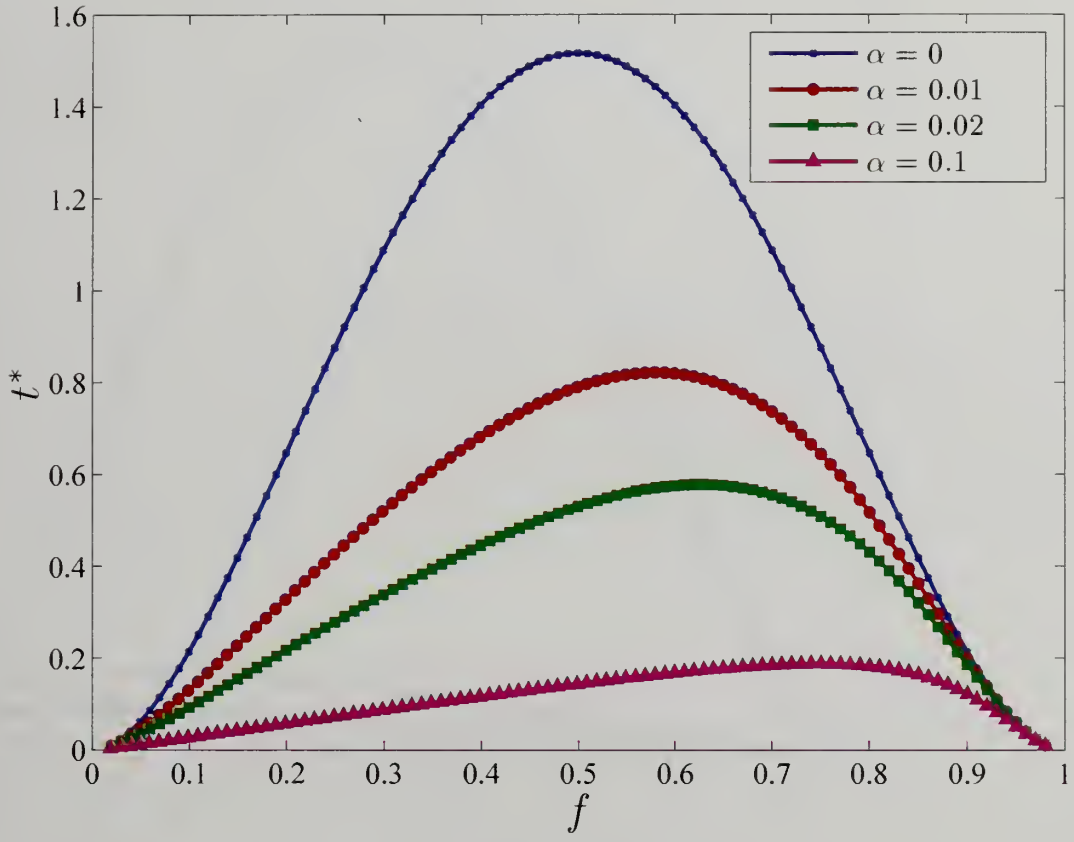

Figure 3.2. Effect of degree of ionization (α) on the stability limit for the disordered phase in polyelectrolytic diblock melt: plots correspond to $N = 1000$ and $\alpha = 0, 0.01, 0.02, 0.1$. Above t^*, disordered phase is stable and below t^*, it becomes unstable.

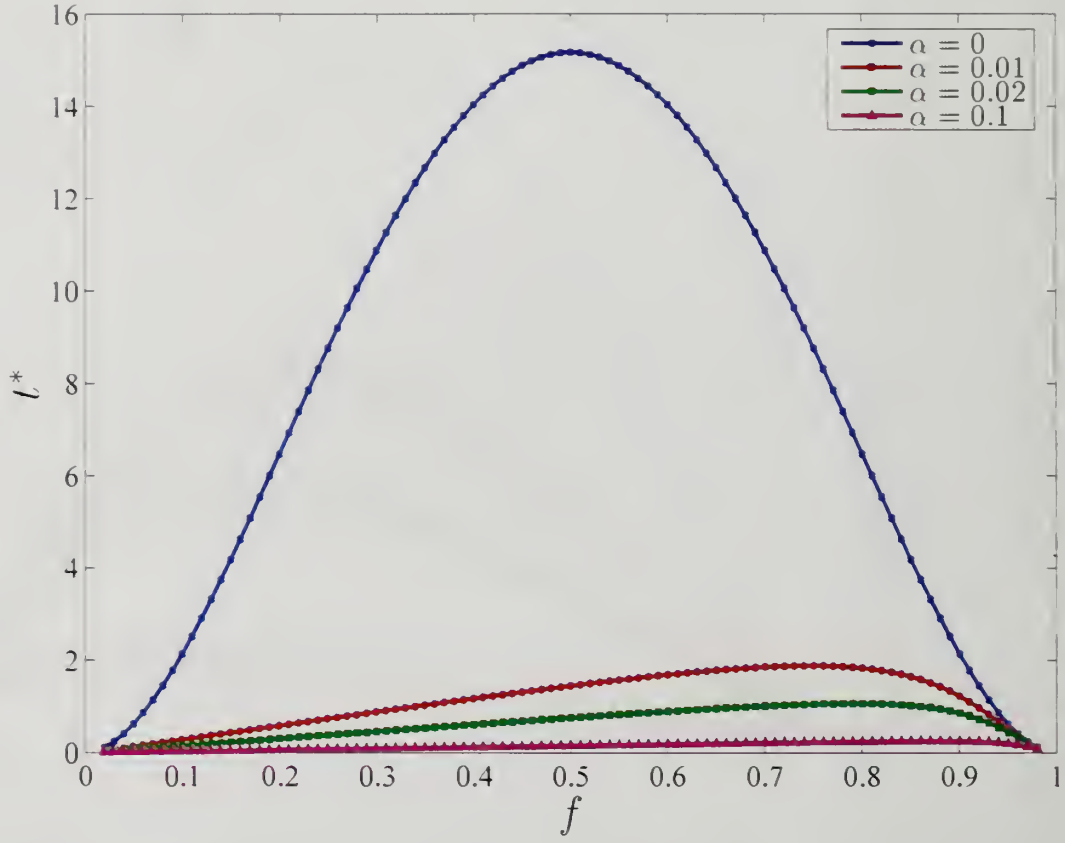

Figure 3.3. Effect of degree of ionization (α) on the stability limit of the disordered phase in polyelectrolytic diblock melt: plots correspond to $N = 10,000$ and $\alpha = 0, 0.01, 0.02, 0.1$.

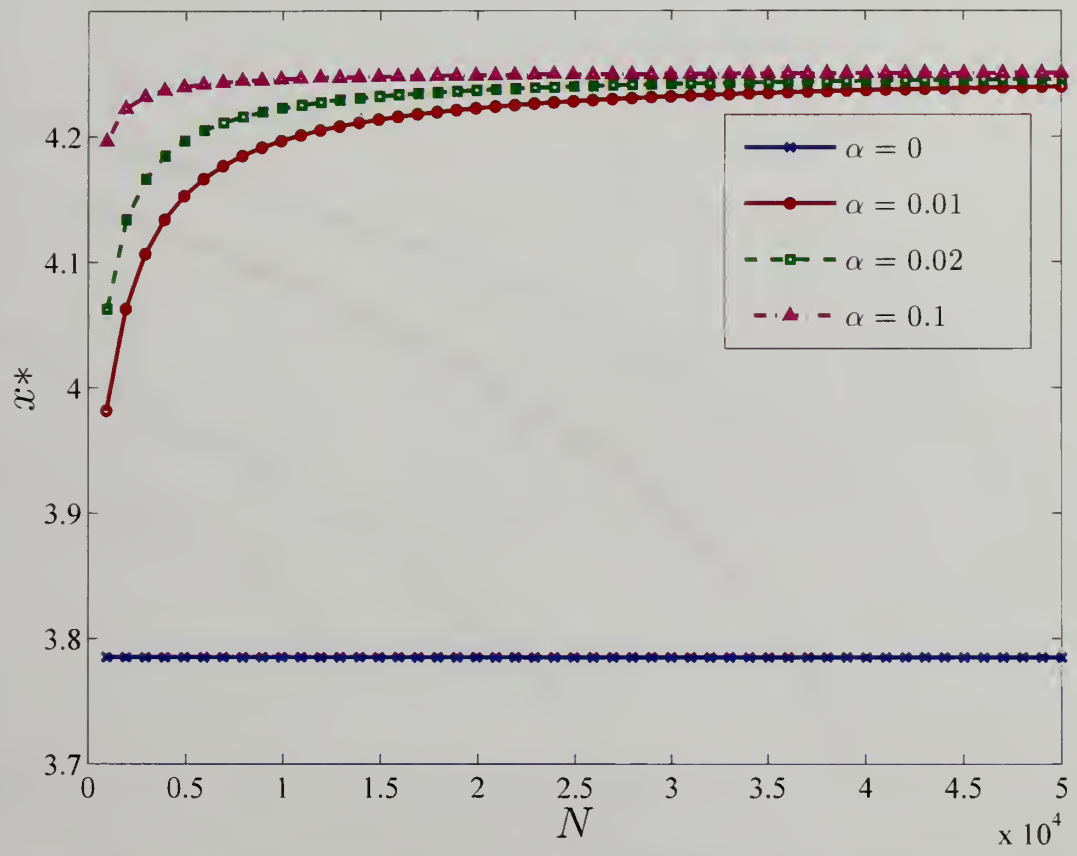

Figure 3.4. RPA Calculations - Effect of degree of polymerization (N) and degree of ionization (α) on critical parameter $x^\star$ for ($f = \frac{1}{2}$) in WSL : $\alpha = 0, 0.01, 0.02, 0.1$.

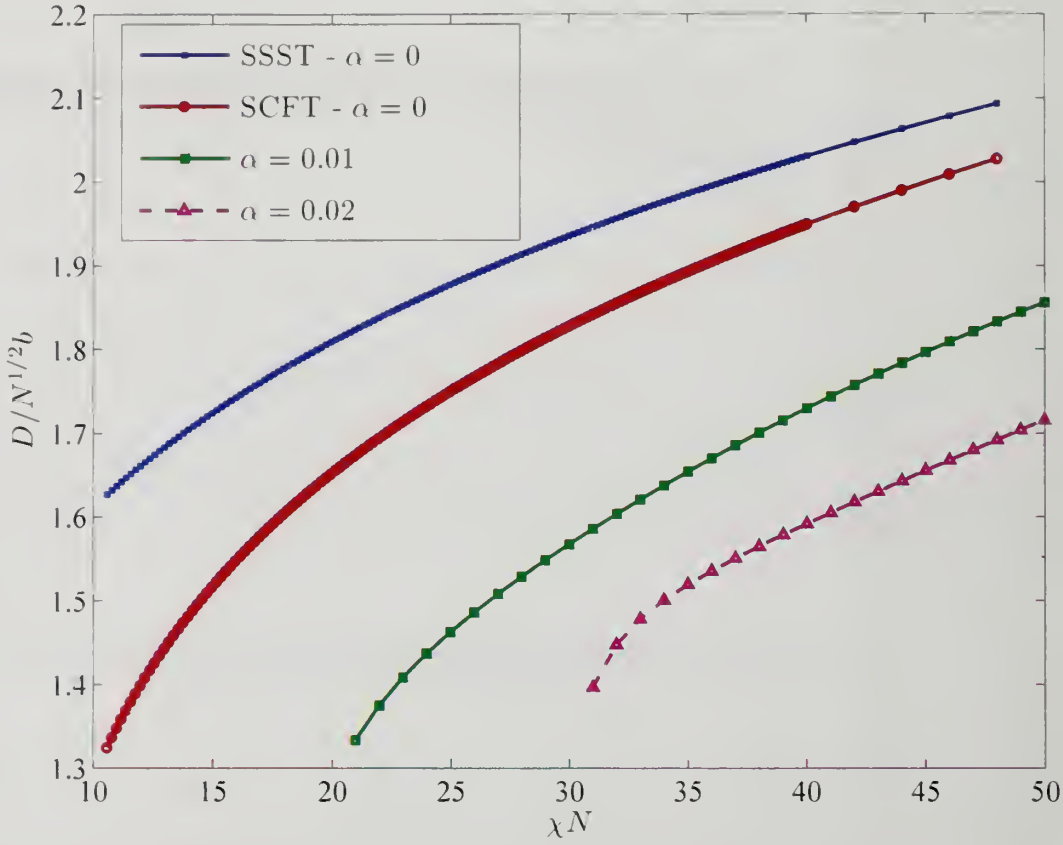

Figure 3.5. SCFT Calculations - Effect of degree of segregation on period of lamellae ($f = 1/2, N = 1000$). Semenov's Strong Segregation Theory (SSST)[30]-[34] which predicts $D/\left(N^{1/2}b\right) = 2\left(8\chi N/3\pi^4\right)^{1/6}$ is also drawn for comparison purposes.

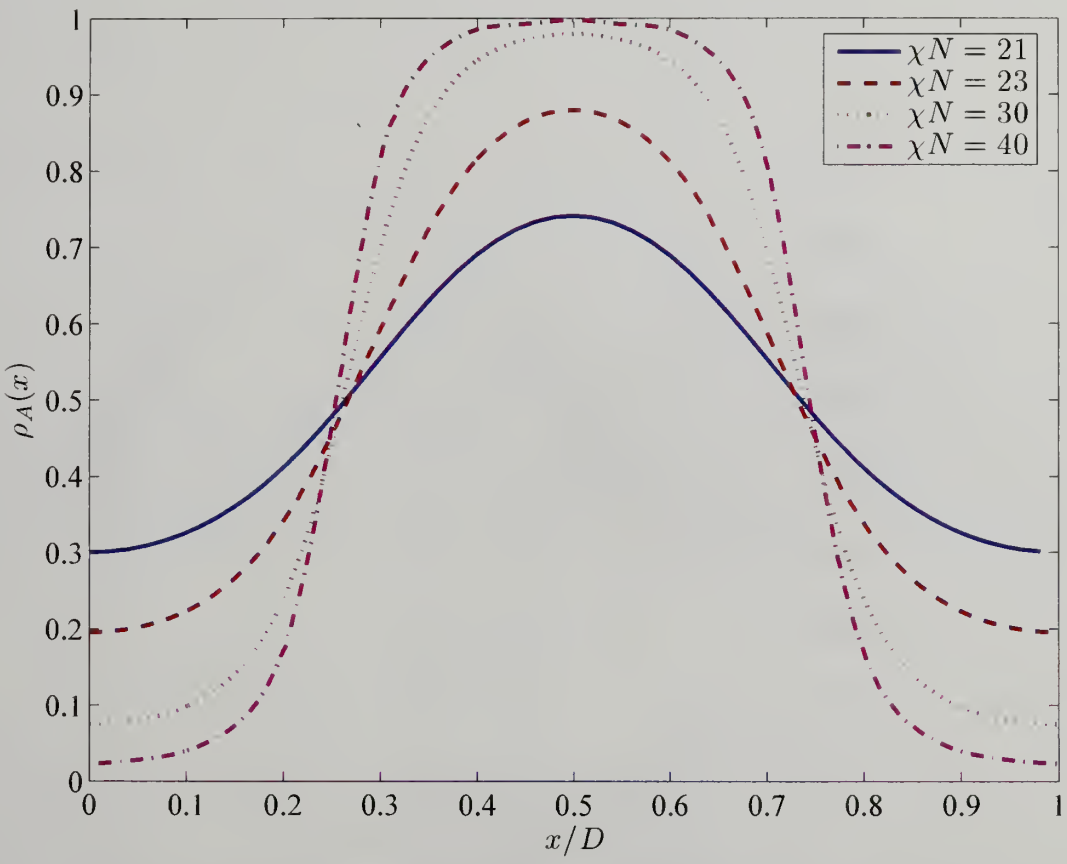

Figure 3.6. Polyelectrolytic block copolymer lamellae ($f = 1/2, \alpha = 0.01, N = 1000$) - monomer densities.

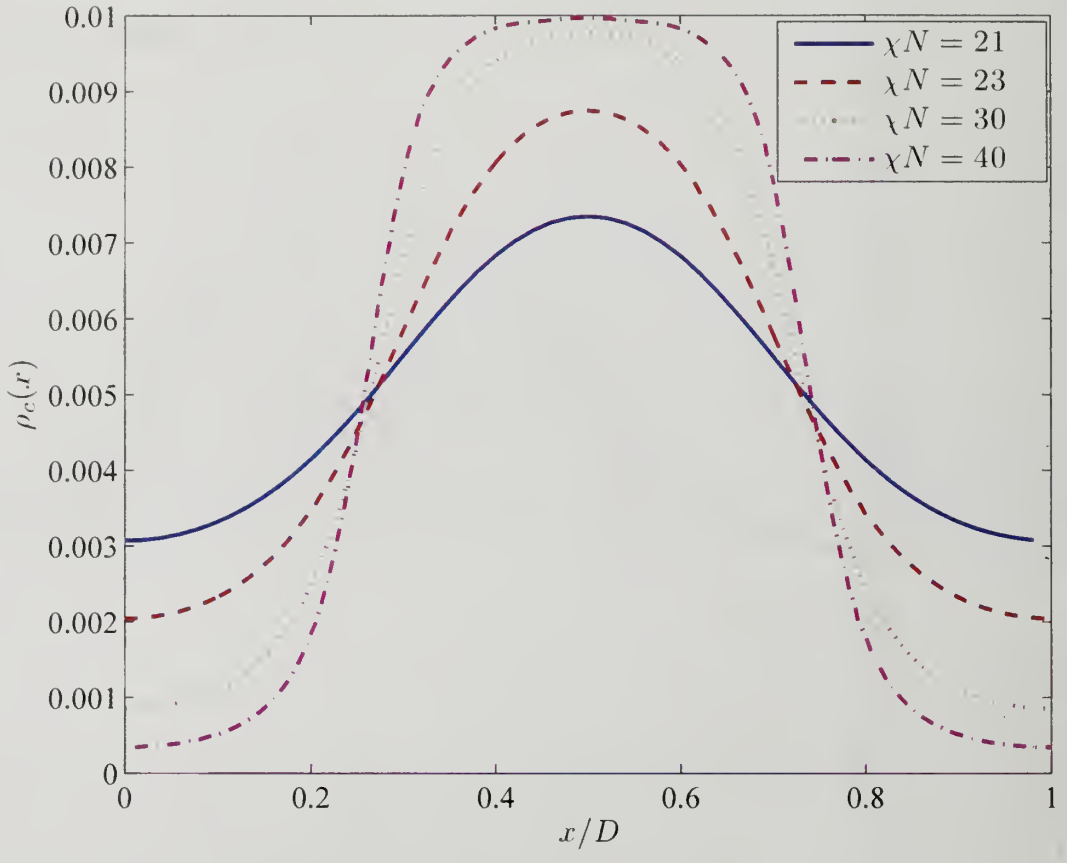

Figure 3.7. Counterion distribution in lamellar phase ($f = 1/2, \alpha = 0.01, N = 1000$).

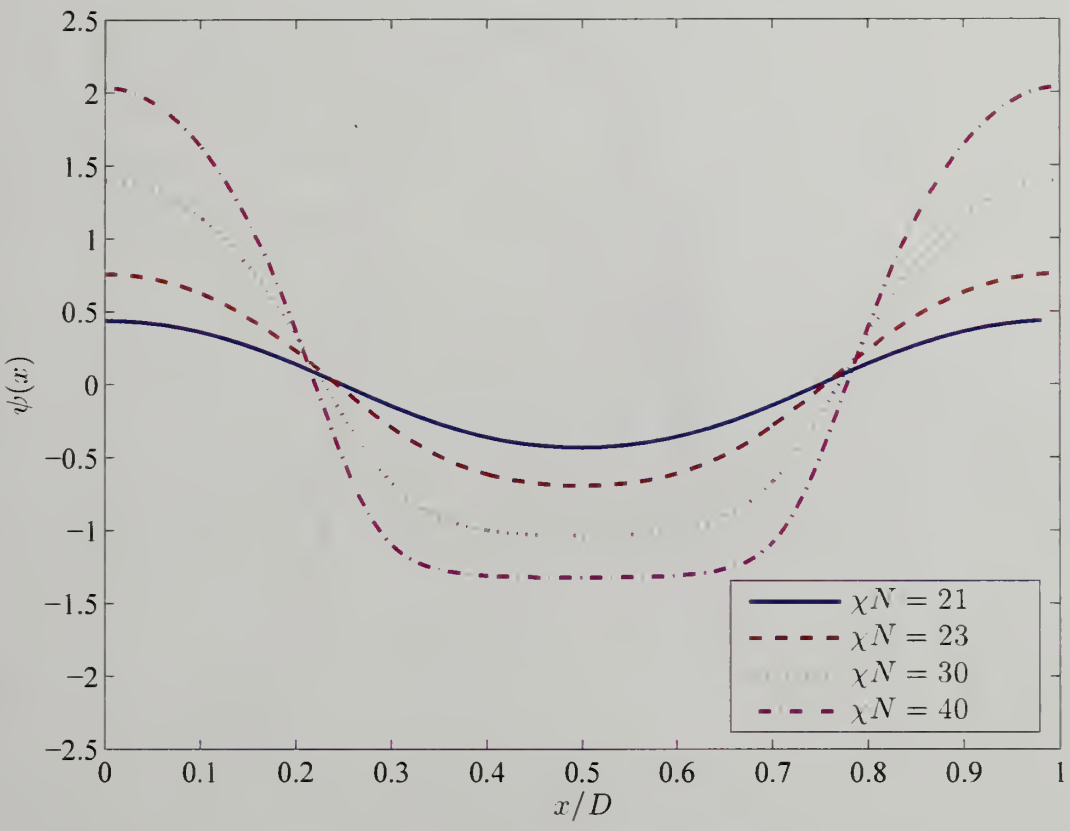

Figure 3.8. Electrostatic potential in lamellar phase ($f = 1/2, \alpha = 0.01, N = 1000$).

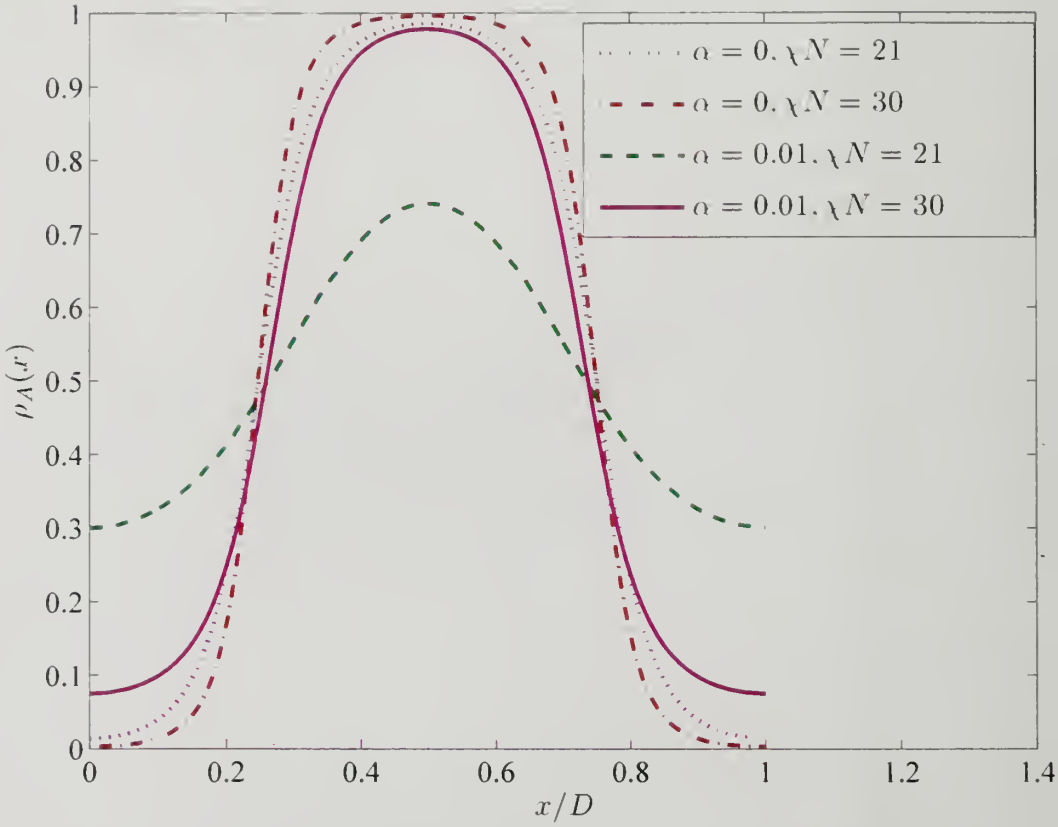

Figure 3.9. Reduction of effective chemical mismatch ($f = 1/2, N = 1000$) - comparison between monomer densities.

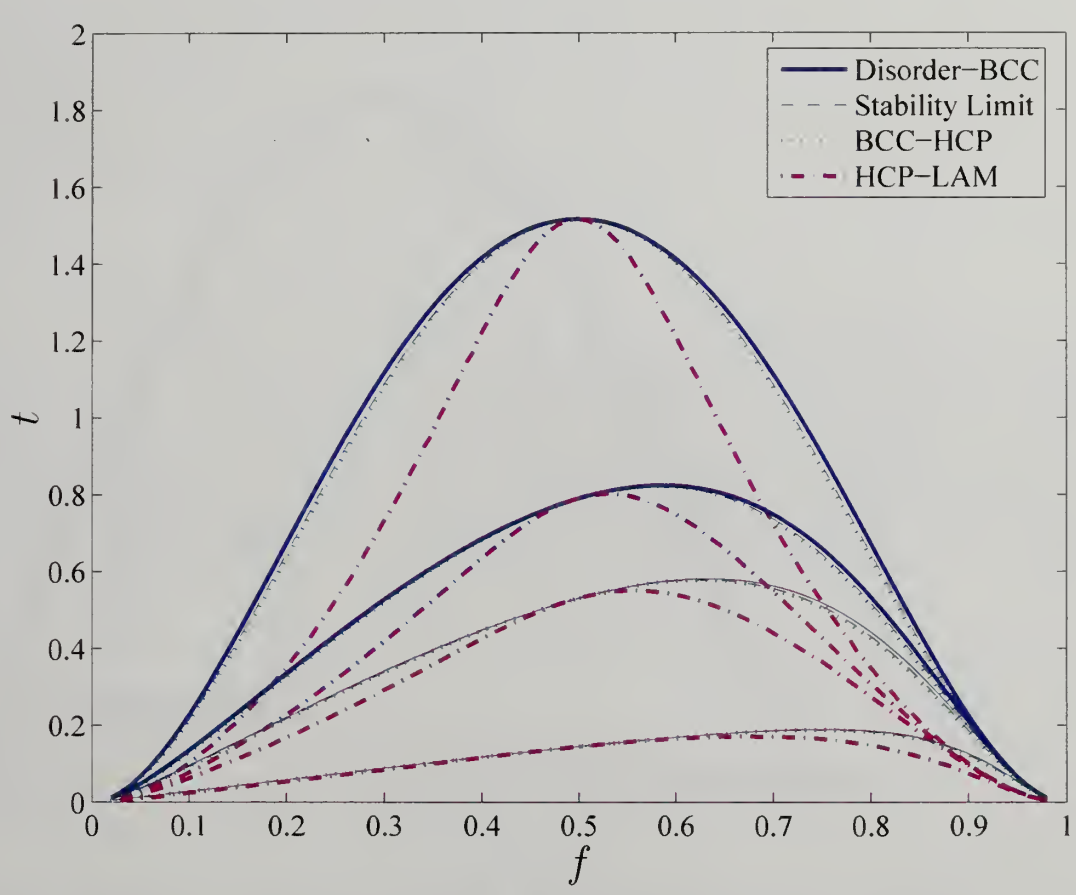

Figure 3.10. RPA Calculations - Morphology diagram for polyelectrolytic diblock copolymer: $N = 1000$ and $\alpha = 0$ for the topmost four boundaries, $\alpha = 0.01$ for the middle four, $\alpha = 0.02$ for the next set and $\alpha = 0.1$ for the lowermost four boundaries.

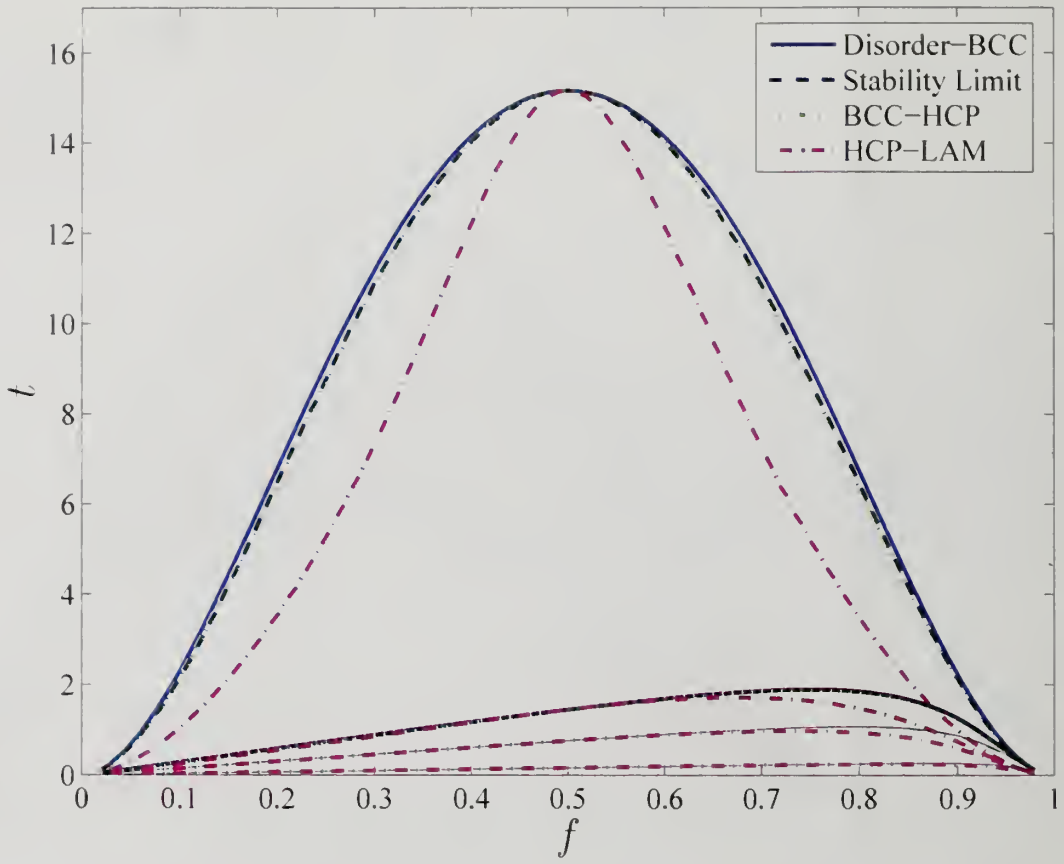

Figure 3.11. RPA Calculations - Morphology diagram for polyelectrolytic diblock copolymer: $N = 10,000$ and $\alpha = 0$ for the topmost four boundaries, $\alpha = 0.01$ for the middle four, $\alpha = 0.02$ for the next set and $\alpha = 0.1$ for the lowermost four boundaries.

CHAPTER 4

CONFINEMENT FREE ENERGY OF FLEXIBLE POLYELECTROLYTES IN SPHERICAL CAVITIES

4.1 Introduction

Polyelectrolytes are ubiquitous in nature and exhibit rich behavior. In the past, a great deal of theoretical[14, 15, 16, 21, 46, 50, 52, 53, 54, 55] and experimental efforts[22, 23, 25, 56, 57, 58] have been made in understanding their characteristics in solutions with concentrations ranging from dilute to concentrated. One of the remarkable discoveries in the last century is the theory of simple electrolytes made by Debye and Hückel[59], where electrostatic interactions get screened (colloquially referred to as the Debye screening). Similar phenomenon was shown to be present in the case of neutral polymers, where monomers interact by short range excluded volume interaction potential (known as Edward's screening[3]). In the case of polyelectrolytes, both kinds of screening effects are present and their coupling via the concept of double screening was introduced by Muthukumar[53], and the behavior of polyelectrolyte solutions was described in terms of these screening phenomena. As a result, different concentration regimes in polyelectrolyte solutions were predicted and verified experimentally[22, 23].

However, most of the computer and real-world experiments involve finite volume, where boundary effects play a significant role and can not be ignored. Recently, there has been a resurgence of interest in studying polymers within confined domains[6, 60, 61, 62, 63, 64, 65, 66, 67, 68, 69, 70]. Unlike neutral polymers, little is known about the physics of polyelectrolytes under confinement, a situation

realized in liposome-mediated delivery of macromolecules to the cells[60], translocation experiments involving RNA/DNA[61, 62], synthetic polyelectrolytes[63] etc. Underlying physics in these experiments is governed by the confinement effects on a *single* polyelectrolyte chain. Physically, confinement forces interaction among the monomers and the conformational entropy of the chain gets lowered due to less number of conformational states available to the chain. If small components like salt ions and solvent molecules are also present in addition to the polymer, then translational entropy of these components gets diminished, making confinement a thermodynamically unfavorable process. Quantitative estimates of these confinement effects are desirable. Recently, a quantitative description of the finite size corrections[71] to free energy for electrolytic systems has been presented. The analog of these calculations for polyelectrolyte systems has not been attempted yet and is one of the goals of this study.

In this study, we focus on a single polyelectrolyte chain confined in a neutral spherical cavity and use radial symmetry to obtain the mean field results. This theoretical model is pertinent in understanding many important physical processes. Few promising applications of this model are the computation of free energy barriers for the chain to move out of the confining space, osmotic pressure of polyelectrolytes, etc. To start with, we consider a situation where inner and outer dielectric constants of medium are different (say ϵ_i and ϵ_o, respectively). For this situation, the electrostatic potential is to be calculated using continuity of electrostatic potential and normal component of displacement vector at the boundary. It turns out that these boundary conditions are equivalent to a continuous dielectric medium (of dielectric constant ϵ_i everywhere) with charges confined within the boundary of sphere for the *radially symmetric globally electroneutral* system. In other words, dielectric mismatch effects disappear due to the use of radial symmetry. We must point out that radial symmetry is strictly valid only at the mean field level and fluctuations break this symmetry. In

the concentrated regime, we have been able to compute the fluctuation contributions without recourse to radial symmetry.

Unlike cylindrical[6] and rectangular[6, 64] confinements, a single self-avoiding chain in a spherical cavity has been shown to be a polymer solution problem[3, 65, 66, 67, 72, 73] with different degrees of confinements corresponding to different concentration regimes as seen in polymer solution theories. We are here interested in estimating different thermodynamic contributions to the free energy of confined polyelectrolytic system. Computing these contributions using simulations is a formidable task. However, self-consistent field theory (SCFT) presents a faster and an accurate way to address this problem. SCFT allows us to explore the role of confinement in free energy at the mean field level (also known as the saddle point approximation) and then capture the role of fluctuations by expanding free energy functional around the mean field solution (one-loop calculations). Unlike earlier studies on single neutral chain[68], we use "explicit solvent model", which captures solvent entropy in a more realistic way. At the mean field level, free energy for a self-avoiding chain under strong confinement (in vacuum) has been shown to be proportional to $w\bar{\rho}_p^2\Omega$, where w is a measure of the strength of excluded volume interactions, $\bar{\rho}_p$ is monomer density and Ω is the volume of the cavity. Remarkably, same proportionality is exhibited by polymer solution theories[3, 72] in the concentrated regime. However, at *low* polymer concentrations (i.e. dilute and semi-dilute regime), fluctuations around the saddle point solution become important and saddle point approximation breaks down. In that case, non-perturbative techniques have to be devised to compute the correct free energy. In this work, we explore the free energy in the concentrated regime, when radius of gyration of the chain is comparable to the radius of the cavity and mean field theory is still applicable.

Dividing the free energy into energetic and entropic parts using thermodynamic arguments, we have identified the role of individual components. Moreover, one

loop calculations provide insight about the corrections to the bulk expressions from fluctuation effects in the concentrated regime. For a globally neutral system with only small ions (i.e. without polyelectrolyte) inside a neutral cavity, local electroneutrality is the equilibrium state. In contrast, local electroneutrality is violated in the presence of a polyelectrolyte chain due to the depletion effects present in the system. We have studied the resulting monomer and charge density distribution for different sets of relevant parameters of the problem. To link with the experiments, we have computed the osmotic pressure and mean activity coefficient for monovalent salt.

This chapter is organized as follows: theory is presented in Sec. 4.2; calculated results and conclusions are presented in Sec. 4.3 and 4.4, respectively.

4.2 Theory

4.2.1 Self-consistent Field Theory

We consider a spherical cavity of radius R containing a single flexible polyelectrolyte chain of total N Kuhn segments, each with length b. The polyelectrolyte chain is represented as a continuous curve of length Nb and an arc length variable t is used to represent any segment along the backbone. We assume that there are n_c monovalent counterions (positively charged) released by the chain (and assuming that the chain is negatively charged for the sake of specificity). In addition, there are n_γ ions of species $\gamma\,(=+,-)$ coming from added salt (in volume $\Omega = 4\pi R^3/3$) so that the whole system is globally electroneutral. Let Z_j be the valency (with sign) of the charged species of type j. Moreover, we assume that there are n_s solvent molecules (satisfying the incompressibility constraint) present in the cavity and for simplicity, each solvent molecule occupies a volume (v_s) same as that of the monomer (i.e. $v_s \equiv b^3$). Subscripts $p, s, c, +$ and $-$ are used to represent monomer, solvent , counterion from polyelectrolyte, positive and negative salt ions, respectively. Degree

of ionization of the chain is taken to be α and we consider smeared charge distribution so that each of the segments carries a charge $e\alpha Z_p$, where e is the electronic charge.

Following the method described in section 2.2.2 in Chapter 2 (cf. Eq. 2.30)[9] to obtain saddle point equations (see Appendix D), the Poisson-Boltzmann equation for electric potential gets coupled to the well-known modified diffusion equation for chain connectivity. In particular, the saddle point equations are given by

$$\phi_p(\mathbf{r}) = \chi_{ps} b^3 \rho_s(\mathbf{r}) + \eta(\mathbf{r}) \tag{4.1}$$

$$\phi_s(\mathbf{r}) = \chi_{ps} b^3 \rho_p(\mathbf{r}) + \eta(\mathbf{r}) \tag{4.2}$$

$$\rho_p(\mathbf{r}) = \frac{1}{Q_p} \int_0^N dt\, q(\mathbf{r}, t) q(\mathbf{r}, N-t) \tag{4.3}$$

$$\rho_s(\mathbf{r}) = \frac{n_s}{Q_s} \exp\left[-\phi_s(\mathbf{r})\right] \tag{4.4}$$

$$\rho_p(\mathbf{r}) + \rho_s(\mathbf{r}) = \rho_0 \tag{4.5}$$

$$\rho_j(\mathbf{r}) = \frac{n_j}{Q_j} \exp\left[-Z_j \psi(\mathbf{r})\right] \quad \text{for} \quad j = c, +, - \tag{4.6}$$

$$\nabla^2_{\mathbf{r}} \psi(\mathbf{r}) = -4\pi l_B \left[\sum_{j=c,+,-} Z_j \rho_j(\mathbf{r}) + Z_p \alpha \rho_p(\mathbf{r}) \right]. \tag{4.7}$$

These equations are equivalent to those derived by Shi and Noolandi[44], and Wang[45] *et al.*, although the method of derivation is different as briefly outlined in Appendix D. In these equations, $\rho_\beta(\mathbf{r})$ and $\phi_\beta(\mathbf{r})$ are respectively the macroscopic number density and the field experienced by particles of type β, due to excluded volume interactions. All charged species experience electrostatic potential represented by $\psi(\mathbf{r})$ above. Note that $\psi(\mathbf{r})$ in above equations is dimensionless (in units of $k_B T/e$) and l_B depicts the Bjerrum length defined as $l_B = e^2/\epsilon k_B T$, where ϵ is the position independent effective dielectric constant of the medium (in units of $4\pi\epsilon_0, \epsilon_0$ being the permittivity of vacuum. Moreover, χ_{ps} is the dimensionless Flory's chi parameter and $\rho_0 = (N + n_s)/\Omega = 1/b^3$. Also, $\eta(\mathbf{r})$ is the well-known pressure field introduced to enforce the incompressibility constraint. The function $q(\mathbf{r}, t)$ is the probability of

finding segment t at location $\mathbf{r}$, when starting end of the chain can be anywhere in space, satisfying the modified diffusion equation[28]

$$\frac{\partial q(\mathbf{r},t)}{\partial t} = \left[\frac{b^2}{6}\nabla^2_{\mathbf{r}} - \{Z_p\alpha\psi(\mathbf{r}) + \phi_p(\mathbf{r})\}\right] q(\mathbf{r},t), \quad t \in (0,N). \tag{4.8}$$

Also, Q_β represents the partition function for the particle of type β in the field experienced by it, given by

$$Q_s = \int d\mathbf{r} \exp\left[-\phi_s(\mathbf{r})\right] \tag{4.9}$$

$$Q_p = \int d\mathbf{r} q(\mathbf{r},N) \tag{4.10}$$

$$Q_j = \int d\mathbf{r} \exp\left[-Z_j\psi(\mathbf{r})\right] \quad \text{for} \quad j = c,+,-. \tag{4.11}$$

Using the above equations, approximated free energy at the extremum (saddle point approximation) is given by

$$\frac{F^\star}{k_BT} = \frac{F_0}{k_BT} - \chi_{ps}b^3\int d\mathbf{r}\rho_p(\mathbf{r})\rho_s(\mathbf{r}) + \frac{1}{8\pi l_B}\int d\mathbf{r}\psi(\mathbf{r})\,\nabla^2_{\mathbf{r}}\,\psi(\mathbf{r}) - \ln Q_p + \sum_j n_j\left[\ln\frac{n_j}{Q_j} - 1\right] - \rho_0\int d\mathbf{r}\eta(\mathbf{r}), \tag{4.12}$$

where $j = s,c,+,-$ and $F_0/k_BT = \frac{\rho_0}{2}\left(Nw_{pp} + n_s w_{ss}\right)$ is the self-energy contribution arising from excluded volume interactions. Using thermodynamic arguments[74] and assuming dielectric constant (ϵ) to be independent of temperature (T), the free energy (Eq. (4.12)) is divided into enthalpic contributions due to excluded volume, electrostatic interactions and entropic part due to small ions, solvent molecules and the polyelectrolyte chain. Denoting these contributions by $E_w, E_e, S_{ions}, S_{solvent}$ and S_{poly}, respectively, the free energy is written as

$$\frac{F^\star - F_0}{k_BT} = \frac{E_w}{k_BT} + \frac{E_e}{k_BT} - \frac{T(S_{ions} + S_{solvent} + S_{poly})}{k_BT} \tag{4.13}$$

$$\frac{E_w}{k_BT} = \chi_{ps}b^3\int d\mathbf{r}\rho_p(\mathbf{r})\rho_s(\mathbf{r}) + \rho_0\int d\mathbf{r}\eta(\mathbf{r}) \tag{4.14}$$

$$\frac{E_e}{k_BT} = \frac{1}{2}\int d\mathbf{r}\,\psi(\mathbf{r})\left(\sum_{j=c,+,-} Z_j\rho_j(\mathbf{r}) + Z_p\alpha\rho_p(\mathbf{r})\right) \tag{4.15}$$

$$\begin{aligned} -\frac{TS_{ions}}{k_BT} &= -\sum_{j=c,+,-}\left[n_j\ln Q_j + \int d\mathbf{r}\, Z_j\rho_j(\mathbf{r})\psi(\mathbf{r})\right] + \sum_{j=c,+,-} n_j\left[\ln n_j - 1\right] \\ &= \sum_{j=c,+,-}\int d\mathbf{r}\,\rho_j(\mathbf{r})\left\{\ln\left[\rho_j(\mathbf{r})\right] - 1\right\} \end{aligned} \tag{4.16}$$

$$\begin{aligned} -\frac{TS_{solvent}}{k_BT} &= -\left[n_s\ln Q_s + \int d\mathbf{r}\,\rho_s(\mathbf{r})\phi_s(\mathbf{r})\right] + n_s\left[\ln n_s - 1\right] \\ &= \int d\mathbf{r}\,\rho_s(\mathbf{r})\left\{\ln\left[\rho_s(\mathbf{r})\right] - 1\right\} \end{aligned} \tag{4.17}$$

$$-\frac{TS_{poly}}{k_BT} = -\ln Q_p - \int d\mathbf{r}\,\left[\left\{Z_p\alpha\psi(\mathbf{r}) + \phi_p(\mathbf{r})\right\}\rho_p(\mathbf{r}) + \rho_0\eta(\mathbf{r})\right]. \tag{4.18}$$

So far, we have presented a general field theoretical treatment for a single polyelectrolyte chain and haven't considered confinement. We study the role of confinement by solving Eqs. (4.1- 4.7) under a particular set of boundary conditions and constraints, which are presented in the next section. Also, the limits of volume integral in Eqs. (4.13- 4.18) vary over the volume of confining spherical cavity.

4.2.2 Boundary Conditions and Constraints

The above treatment leads to coupling of non-linear Poisson-Boltzmann equation with modified diffusion equation. Both of these equations are second order differential equations and hence, two conditions are required for each, in order to obtain a unique solution. In addition, for t dependent diffusion equation, an initial condition is needed to start the computations. To solve these equations, we exploit the assumed spherical symmetry of the system so that $q(\mathbf{r},t) \rightarrow q(r,t)$, where $r = |\mathbf{r}|$ and the Laplacian is given by

$$\nabla^2_{\mathbf{r}} = \frac{1}{r^2}\frac{\partial}{\partial r}\left(r^2\frac{\partial}{\partial r}\right) \tag{4.19}$$

Due to symmetry of the system, additional requirements need to be fulfilled by the solution. Here, we summarize all these conditions:

$$\text{Boundary Conditions :} \quad \frac{\partial \psi(r)}{\partial r} \mid_{r=R} = 0, q(R,t) = 0 \quad \text{for all } t \tag{4.20}$$

$$\text{Initial Conditions :} \quad q(r,0) = 1 \quad \text{for all } r \neq R \tag{4.21}$$

$$\text{Symmetry Conditions:} \quad \frac{\partial \psi(r)}{\partial r} \mid_{r=0} = \frac{\partial q(r,t)}{\partial r} \mid_{r=0} = 0 \quad \text{for all } t \tag{4.22}$$

Boundary and initial conditions for $q(r,t)$ correspond to the facts that (a) segments are excluded from boundary so probability of finding any segment at the boundary is zero and (b) the ends can be anywhere inside sphere. Symmetry condition for $q(r,t)$ is invoked because we are looking for a symmetrical solution of monomer density about the center without any discontinuity. Boundary condition and symmetry conditions for electrostatic potential are obtained by using the Gauss law at the boundary and the fact that net force experienced by an ion at the center of the sphere must be zero.

Along with the above initial and boundary conditions, solution of SCF equations need to be obtained under additional constraints due to the fixed number of monomers (N), ions (n_j) and global electroneutrality so that

$$Z_p \alpha N + Z_c n_c = 0, \quad Z_+ n_+ = -Z_- n_- = 0.6023\, c_s \Omega, \tag{4.23}$$

where c_s is salt concentration in moles per liter (molarity) and Ω is in units of nm^3.

In this work, we are interested in studying confinement effects on a single flexible polyelectrolyte chain. That's why we have chosen a non-adsorbing neutral spherical cavity. In studies focussing at the adsorption on to *charged* impermeable/permeable surfaces, electrostatic boundary conditions have to be changed. The boundary conditions for the electrostatic potential can be written by relating the discontinuity of the normal component of the displacement vector to the surface charge density. In case,

the short range interactions coming from hard surfaces are also under investigation. the boundary condition for the function $q(r,t)$ has to be modified too. A popular boundary condition[6] for studying the effect of short range interactions is to use the condition

$$\frac{\partial \ln q(r,t)}{\partial r} \mid_{r=R} \;=\; -\frac{1}{c}, \tag{4.24}$$

where c is the parameter, which characterizes the attractive or repulsive nature of the hard surface.

4.2.3 Numerical Technique

We have solved SCF equations (Eqs. (4.1 - 4.8)) in real space using an explicit finite difference scheme for Poisson-Boltzmann-like equation (Eq. (4.7)) and the standard Crank-Nicolson[75] scheme for solving modified diffusion equation (Eq. (4.8)). Due to the use of properly normalized equations for densities, all the constraints mentioned earlier are always satisfied during the computation.

As the solution of SCF equations is invariant when an arbitrary constant is added to the fields, so this constant needs to be fixed in order to obtain a unique solution. Choice of fixing this constant depends on the numerical scheme used in solving the SCF equations. We simply choose $\psi(R) = 0$ and $\int d\mathbf{r}\eta(\mathbf{r}) = 0$. We must point out that any method of fixing this constant does not affect the densities but the free energy gets changed by a constant.

To realize the constraint $\int d\mathbf{r}\eta(\mathbf{r}) = 0$, $\frac{1}{\Omega}\int d\mathbf{r}\eta(\mathbf{r})$ is subtracted from the computed $\eta(\mathbf{r})$ at each iteration. This procedure leads to $\int d\mathbf{r}\eta(\mathbf{r}) = 0$ in the final solution. Also, all the integrals are evaluated by the standard Trapezoidal[75] rule and Broyden's method[75] is used to solve the set of non-linear equations.

4.2.4 Reference System

The choice of a reference system in free energy calculations depends on the physical quantity of interest. One of our goals in this study is to investigate the role of the polyelectrolyte chain in the free energy of the system. To study the role of the chain, the spherical cavity without any polymer (with small ions and solvent inside) is the appropriate choice.

In the absence of the chain, free energy becomes

$$\frac{F\{\bar{\rho}_p = 0\} - F_0\{N = 0\}}{k_B T} = \sum_{j=+,-,s} n_j \left[\ln \frac{n_j}{\Omega} - 1\right]. \tag{4.25}$$

Note that in the absence of the chain, $n_s b^3 = \Omega$, due to the incompressibility condition.

4.2.5 Osmotic Pressure: Contact Value Theorem

Although we have computed the free energy of a confined chain, it is worthwhile to compute a physical observable, which is readily measurable experimentally. So, we have computed the osmotic pressure of a confined chain by carrying out the variation of free energy (Eq. (4.12)) with respect to the number of solvent molecules, but keeping the number of monomers and salt ions fixed (and taking care of the fact that volume has to be changed to alter the number of solvent molecules for the incompressible system under investigation here). The osmotic pressure is given by[73]

$$\frac{\Pi b^3}{k_B T} = -\left[\frac{\delta}{\delta n_s}\left(\frac{F - F_0}{k_B T}\right)_{N,n_j} - \frac{\delta}{\delta n_s}\left(\frac{F - F_0}{k_B T}\right)_{N,n_j=0}\right]. \tag{4.26}$$

where $j = c, +, -$. Within the saddle point approximation, $F = F^\star$ and $(F^\star - F_0)/k_B T = -n_s$ for pure solvent (i.e. when $N, n_j = 0$). Using the above formula, osmotic pressure comes out to be (within radial symmetry)

$$\frac{\Pi^\star}{k_BT} = \sum_{j=c,+,-} \rho_j(R^-) - \rho_p(R^-) - \ln \rho_s(R^-) + \frac{q(R^-,N)}{\int d\mathbf{r}\, q(\mathbf{r},N)} - \chi_{ps} b^3 \rho_p^2(R^-) + \rho_e(R^-)\psi(R^-), \tag{4.27}$$

where $\rho_e(R^-)$ is the total charge density (in units of electronic charge) at a point close to the surface of the cavity and $\star$ in the superscript depicts the fact that saddle point approximation for the free energy has been used in deriving the result. Due to the coarse grained model used in studying the single chain, information at a length scale below Kuhn's segment length is not correctly captured by the model. So. R^- represents the point, which is at a distance of one Kuhn segment length from the surface. This point is well-discussed in the literature[76, 77] and will not be pursued further.

If we were to imagine a system, where densities and fields are constant (as in the concentrated bulk system), then the above expression simplifies to the well-known[3] expression for the osmotic pressure of a homogeneous system (represented by $\Pi_h^\star$)

$$\frac{\Pi_h^\star}{k_BT} = \sum_{j=c,+,-} \frac{n_j}{\Omega} - \frac{\bar{\rho}_p}{b^3} - \ln \frac{1-\bar{\rho}_p}{b^3} + \frac{\bar{\rho}_p}{Nb^3} - \frac{\lambda_{ps}}{b^3}\bar{\rho}_p^2, \tag{4.28}$$

where $\bar{\rho}_p = Nb^3/\Omega$. In the literature[77], osmotic pressure for fluids near surfaces is given by the fluid densities near surfaces (the so called "contact value theorem") and Eq. (4.27) is nothing but the analog of the "contact value theorem" for the inhomogeneous system *with interactions*.

4.2.6 Mean Activity Coefficient

Using the saddle point approximation for the free energy, we have computed the electrostatic chemical potential of small ions. Carrying out the variation of free energy

(Eq. (4.12)) with respect to number of small ions, the mean field estimate for the electrostatic chemical potential[59] of small ions comes out to be

$$\mu_j^{el} = \frac{\delta}{\delta n_j}\left(\frac{F-F_0}{k_BT}\right)_{N,V,n_{m\neq j}} = \ln\left[\frac{n_j}{\int d\mathbf{r}\exp\left(-Z_j\psi(\mathbf{r})\right)}\right] \tag{4.29}$$

for $j = c, +, -$. This is a straightforward generalization of the electrostatic chemical potential for homogeneous system to an inhomogeneous one. Using these expressions, chemical potential for the salt $A_{\nu_+}B_{\nu}$ (so that $\nu_+ = \nu_- = 1$ for the monovalent salt) can be written as

$$\mu_{salt} = \nu_+\mu_+^{el} + \nu_-\mu_-^{el}. \tag{4.30}$$

However, individual activity coefficients or the chemical potential can not be measured experimentally. So, we construct the mean activity coefficient ($\gamma_\pm$) for the binary salt[59] defined by

$$\mu_{salt} = \ln\left[\left(\frac{n_+}{\Omega}\right)^{\nu_+}\left(\frac{n_-}{\Omega}\right)^{\nu_-}\gamma_\pm^{\nu}\right], \tag{4.31}$$

where $\nu = \nu_+ + \nu_-$. Using Eq. (4.30) and (4.31), mean activity coefficient is given by

$$\gamma_\pm^{\nu} = \left[\frac{\Omega}{\int d\mathbf{r}\exp\left(-Z_+\psi(\mathbf{r})\right)}\right]^{\nu_+}\left[\frac{\Omega}{\int d\mathbf{r}\exp\left(-Z_-\psi(\mathbf{r})\right)}\right]^{\nu_-}. \tag{4.32}$$

Using Schwarz's inequality[78], it can be shown that the mean activity coefficient is always less than or equal to unity. For the spherical cavity with pure solvent and monovalent salt ions, potential is essentially constant everywhere (local electroneutrality) and that leads to mean activity coefficient being unity. Note that the Eq.

(4.32) can also be derived by considering a Donnan equilibrium between the interior containing polyelectrolyte chain and the exterior containing salt ions with salt concentration c_s.

4.3 Results

Having presented the field theoretical treatment of a single flexible chain in the presence of solvent, we present the results obtained after solving SCFT equations for a negatively charged chain ($Z_p = -1$) with monovalent salt. In this study, we have taken all small ions (counterions and co-ions) to be point charges and while calculating counterion density profiles, we have added contributions coming from the counterions released by the polyelectrolyte chain and the salt. Also, it should be noticed that due to the point nature of these charges, counterions and co-ions are not excluded from the confining boundary, which can be done, in principle, by the introduction of an arbitrary wall potential[79]. Here, we simply assume that the *depletion layer*[8] for counterions and co-ions is very small as compared to the monomer due to an order of difference in their sizes and its negligible effects on the system properties.

All the results reported in this work have been obtained with a grid spacing of $\Delta r = 0.1$ and chain contour discretization of $\Delta t = 0.01$ after putting $b = 1$ nm.

4.3.1 Monomer and Charge Distribution

To study the effect of confinement, we have varied degree of polymerization (N) keeping all other parameters fixed. Increase in N with fixed R leads to a more confined environment with the increase in monomer density everywhere inside the cavity. This can be seen in Fig. 4.1, where we have plotted monomer densities for a single polyelectrolyte chain for different values of N after choosing a particular set of parameters ($\chi_{ps} = 0.45, \alpha = 0.1, l_B/b = 0.7, R/b = 5, c_s = 0.1M$). These values for the parameters were chosen to mimic a salty flexible polyelectrolyte chain under

spherical confinement in the presence of water as a solvent. Also, for comparison purposes, we have plotted monomer densities for the corresponding neutral chains in an athermal solvent ($\chi_{ps} = 0$) and in an equivalent solvent condition ($\chi_{ps} = 0.45$). Comparing the monomer density for the neutral chain in athermal solvent with a poorer solvent, it is clear that the exclusion of solvent molecules from the core of the coil is stronger as the solvent quality is decreased, as expected. Now, when the polymer in the less good solvent is charged, the solvent exclusion effect is slightly weaker. This difference becomes negligible as the monomer volume fraction increases. Moreover, monomer density profiles for neutral and the polyelectrolyte chain in the same solvent are almost identical, which corroborates the coil conformation of the polyelectrolyte.

We have also varied R by keeping the number of salt ions and a fixed, and the results obtained for radial densities are shown in Fig. 4.2 for a particular value of N (number of salt-ions corresponds to $c_s = 0.1M$ for $R/b = 5$). The observed difference in small ion density profiles for different R's is attributed to the fact that total salt concentration (c_s) is changing when R is being changed with the number of small ions kept fixed during this variation. In this figure, we have chosen $N = 100$ and the rest of the parameters are the same as in Fig. 4.1 for the polyelectrolyte chain. From Fig. 4.2, it is evident that due to exclusion of the monomers from confining sphere surface, decrease in R leads to an increase in concentration of monomers in the interior. Had it been a bulk situation ($R \to \infty$), small ion densities would have reached their bulk value (c_s). Looking at small ions' densities in Fig. 4.2, it is clear that for the confined spherical system, this common presumed result is no more valid and small ion density profiles haven't reached their bulk value. In other words, net radial charge density is no more zero near the confining boundary (as shown in Fig. 4.3) and a double layer system[80] is set up as a result of depletion of the chain from the surface.

In this study, small ions are treated as point charges and hence, are not excluded from the surface of the spherical cavity in contrast to the monomer. As a result, when N is increased keeping α fixed at stronger confinements (in terms of higher monomer densities), there are more counterions (positively charged) generated by the chain and hence, charge density near the surface of the cavity increases (Fig. 4.3). On the other hand, near the center of the cavity, the local charge density curves move toward zero as N is increased (i.e. interior of the cavity is becoming locally electroneutral). For lower degrees of confinements (i.e. low $\bar{\rho}_p$), increase in N leads to increase in charge density everywhere due to more number of ions in the system. However, this behavior is seen over a very small density regime.

We have also varied other parameters (c_s, α and l_B). Effects of all these parameters on monomer densities are consistent with the observation that a polyelectrolyte[53] chain at high salt concentration is equivalent to a neutral chain with an effective excluded volume parameter given by

$$w_{eff} = \frac{1}{1-\bar{\rho}_p} - 2\chi_{ps} + \frac{4\pi l_B \alpha^2 Z_p^2}{\kappa^2}. \tag{4.33}$$

So, the polyelectrolyte chain shows higher expansion[81] as compared to its neutral analog[82].

On the other hand, at low salt concentrations, the chain can tend to attain a rod-like conformation due to dominance of electrostatic repulsions along the backbone and spherical symmetry is broken. In our mean field study, we use spherical symmetry and Gaussian model for the polyelectrolyte chain. Due to these limitations, spherical symmetry breaks down in the extremely low salt regime and we are not allowed to explore the low salt regime using the current model.

These results show that confinement of the chain leads to the development of a charge density wave inside the cavity and an outcome of this charge density wave is

that there is a potential difference across the center of the cavity and the surface. It is to be noted that for a confined system with only small ions inside, potential is constant everywhere and local electroneutrality is the equilibrium state (trivial solution of SCF equations). However, it is the depletion of the chain from the cavity surface, which leads to the accumulation of charges near the surface and as a result inhomogeneous charge distribution is attained. To study the role of polyelectrolyte in the free energy, we compare the free energies of the inhomogeneous phase with the cavity containing pure solvent and salt-ions in the next section.

4.3.2 Free Energy within Saddle Point Approximation

In Fig. 4.4, we have plotted different contributions to free energy for a salty system using Eqs. (4.13 - 4.17). Analyzing the contributions to free energy, it is clear that the free energy has four major contributions. At lower polymer volume fractions, free energy is dominated by entropy of small ions ($-TS_{ions}/k_BT$) and solvent ($-TS_{solvent}/k_BT$). As volume fraction is increased, chain conformational entropy and polymer-solvent interaction energy also become important. Also, electrostatic energy part in free energy is small compared to other terms, stressing a minor role played by electrostatic energy in the crowded environment under investigation here. Share of each contribution to the free energy depends on the degree of confinement. For instance, when degree of confinement is extremely high ($Nb^3/\Omega \rightarrow 1$), solvent entropy and polymer-solvent interaction energy terms are negligible and free energy has two major contributions - small ion entropy and chain conformational entropy. Strictly speaking, our theoretical model breaks down as soon as monomer density inside the cavity is close to unity because the finite size of small ions and nature of interactions between the various species become important. All these effects can not be captured with our theory, which involves only two body interaction potential.

A few comments about the shape of the plots in Fig. 4.4 are due here. Shape of small ions entropy term is governed by number of small ions term ($\sum_j \int d\mathbf{r}\rho_j(\mathbf{r})$ in Eq. (4.16)) and when N is increased keeping degree of ionization (α) and R fixed, number of counterions increases and hence, $-TS_{ions}/k_BT$ decreases with increase in N (almost linearly). Similarly, when N is increased while keeping R fixed, total number of solvent molecules in the cavity decreases (due to incompressibility) and hence, $-TS_{solvent}/k_BT$ increases. Increase in N for a fixed R/b leads to lower number of conformations available to the chain and hence, entropy of the chain decreases or $-TS_{poly}/k_BT$ increases. Shape of excluded volume interaction energy and electrostatic interaction energy can be understood by the fact that in the asymptotic limit with respect to degree of confinement, the product of densities (monomer and solvent) as well as the electric potential are small.

In implicit solvent computations[68], free energy goes linearly with N^2/Ω. In order to see whether the same linear law is followed by free energy in explicit solvent model, we have plotted free energy as a function of N^2/Ω for different values of R/b in Fig. 4.5. It is found that free energy follows the linear law only for lower values of $\bar{\rho}_p$. For higher $\bar{\rho}_p$, there are deviations from this linear law due to the conformational entropy of the chain. Overall, the shape of the free energy curve is of the form $\sum_{j=c,+,-,s} n_j \left[\ln(n_j/\Omega) - 1\right]$ for lower $\bar{\rho}_p$ and systematic deviations are seen for higher $\bar{\rho}_p$.

Also, to highlight the role of the polyelectrolyte in the free energy of confinement, we have plotted the *difference* between the free energy of the spherical cavity with and without chain (i.e. $\Delta F^\star = F^\star - F\{\bar{\rho}_p = 0\}$) for different radii of the confining cavity and monomer densities in Fig. 4.6. In these computations, it has been assumed that $w_{pp} = w_{ss}$ to get rid of an uninteresting constant. The results reveal that the confinement of the chain is a thermodynamically unfavorable process and for the same density, larger value of $\Delta F^\star$ for larger spherical cavity can be attributed to

the difference in conformational entropy and polymer-solvent interaction energy for chains of different lengths in spheres of different radii.

In scaling theories[6], it is commonly asserted that the confinement free energy is extensive in N. In order to confirm this assertion, we have plotted $(F^* - F_0)/Nk_BT$ for various values of monomer densities at different values of R (see Fig. 4.7). Our results clearly show that the free energy under spherical confinement is not extensive in N, in contrast to the rectangular and cylindrical confinements[6].

4.3.3 Osmotic Pressure and Mean Activity Coefficient

In Fig. 4.8, we have plotted the osmotic pressure obtained from Eq. (4.27) as a function of monomer density. For comparison purposes, we have also plotted the osmotic pressure of the homogeneous phase (Eq. (4.28)). It is found that the osmotic pressure is the same for the homogeneous and the inhomogeneous phase at lower monomer densities and ideal gas law for osmotic pressure is obtained in this regime. However, at higher densities, deviations from ideal gas law are seen and these deviations are larger for the inhomogeneous phase in comparison with the homogeneous phase. Comparing each term in Eqs. (4.27) and (4.28), it is found that the discrepancy between the inhomogeneous and homogeneous phase arises as a result of the depletion of the chain from the spherical surface. Due to the depletion, the monomer density at one Kuhn step away from the surface is higher for the inhomogeneous system in comparison with the homogenous system. Moreover, the log term involving solvent density and quadratic excluded volume interaction term involving the chi parameter add to the discrepancy. Other than these terms, electrostatic and small ions terms do not change much. Effect of the cavity radius on the osmotic pressure profiles can be easily explained using Eq. (4.28) and the fact that number densities of salt ions is higher for smaller cavity, when number of ions is kept fixed during the computation.

In the absence of the polyelectrolyte, the local electroneutrality is the equilibrium state for the small ions. That means the mean activity coefficient for the salt is unity. However, due to the depletion of the chain from the surface, local electroneutrality gets broken and that leads to a deviation from unity. In Fig. 4.9, we have plotted the mean activity coefficient for the monovalent salt and it is clear that the presence of the polyelectrolyte chain leads to deviation from ideal behavior (local electroneutrality). The shape of the activity coefficient curves can be understood by the fact that local electroneutrality is attained for very large densities also, where number of small ions is large and almost uniformly distributed. Effect of R on these plots can be explained by the fact that the extent of inhomogeneity in electrostatic potential increases with an increase in R.

4.3.4 One-loop Fluctuation Corrections : Narrow Depletion Zone Approximation

The saddle point approximation used in computing free energy (Eq. (4.12)) is valid when the number densities of small molecules and monomers is high (i.e. concentrated regime). In order to capture the role of fluctuations in the concentrated regime, we have expanded the integrand of functional integrals over fields around the saddle point solution up to quadratic terms in fields (Appendix E) so that the functional integrals to be carried out are Gaussian (one-loop calculations). For low concentrations (dilute and semi-dilute regimes), this treatment breaks down and other techniques have to be employed.

Even at the one-loop level, it is very difficult to sum the infinite series, which emerge as a result of Gaussian integrals . Moreover, these sums are plagued with ultraviolet divergences, which have to be regularized. However, we have been able to sum these series in the long chain limit ($N \to \infty$) when $\kappa R \to \infty$ and $\xi^{-1} R \to \infty$, where κ^{-1} and ξ are Debye and Edwards' screening lengths, respectively. In the

concentrated regime for a very long chain, the width of the depletion zone near the surface of the sphere is very small as compared to the radius of the sphere and we can suppress the radial dependence of the densities (cf. Fig. 4.1 and 4.2). Taking this approximation and ignoring the correlation energy of the charges along the backbone of the chain (which is very small for a weakly charged polyelectrolyte), the free energy at one-loop level can be written as (Appendix E)

$$\frac{F}{k_BT} = \frac{F^*}{k_BT} + \frac{1}{2}\sum_{k=1}^{\infty}\sum_{l=0}^{\infty}(2l+1)\left[\ln\left(1+\frac{R^2/\xi^2}{\nu_{kl}^2}\right)+\ln\left(1+\frac{\kappa^2R^2}{\nu_{kl}^2}\right)\right], \quad (4.34)$$

where $\kappa^2 = 4\pi l_B\sum_{c,+,-} Z_j^2 n_j/\Omega, \xi^{-2} = 12(\frac{1}{1-\rho_p} - 2\chi_{ps})Nb/\Omega$ and ν_{kl} is k^{th} zero of the spherical Bessel function of order l (i.e. $j_l(\nu_{kl}) = 0$). The infinite sum over k can be computed exactly. However, the sum over l diverges. The divergence can be regularized by introducing an upper cutoff M on l and identifying cut-off independent part. The *finite* sum over l has been computed in Ref. [71]. The cut-off independent part gives

$$\begin{aligned}\frac{F}{k_BT} &= \frac{F^*}{k_BT} - \frac{(\kappa^3+\xi^{-3})\Omega}{12\pi} + \frac{\kappa^2 S}{32\pi}\left(1+2\ln\kappa R\right) + \frac{\xi^{-2}S}{32\pi}\left(1+2\ln\xi^{-1}R\right) \\ &\quad + \frac{1}{3}(\kappa+\xi^{-1})R, \end{aligned} \quad (4.35)$$

where S is the surface area of the sphere ($= 4\pi R^2$). In the above expression, cubic terms in κ and ξ^{-1} represent the bulk contribution of fluctuations to the free energy and other terms correspond to the finite size corrections, which arise as a result of confinement. Note that for $R \to \infty$, these finite size contributions vanish and the well-known screening result is obtained. Also, the finite size contributions are smaller than the bulk contributions in the limit discussed here and hence, overall, fluctuations lower the total free energy.

Fluctuation corrections to the osmotic pressure and the mean activity coefficient can be estimated in a straightforward way by using Eq. (4.35). It must be kept in mind that Eq. (4.35) is strictly valid in the strong screening regime for an infinitely long chain. In order for these conditions to be realized, spherical cavity has to be very large to accommodate the long chain (because of incompressibility condition). On the other hand, numerical solution of SCF equations for large spherical cavities with a very long chain becomes very expensive. So, in this study, we limit ourselves to a qualitative discussion about the fluctuation corrections to osmotic pressure and mean activity coefficient.

Qualitatively, the osmotic pressure is decreased due to fluctuations (because the fluctuations at one loop level lower the free energy). It can be shown quite easily that the leading corrections to the pressure profiles[3, 59] will be of the form $-\kappa^3/24\pi$ and $-\xi^{-3}/24\pi$. In the thermodynamic limit of infinite volume for an infinitely long chain, these expressions become exact. As the osmotic pressure must be positive, this analysis sets the range of validity of the one-loop calculations[3] to be well above the overlap concentration (in the concentrated regime). In fact, below those concentrations, perturbative treatment to capture the role of fluctuations fails and non-perturbative methods to capture the role of higher order terms in the expansion of the integrand have to be used (e.g. in dilute and semi-dilute regime)[3, 53].

The finite size corrections to these laws (originating from the last three terms on the right hand side in Eq. 4.35) are small but positive and overall, increase the range of validity of the fluctuation analysis. Similar analysis can be carried out for the mean-activity coefficient of the monovalent salt and the leading corrections coming from fluctuations[59] are of the form $\exp(-\kappa l_B/2)$. Of course, the analysis is valid for the low salt concentrations (Debye-Hückel regime) because the size and the nature of the short-range interactions of salt ions become important at higher concentrations.

4.4 Conclusions & Future Work

We have studied a weakly charged flexible polyelectrolyte chain under spherical confinement using SCFT. In Sections 4.2 and 4.3, we have demonstrated that SCFT predicts creation of a charge density wave and a potential difference across the center of the sphere and the boundary.

We have also shown that for a given charge density along the backbone, free energy of a flexible chain ($F^* - F_0$) has four major contributions - entropy of small ions, entropy of solvent , energy due to polymer-solvent interactions and conformational entropy of the chain. Share of each contribution to the free energy depends on the monomer density, degree of ionization and salt-concentration inside the sphere. However, electrostatic interaction energy plays a minor role in free energy for the weakly charged flexible polyelectrolyte. Our results show that the free energy is not extensive in the number of monomers.

Osmotic pressure for the polyelectrolyte chain follows ideal gas law in the low monomer density regime and substantial deviations are seen as the monomer density is increased. Mean activity coefficient for the monovalent salt show a small, yet systematic deviation from unity, highlighting the role of the polyelectrolyte in breaking the local electroneutrality condition seen in the absence of the polyelectrolyte.

One-loop fluctuation analysis (within the approximation of narrow depletion zone) reveals that fluctuations lower the free energy and the free energy has additional contributions coming from screening effects due to monomers as well as small-ions. Without any confinement, the fluctuations corrections at one-loop level[3] have been shown to lower the free energy and the range of validity of the fluctuation analysis is set by the condition that osmotic pressure must be positive. The concentrations over which the condition is satisfied, come out to be well-above the overlap concentration in polymer solution theories. As the finite size corrections to the fluctuation

contributions in the free energy are positive, so the range of validity of the fluctuation analysis gets widened due to the confinement.

Finally, we comment on the assumptions used in arriving at the above conclusions: (1) We have used the spherical symmetry of the system which is valid as long as coil conformation of the chain is retained and a rod like conformation is avoided. Also, we have used SCFT for a flexible polyelectrolyte chain, which means the chain must not be stiffened due to charges on the backbone and large torsional barriers. These criteria are realized in the presence of high salt, where electrostatic interactions get screened and become short ranged.

(2) Saddle-point approximation breaks down in the extremely dilute limit for monomers, solvent and small-ions. The approximation is strictly valid in the concentrated regime in the presence of enough salt and solvent. The necessity to have many solvent molecules, sets upper limit to be away from extremely dense regime, where $Nb^3/\Omega \to 1$.

In this study, fluctuations in densities and fields about the mean field solution of SCF equations have been treated perturbatively by expanding free energy functional up to quadratic order about the saddle point. This fluctuation analysis breaks down for low density regime, where higher order terms also contribute and need to be taken into account using an appropriate non-perturbative treatment.

(3) Role of solvent is taken into account by taking the volume of a solvent molecule as the same as that of a monomer. In reality, solvent size may be smaller than Kuhn step length and incompressibility constraint is violated near the boundary. For the present study, we have simply assumed that the effect of the depletion zone for solvent on the system properties is negligible and can be ignored. All these limitations of the current model can be removed by taking the solvent size to be different from the

monomer[83] and using $\rho_p(r) + \rho_s(r) = \rho(r)$, where $\rho(r)$ is a suitable function, which is ρ_0 away from the boundary and falls from ρ_0 to zero in a smooth fashion within the depletion zone[83]. However, the choice of $\rho(r)$ and width of depletion zone is arbitrary and depends on the numerics of the problem.

Similarly, small ions have been treated as point charges, which might not be a bad approximation knowing the fact that typical ion radii for monovalent cations and anions lie in the range $\sim 0.06 - 0.22$ nm[84].

(4) In principle, the degree of ionization (α) should also be computed by minimization of free energy[85] with respect to α. In order to simplify the numerical work, we have taken the degree of ionization (α) to be independent of l_B and avoided any ion condensation effects.

(5) While splitting the free energy into energy and entropy, we have assumed that dielectric constant (ϵ) of the solvent is insensitive to temperature. However, the temperature dependence of the dielectric constant[74, 86] can be easily incorporated in our theory.

We have extended the work to develop a theory of genome packing[87] in spherical viruses, where the confining spherical cavity is decorated with flexible charged chains, which bear charges of the sign opposite to that of the genome packed inside the viral capsid. The focus of the study has been the spontaneous selection of the genome length for a given viral capsid based on the field theoretical description of the system. Effect of the amount of added salt on the spontaneous selection of the genome length is studied to make relation with the experiments.

Future directions for the extensions of the current work include the study of a single semi-flexible polyelectrolyte chain in spherical cavities, adsorption of a single

polyelectrolyte chain as well as many chains on to a charged spherical surface, and the study of polyelectrolytes at spherical dielectric interfaces.

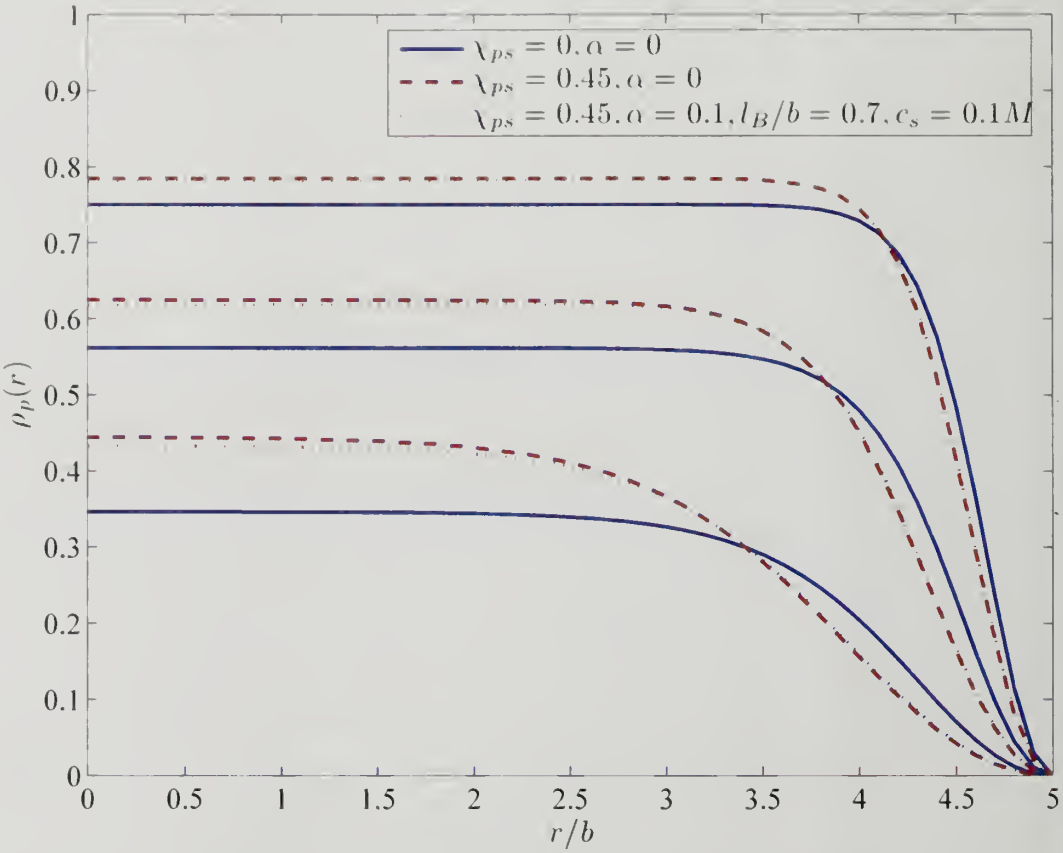

Figure 4.1. Effect of N on monomer densities - comparison with the corresponding neutral chains . In above plots, we have chosen $R/b = 5$ and $N = 100$, $N = 200$ and $N = 300$ from bottom to top, respectively .

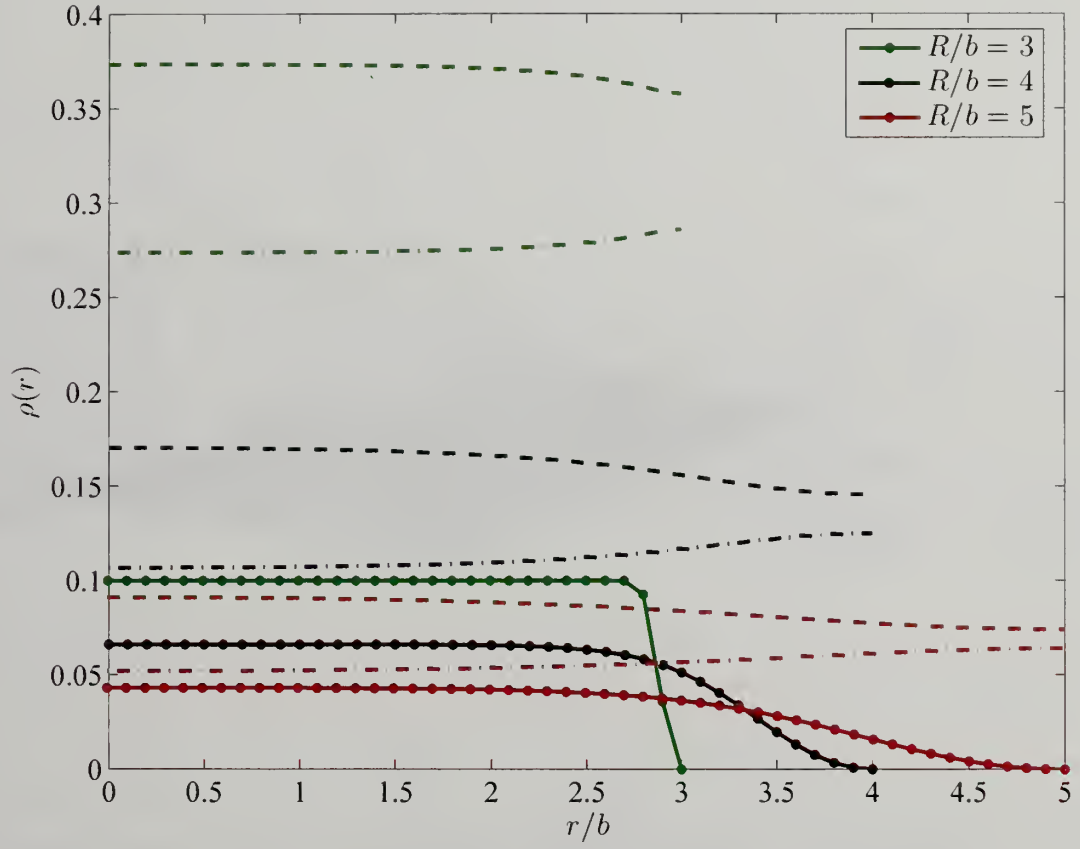

Figure 4.2. Effect of cavity radius (R) on ion densities. In these plots, we have chosen $N = 100, \alpha = 0.1, l_B/b = 0.7, \chi_{ps} = 0.45$ and number of salt ions is kept fixed (in all these plots, number of salt ions is equivalent to salt concentration of $0.1M$ for a sphere of radius $R/b = 5$). Solid, dashed and dash-dotted lines represent $\rho(r) = \alpha\rho_p(r)$, $\rho_c(r) + \rho_+(r)$ and $\rho_-(r)$, respectively.

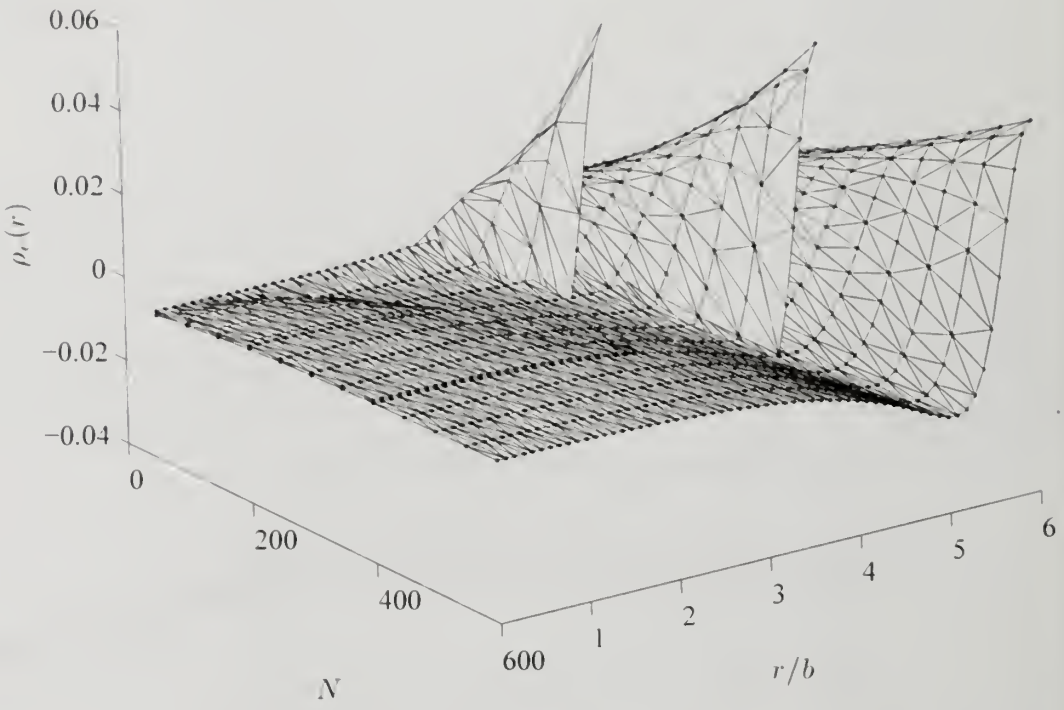

Figure 4.3. Effect of cavity radius (R) on net charge density, $\rho_e(r) = \sum_{j=c,+,-} Z_j\rho_j(r) + Z_p\alpha\rho_p(r)$. In these plots, we have chosen $\alpha = 0.1, l_B/b = 0.7, \chi_{ps} = 0.45$ and number of salt ions is kept fixed (in all these plots, number of salt ions is equivalent to salt conc of $0.1M$ for sphere of radius $R/b = 5$). N is increased in steps of 50 starting from 50.

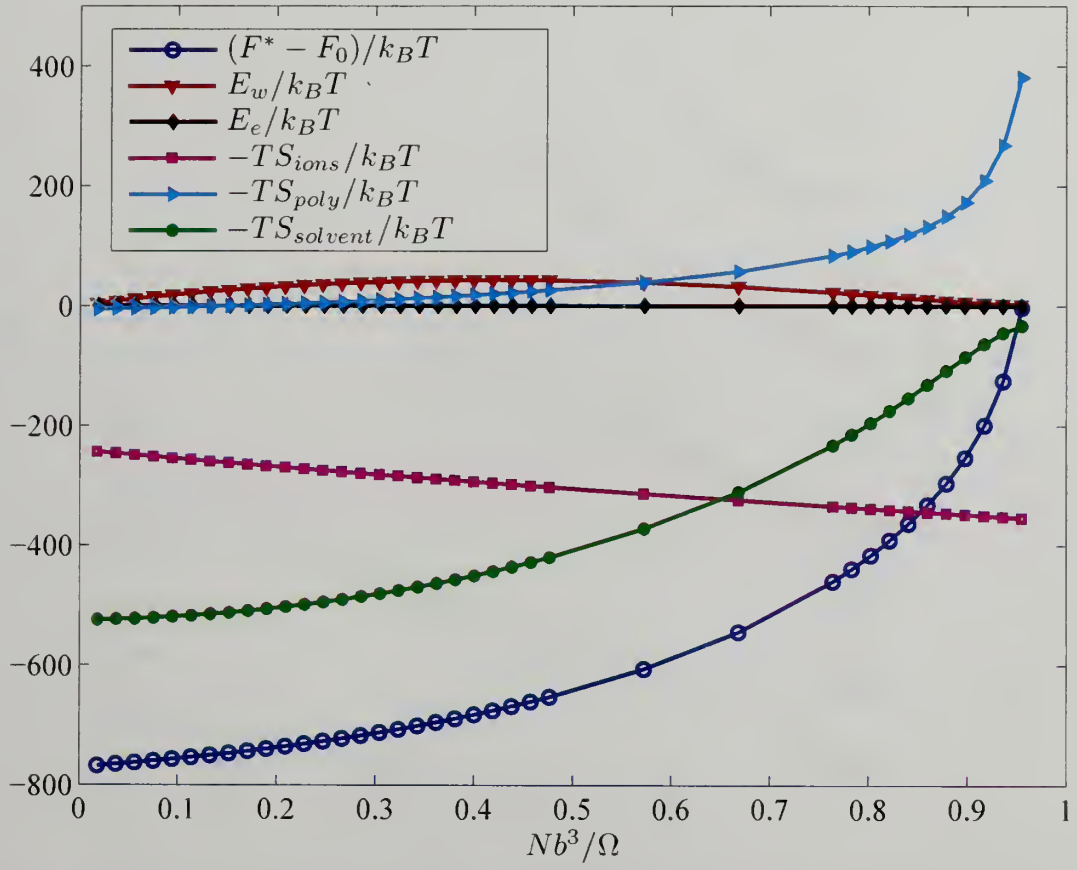

Figure 4.4. Different contributions to the free energy within the saddle point approximation for salty systems. Here, we have chosen $N = 100, \alpha = 0.1, l_B/b = 0.7, \chi_{ps} = 0.45, c_s = 0.1M, R/b = 5$.

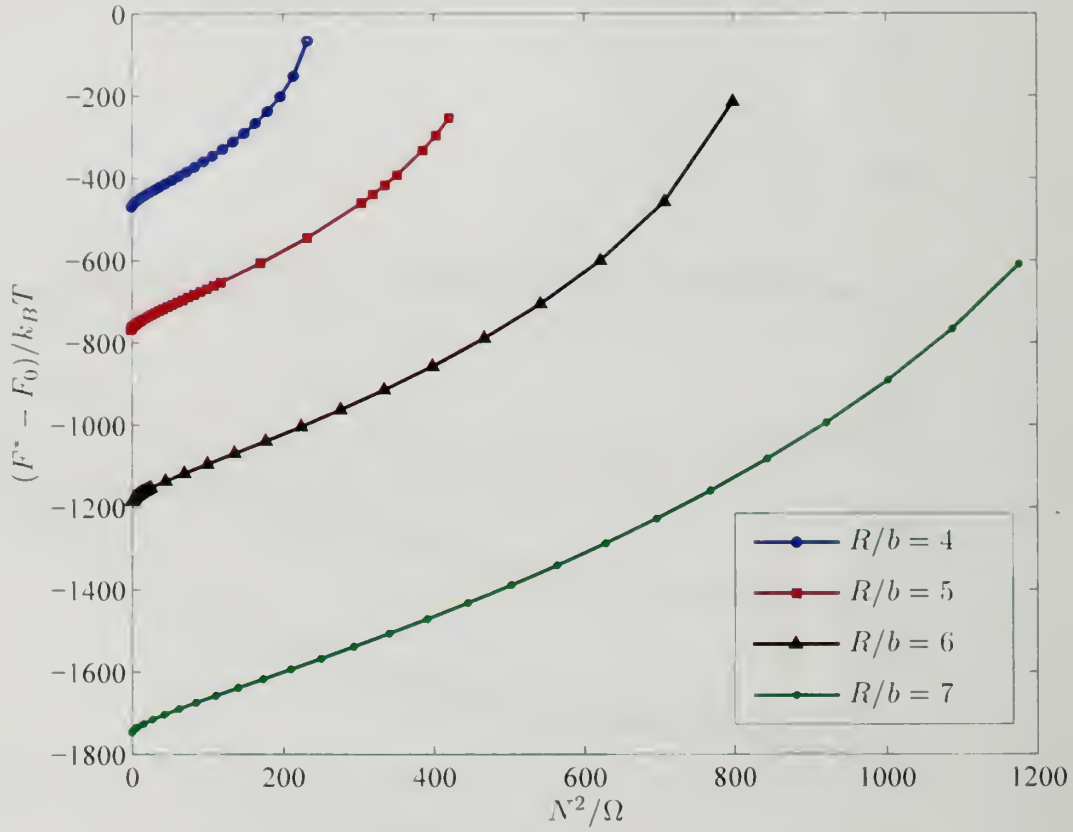

Figure 4.5. Effect of confinement on the free energy within the saddle point approximation. Here, we have chosen $\alpha = 0.1, l_B/b = 0.7, \chi_{ps} = 0.45$ and number of salt ions is kept fixed so that the number of salt ions is equivalent to salt concentration of $0.1M$ for sphere of radius $R/b = 5$.

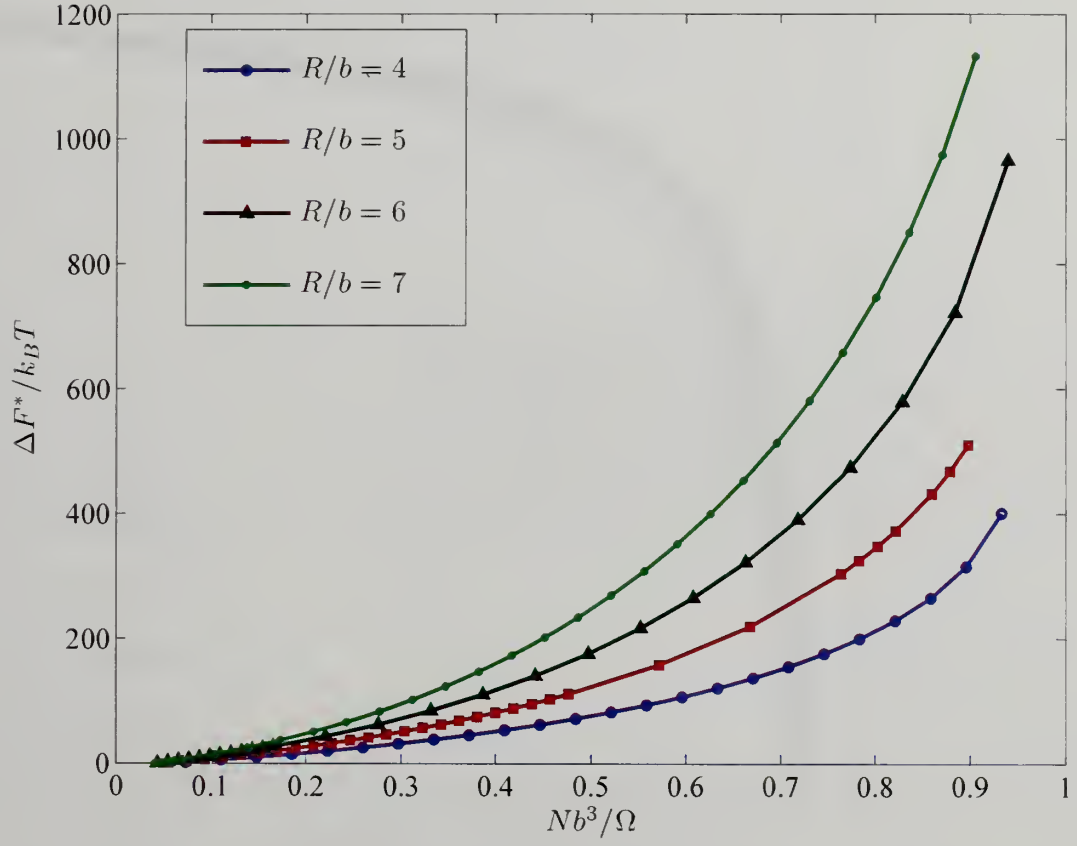

Figure 4.6. Difference in free energy of the spherical cavity with and without polyelectrolyte chain. $\Delta F^\star = F^* - F\{\bar{\rho}_p = 0\}$. All other parameters are the same as in Fig. 4.5.

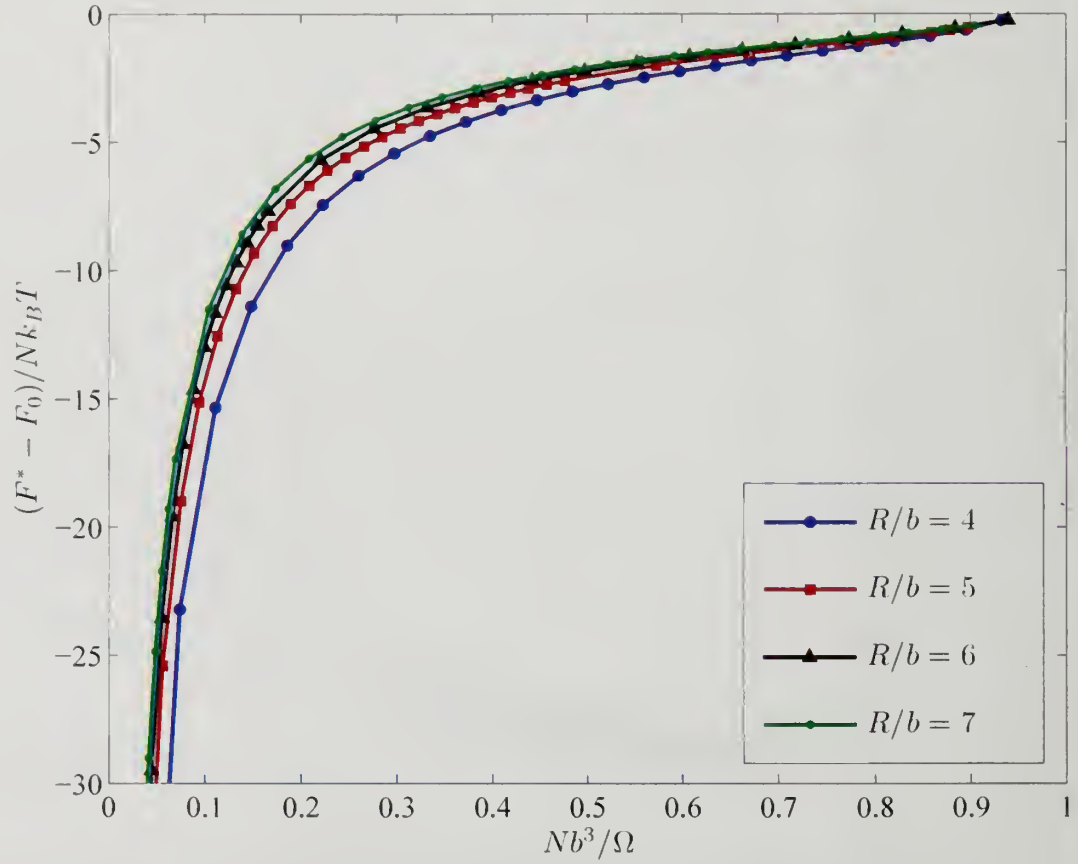

Figure 4.7. Non-extensive nature of free energy of confinement. Parameters are the same as in Fig. 4.5.

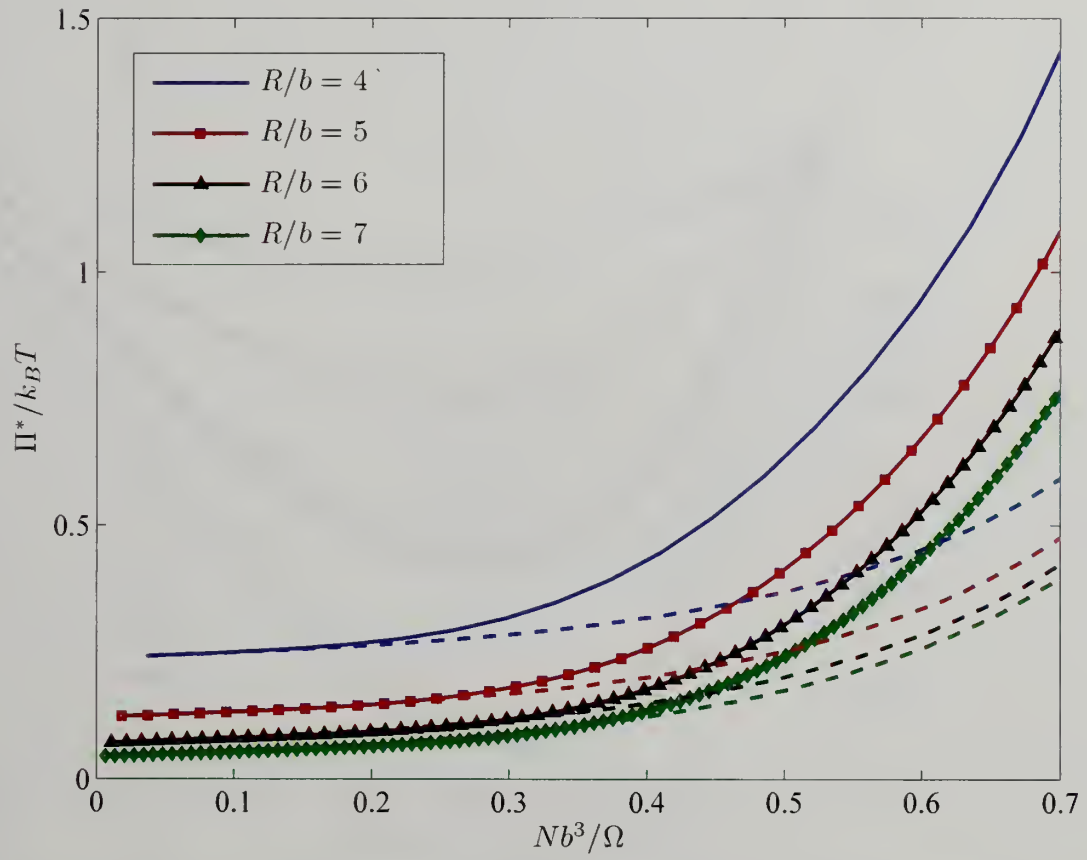

Figure 4.8. Comparison between osmotic pressure for the confined polyelectrolyte chain and the homogeneous phase (cf. Eq. (4.28)). Solid lines correspond to the inhomogeneous case and dashed lines represent the homogeneous system. Parameters are the same as in Fig. 4.5.

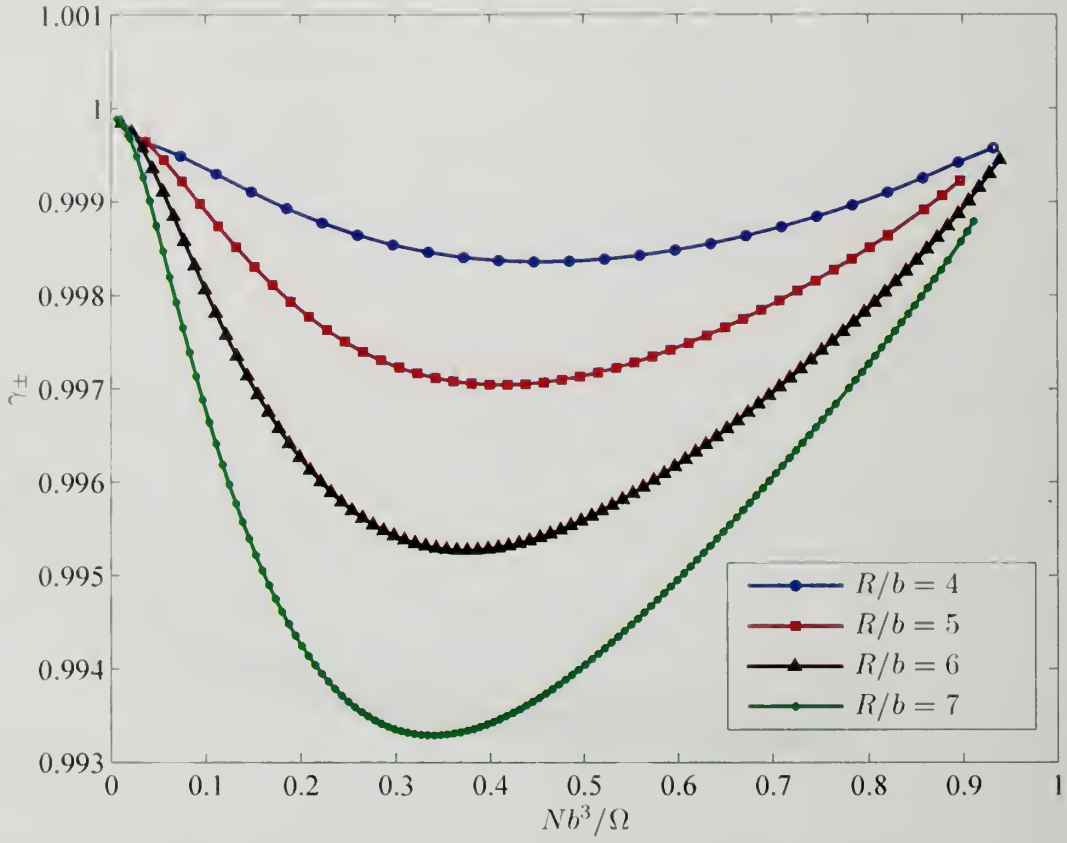

Figure 4.9. Mean activity coefficients for monovalent salt as a function of monomer density of the polyelectrolyte. For comparison purposes, parameters have been chosen to be the same as in Fig. 4.5.

CHAPTER 5

COUNTERION ADSORPTION ON FLEXIBLE POLYELECTROLYTES: COMPARISON OF THEORIES

5.1 Introduction

Counterion adsorption in polyelectrolyte solutions is one of the fundamental problems in polyelectrolyte physics, which has been a topic of extensive research[81, 85, 88, 89, 90, 91, 92, 93, 94, 95, 96, 97, 98, 99, 100, 101, 102, 103, 104, 105, 106, 107, 108, 109, 110, 111, 112, 113] for decades. Historically[88, 89, 90, 91], the counterion adsorption in polyelectrolyte solutions was described as an analog of ion-pairing in simple electrolyte solutions, and deviations from the Debye-Hückel limiting laws in colligative properties of polyelectrolyte solutions in dilute concentration regime had been attributed to counterion adsorption. Ignoring interactions among different chains in dilute solutions, modeling a polyelectrolyte chain by an infinite rod and using bulk dielectric constant of the medium for describing electrostatic interactions, counterion adsoprtion (or "Manning condensation") was predicted to be a result of a singularity in the partition function arising due to a singular electrostatic potential near the rod. In particular, it was predicted that for monovalent monomers and counterions if $l_B/l > 1$, where l_B is Bjerrum length ($= e^2/4\pi\epsilon_0\epsilon k_B T$, e being the electronic charge, ϵ_0 being the dielectric constant of the vacuum, ϵ being the dielectric constant of the medium and $k_B T$ being the Boltzmann constant times temperature) and l is the charge spacing on the backbone of the chain, then some of the counterions from the solution adsorb on the chain until $l_B/l = 1$. On the other hand, if $l_B/l < 1$, the Debye-Hückel approximation (i.e., the linearization of Poisson-Boltzmann) can be

used to describe the electrostatics, and there is no adsorption. In other words, counterion adsorption was described as a kind of phase transition (such as the condensation of vapors) driven by electrostatic energy only.

Over the years, simulations[92, 93, 94, 95, 96, 97, 98, 99] and experiments[81, 100, 101, 102, 103, 104, 105] have provided a useful insight into the counterion adsorption mechanism in polyelectrolyte solutions. Most importantly, it was revealed that a polyelectrolyte chain never attain a perfect rod conformation[92], even in salt-free solutions where the rod conformation is usually expected. Also, it has been shown that the effect of ion-pairing[93, 103] on the backbone and dielectric constant[104] has to be considered in order to treat a realistic polyelectrolyte chain. Furthermore, simulations[94, 95] reveal that the counterions retain their translational degrees of freedom along the backbone of the chain after being adsorbed.

These insights obtained from the simulations and experiments have led to a number of theoretical descriptions[85, 106, 107, 108, 109, 110, 111, 112, 113] of the counterion adsorption in polyelectrolyte solutions (containing monovalent or multivalent salts) over the last two decades. For an isolated, *single* polyelectrolyte chain, it was shown that there is no singularity in the partition function when the polyelectrolyte chain is modeled as a flexible one[85]. An important prediction of the theory[85] emphasized the role played by the dielectric mismatch between the local environment of the backbone and the bulk solution in driving counterion adsorption, and that had not been highlighted earlier in the literature. In particular, it was shown that counterion adsorption arises as an interplay of adsorption energy and translational entropy of ions. Entropically, higher degree of ionization, an effect which is opposed by the lowering of electrostatic energy by the formation of ion pairs at the backbone of the chain, is preferred. To carry out the calculations analytically, the Debye-Hückel potential was used to describe the electrostatic interactions between charged species, and a novel variational method was used to express the chain conformational entropy

and excluded volume effects. Finally, the complete free energy of the system (consisting of the chain, the counterions, and the solvent) was simultaneously minimized in terms of the degree of counterion adsorption and the size of the polyelectrolyte chain to self-consistently obtain the equilibrium values of the respective variables. The theory is in qualitative agreement with the known simulation results. Recently, this single chain theory has been extended to describe the competitive counterion adsorption[113] phenomenon in the presence of multivalent and monovalent counterions. Despite the qualitative agreements to simulations and experiments (especially, regarding the phenomena of charge reversal and reentrant transition), the approximations used in the theory have not rigorously been assessed so far.

In this work, we consider the counterion adsorption on a flexible polyelectrolyte chain using the self-consistent field theory (SCFT). SCFT computes the free energy of the system by summing over all possible conformations of the chain, and hence, provides a more accurate description of the system (in fact, it provides the exact free energy at the mean-field level) compared to the variational formalism. Also, as the electrostatics in SCFT is treated at full, non-linear Poisson-Boltzmann level, we can assess the validity of the Debye-Hückel potential to describe the electrostatic energy in the variational formalism. Although SCFT provides an accurate and clear picture, it is computationally expensive to calculate the degree of ionization due to a vast parameter space in the case of polyelectrolytes. On the other hand, the variational theory put forward by Muthukumar[85] is transparent, analytically tractable (to some extent), and very inexpensive in terms of the computational needs. Aim of this study is to provide a simple, accurate, and easy-to-use method to compute the degree of ionization and assess the approximations used in the variational formalism.

This chapter is organized as follows: the theoretical formalisms are presented in Sec. 5.2; calculated results and conclusions are presented in Sec. 5.3 and 5.4, respectively.

5.2 Comparison of Theories : SCFT and Variational Formalism

We consider a single flexible polyelectrolyte chain of total N Kuhn segments, each with length b, confined in a spherical cavity of volume $\Omega = 4\pi R^3/3$. The polyelectrolyte chain is represented as a continuous curve of length Nb, and an arc length variable t is used to represent any segment along the backbone so that $t \in [0, Nb]$. Now, we assume that the chain (negatively charged) is surrounded by n_c monovalent counterions (positively charged) released by the chain along with n_γ ions of species $\gamma\,(= +, -)$ coming from added salt so that the whole system is globally electroneutral. Let Z_j be the valency (with sign) of the charged species of type j, and n_s be the number of solvent molecules (satisfying the incompressibility constraint after assuming the small ions to be pointlike) present in the cavity. For simplicity, we have taken the volume of a solvent molecule (v_s) to be equal to the volume of the monomer (i.e., $v_s \equiv b^3$). Subscripts $p, s, c, +$ and $-$ are used to represent monomer, solvent , counterion from polyelectrolyte, positive and negative salt ions, respectively.

In order to study counterion adsorption, we use the so-called "two-state" model for the counterions so that there are two populations of counterions in the system. One population of the counterions is free to enjoy the available volume (called the "free" counterions) and the other population is "adsorbed" on the backbone. However, the adsorbed counterions are allowed to enjoy translational degrees of freedom along the backbone, maintaining a total charge of $e\alpha NZ_p$ on the chain, where e is the electronic charge and α is the degree of ionization of the chain (i.e., there are $-(1-\alpha)NZ_p/Z_c$ "adsorbed" counterions on the chain). In the literature, this kind of charge distribution has been referred to as a "permuted" charge distribution[12].

For a particular set of parameters, we compute the free energy of the system comprising of the single chain, its counterions, the salt ions, and the solvent as a function of the degree of ionization (α). As mentioned before, we compute the free energy using

two different computational frameworks: SCFT[9, 114] and the variational[50, 72, 85] formalism. In both the formalisms, we ignore the electrostatic interactions between solvent molecules and the small ions, and model the dielectric constant (ϵ) of the medium to be independent of temperature (T) to extract energy and entropy of the system. Also, for comparison purposes, we divide the free energy into a mean field part and an additional part, which goes beyond the mean field theory. Mean field part is further divided into the contributions coming from the "adsorbed" counterions ($F_a^\star$) and the "free" ions, and from the chain entropy etc., ($F_f^\star$). All contributions are properly identified(or subdivided into) as the enthalpic or(and) entropic parts. In all of what follows, the superscript $\star$ represents the mean field part. A brief description of the derivation for the two formalisms is presented in Appendix F, and the original references[85, 114] may be consulted for details.

To start with, we note that the contributions coming from "adsorbed" counterions are the same in both formalisms, and are given by

$$F_a^\star = E_a - TS_a, \tag{5.1}$$

$$E_a = -(1-\alpha)N\delta l_B/b, \tag{5.2}$$

$$-TS_a = N\left[\alpha\ln\alpha + (1-\alpha)\ln(1-\alpha)\right], \tag{5.3}$$

so that E_a is the electrostatic binding energy of the ion-pairs formed on the polymer backbone due to the adsorption of ions and S_a is the translational entropy of the "adsorbed" counterions along the backbone. Parameter $\delta = \epsilon b/\epsilon_l d$, reflects the deviation of the dielectric constant at the local environment of the chain (ϵ_l) from the bulk value (ϵ), and d represents the length of the dipole formed due to ion-pairing.

5.2.1 Self-Consistent Field Theory

Although $F_a^\star$ is the same in both formalisms, other contributions involving the "free " ions, the chain entropy etc. (i.e., $F_f^\star$) differ from each other significantly in

terms of computational details. In SCFT, F_f^* is computed after solving for fields experienced by different components in the system, which arise as a result of interactions of a particular component with the others. For a single polyelectrolyte chain in a spherical cavity, each charged component (monomers and small ions) experience a dimensionless field ψ (in units of k_BT/e), which is given by the solution of the Poisson-Boltzmann equation

$$\nabla_{\mathbf{r}}^2 \psi(\mathbf{r}) = -4\pi l_B \rho_e(\mathbf{r}), \tag{5.4}$$

where $\rho_e(\mathbf{r}) = \sum_{j=c,+,-} Z_j \rho_j(\mathbf{r}) + Z_p \alpha \rho_p(\mathbf{r})$ is the local charge density and $\rho_\beta(\mathbf{r})$ is the collective number density of species of type $\beta = p, c, +, -$. Collective number densities for small ions are given by the Boltzmann distribution with the prefactor determined by the constraint that the number of small ions are fixed in the system. Explicitly,

$$\rho_j(\mathbf{r}) = \frac{n_j \exp\left[-Z_j \psi(\mathbf{r})\right]}{\int d\mathbf{r} \exp\left[-Z_j \psi(\mathbf{r})\right]} \tag{5.5}$$

for $j = c, +, -$. In Eq. (5.4), $\rho_p(\mathbf{r})$ is the monomer density, which is related to the probability of finding a particular monomer (described by the contour variable t) at a particular location $\mathbf{r}$, when the starting end of the chain can be anywhere in space (say, $q(\mathbf{r}, t)$), by the relation

$$\rho_p(\mathbf{r}) = \frac{\int_0^N dt\, q(\mathbf{r}, t) q(\mathbf{r}, N-t)}{\int d\mathbf{r} q(\mathbf{r}, N)}. \tag{5.6}$$

Furthermore, it can be shown that $q(\mathbf{r}, t)$ satisfies the modified diffusion equation[1, 9]

$$\frac{\partial q(\mathbf{r}, t)}{\partial t} = \left[\frac{b^2}{6} \nabla_{\mathbf{r}}^2 - \{Z_p \alpha \psi(\mathbf{r}) + w_p(\mathbf{r})\}\right] q(\mathbf{r}, t), \quad t \in (0, N), \tag{5.7}$$

w_p being the field experienced by monomers due to non-electrostatic interactions. At the saddle point, it is given by

$$w_p(\mathbf{r}) = \chi_{ps} b^3 \rho_s(\mathbf{r}) + \eta(\mathbf{r}), \tag{5.8}$$

where χ_{ps} is the dimensionless Flory's chi parameter and $\eta(\mathbf{r})$ is the Lagrange's multiplier to enforce the incompressibility constraint

$$\rho_p(\mathbf{r}) + \rho_s(\mathbf{r}) = \rho_0 \tag{5.9}$$

at all points in the system. Here, ρ_0 is the total number density i.e., $\rho_0 = (N+n_s)/\Omega = 1/b^3$. Finally, $\rho_s(\mathbf{r})$ is the collective number density of solvent molecules given by the Boltzmann distribution in terms of the field experienced by a solvent molecule (w_s). Within the saddle-point approximation, ρ_s and w_s are related by

$$\rho_s(\mathbf{r}) = \frac{n_s \exp\left[-w_s(\mathbf{r})\right]}{\int d\mathbf{r} \exp\left[-w_s(\mathbf{r})\right]}, \tag{5.10}$$

$$w_s(\mathbf{r}) = \chi_{ps} b^3 \rho_p(\mathbf{r}) + \eta(\mathbf{r}). \tag{5.11}$$

These equations also close the loop of self-consistent equations, and Eqs.(5.4 - 5.11) form the set of coupled non-linear equations that defines the system.

After solving these equations for fields (and in turn, for densities), the free energy at the saddle point, $F_f^\star$, is divided into enthalpic contributions due to the excluded volume and electrostatic interactions and into entropic contributions because of small ions, solvent molecules and the polyelectrolyte chain. Denoting these contributions by E_w, E_e, S_i, S_s, and S_p, respectively, $F_f^\star$ is given by

$$F_f^\star - F_0 = E_w + E_e - T(S_i + S_s + S_p), \tag{5.12}$$

where $F_0 = \frac{\rho_0}{2}(N w_{pp} + n_s w_{ss})$ is the self-energy contribution arising from the excluded volume interactions characterized by the excluded volume parameters w_{ij} between species i and j. Explicit expressions for different constituents of F_f^* are presented in Table 3.1 in terms of densities and fields at the saddle point. Within the saddle-point approximation, the total free energy (F_{SCFT}) of the system is given by $F_{SCFT} \simeq F_a^* + F_f^*$. In order to compare the free energies obtained from SCFT and the variational formalism for a given N and R, a single Gaussian chain of contour length Nb in the volume Ω is chosen as the reference frame, whose free energy is taken to be zero. This reference free energy of confinement for a single Gaussian chain has been subtracted from the polymer conformational entropy in Table 5.1. The free energy of confining a single Gaussian chain with N Kuhn segments of length b each in a spherical cavity of radius R can be computed exactly and is given by[115]

$$F_{gaussian} = -\ln\left[\int d\mathbf{r} q_0(\mathbf{r}, N)\right] = -\ln\left[\frac{6\Omega}{\pi^2}\sum_{k=1}^{\infty}\frac{1}{k^2}\exp\left[-\frac{k^2\pi^2 N b^2}{6R^2}\right]\right]. \quad (5.13)$$

5.2.2 Variational Formalism

In variational calculations[85], a single polyelectrolyte chain, whose monomers interact with the excluded volume and the electrostatic interactions in the presence of the small ions is approximated by an *effective* Gaussian chain, whose conformational statistics are dependent on the different kinds of interactions in the system. To compute the equilibrium free energy, its variational *ansatz* is minimized with respect to the variational parameter b_1, which is related to the radius of gyration (R_g) of the chain by $R_g^2 = N b b_1/6$. Physically, this corresponds to the minimization of the free energy of the single chain system with respect to the size of the chain. For the computations of the equilibrium degree of ionization, an additional minimization of the free energy with respect to the degree of ionization has to be carried out.

Term	SCFT	Variational Formalism
$E_w - TS_s$	$\chi_{ps} l^3 \int d\mathbf{r} \rho_p(\mathbf{r}) \rho_s(\mathbf{r})$ $+\rho_0 \int d\mathbf{r} \eta(\mathbf{r}) + \int d\mathbf{r}\, \rho_s(\mathbf{r}) \{\ln[\rho_s(\mathbf{r})] - 1\}$	$\frac{4}{3}\left(\frac{3}{2\pi}\right)^{3/2} (1 - 2\chi_{ps}) \sqrt{N} / \tilde{b}_1^{3/2}$ $+\chi_{ps} N b^3 - \Omega$
E_e	$\frac{1}{2} \int d\mathbf{r}\, \psi(\mathbf{r}) \rho_e(\mathbf{r})$	$2\sqrt{\frac{6}{\pi}} \alpha^2 \tilde{l}_B N^{3/2} \Theta_0(a) / \tilde{b}_1^{1/2}$
$-TS_i$	$\sum_{j=c,+,-} \int d\mathbf{r}\, \rho_j(\mathbf{r}) \{\ln[\rho_j(\mathbf{r})] - 1\}$	$(fN + n_+) \ln(fN + n_+)/\Omega$ $+n_- \ln n_- / \Omega$ $-(fN + n_+ + n_-)$
$-TS_p$	$-\ln\left[\int d\mathbf{r} q(\mathbf{r}, N) / \int d\mathbf{r} q_0(\mathbf{r}, N)\right]$ $-\rho_0 \int d\mathbf{r} \eta(\mathbf{r}) - \int d\mathbf{r}\, Z_p \alpha \psi(\mathbf{r}) \rho_p(\mathbf{r})$ $- \int d\mathbf{r} w_p(\mathbf{r}) \rho_p(\mathbf{r})$	$\frac{3}{2}\left[\tilde{b}_1 - 1 - \ln \tilde{b}_1\right]$

Table 5.1. Comparison of contributions to $F_f^\star$ in SCFT and variational formalism.

However, due to the intricate coupling between the size of the chain and the degree of ionization, the minimizations have to be carried out self-consistently.

The variational *ansatz* of the total free energy ($F_{variational}$) is given by $F_{variational} = F_a^\star + F_f^\star + \Delta F$, where ΔF involves one-loop fluctuation corrections, addressing the density fluctuations of the small ions, to the free energy. As mentioned before, the free energy of the adsorbed counterions (i.e., $F_a^\star$) is the same in both SCFT and the variational formalisms (cf. Eq. (5.1)). The $F_f^\star$ part of the free energy[85] is tabulated in Table 5.1. The function $\Theta_0(a)$ in Table 5.1 is a cross-over function given by[50, 85]

$$\Theta_0(a) = \frac{\sqrt{\pi}}{2}\left(\frac{2}{a^{5/2}} - \frac{1}{a^{3/2}}\right) \exp(a)\mathrm{erfc}(\sqrt{a}) + \frac{1}{3a} + \frac{2}{a^2} - \frac{\sqrt{\pi}}{a^{5/2}} - \frac{\sqrt{\pi}}{2a^{3/2}}, \quad (5.14)$$

where $a \equiv \kappa^2 N b b_1/6$, and κb is the dimensionless inverse Debye length. Furthermore, $\tilde{b}_1 = b_1/b, \tilde{l}_B = l_B/b$. The number of salt ions (n_+, n_-) are related to the salt concentration (c_s) by the relation $Z_+ n_+ = -Z_- n_- = 0.6023 c_s \Omega$, where c_s is in units of moles per liter (molarity). Also, all the terms in the free energies are in units of $k_B T$.

In this work, we have ignored one-loop corrections to the free energy within SCFT. However, one-loop corrections to the free energy coming from the density fluctuations of the small ions, within the variational formalism, is given by

$$\Delta F = -\frac{\Omega \kappa^3}{12\pi}. \tag{5.15}$$

where $\kappa^2 = 4\pi l_B (aN + n_+ + n_-)/\Omega$ and κ is the inverse Debye length.

5.2.3 Numerical Techniques

We solve SCFT Eqs. [(5.4) - (5.11)] within spherical symmetry (i.e. $\mathbf{r} \rightarrow r = |\mathbf{r}|$), using the Dirichlet boundary conditions for $q(r,t)$ and all the fields except $\eta(r)$. Also, due to the use of spherical symmetry in these calculations, we use

$$\frac{\partial \psi(r)}{\partial r}\,|_{r=0} = \frac{\partial q(r,t)}{\partial r}\,|_{r=0} = 0 \quad \text{for all } t. \tag{5.16}$$

Starting from an initial guess for fields, new fields and densities are computed after solving the modified diffusion and Poisson-Boltzmann equation by finite difference methods[75]. Broyden's method[75] has been used to solve the set of non-linear equations. The equilibrium value of the degree of ionization $(\alpha^\star)$ is obtained after minimizing the free energy with respect to α. We carry out the numerical minimization of free energy over α using Brent's method[75]. The results presented in this chapter were obtained by using a grid spacing of $\Delta r = 0.1$ and contour steps of $\Delta t = 0.01$.

On the other hand, the self-consistent minimization of the free energy in the variational method has been carried out by assuming a uniform expansion of the

chain within spherical symmetry. In this formalism, the free energy is minimized simultaneously with respect to α and b_1, and both these quantities at equilibrium $(\alpha^\star, b_1^\star)$ are computed self-consistently. The radius of gyration of the chain (which is confined to a finite volume, $\Omega = 4\pi R^3/3$) is obtained from the equilibrium value of the expansion factor $b_1^\star$. For these calculations, the upper bound for the radius of gyration of the chain is specified to be the radius of the confining volume (i.e. $R_g \leq R$) to mimic the confinement effects. Also, the Kuhn step length b is taken to be unity in both variational as well as SCFT calculations.

5.3 Results

5.3.1 Degree of Ionization

We have carried out an exhaustive comparison between the SCFT and variational formalisms by calculating the equilibrium degree of ionization $(\alpha^\star)$ of a negatively charged single flexible polyelectrolyte chain (i.e. $Z_p = -1, Z_c = 1$) in the presence of a monovalent salt in both cases. For all sets of parameters, the $\alpha^\star$ obtained by the minimization of SCFT free energies is indistinguishable from that obtained using variational free energies without one-loop corrections (i.e., $F_{variational} - \Delta F$). To demonstrate this, we have plotted $\alpha^\star$ as a function of l_B/b for different spherical volumes (i.e., different R) in Fig. 5.1. This clearly supports the validity of variational theory to predict the degree of ionization of the polyelectrolyte chain in an efficient way. Taking into account its computational ease and transparency, the comparison shows that the theory is a better candidate for the computation of $\alpha^\star$.

However, inclusion of one-loop corrections to the free energy because of the density fluctuations of the small ions within the variational formalism (i.e., considering $F_{variational}$), leads to deviations from the observed agreement at the mean field level. In Fig. 5.2, we have plotted $\alpha^\star$ as obtained from SCFT (without one-loop corrections) and the variational theory with one-loop corrections due to the small ions. It is to

be noted that the degree of ionization is essentially zero in SCFT for experimentally relevant values of l_B/b (around 3) for aqueous solutions, whereas α^* is reasonable in the variational theory. The increase in α^* with the inclusion of ΔF can be understood by the fact that the density fluctuations of the small ions lower the free energy, and its contribution to the total free energy increases with the increase in the number of "free" ions (goes like $-n^{3/2}$ in salt-free case, where n is the number of "free" ions - cf. Eq. (5.15)). Also, term-by-term comparison of the free energy components reveals that the discrepancy arises solely due to the term accounting for the density fluctuations of the small ions. This disagreement highlights the fact that the effect of density fluctuations of the small ions is not included in SCFT within the saddle point approximation.

5.3.2 Term-by-term Comparison of Free Energy: SCFT and Variational Formalism

To assess the approximations used in the variational theory and to find out the origin of the remarkable agreement in terms of α^* obtained from SCFT and variational theory (without one-loop corrections, in order to make a fair comparison with SCFT), we have compared individual contributions to the free energies in these two formalisms. In Fig. 5.3, we have plotted these free energies for $Z_p = -Z_c = -1, R/b = 10, N = 100, c_s = 0.1M, \delta = 3$ and $\chi_{ps} = 0.45$. It is clear that the total free energies obtained from SCFT and the variational theory are in quantitative agreement with each other.

In Figs. 5.4 and 5.5, we have compared different constituents of the free energies obtained from SCFT and the variational formalism for low monomer densities. It is evident that both the theories predict that the major contributions to the free energy are due to the ion-pair energy(Fig. 5.4a), the "adsorbed" counterion translational entropy (Fig. 5.4b), the polymer-solvent interaction energy and the solvent entropy

(Fig. 5.4c); and the "free" ions translational entropy (Fig. 5.4d). Contributions due to the chain conformational entropy (Fig. 5.5a) and electrostatic energy (Fig. 5.5b) are almost negligible (less than 0.1% in the total free energy) as compared to others. For low monomer densities, the dominant contributions to the total free energies come from the polymer-solvent interaction energy and the solvent entropy. For the particular single chain dilute system investigated here, these contributions account for more than 50% of the total free energy. Although large, these contributions are found to be almost insensitive to α (note the scale in (Fig. 5.4c)). In fact, these contributions have been shown to depend on the monomer density and solvent quality in a sensitive way[114]. The α dependent terms, which contribute significantly to the total free energy are the ion-pair energy and the "free" ions translational entropy. At lower electrostatic interaction strengths (i.e., low l_B/b), the translational entropy of the "free" ions dominates and at higher electrostatic strengths, the ion-pair energy term contributes significantly to the free energy. Together, these two contributions account for as high as 99% of the f dependent part in the total free energy (cf. Figs. 5.3, 5.4a and 5.4d). Relatively very small contributions ($\sim 1\%$) to the free energies come from the translational entropy of the "adsorbed" ions.

An excellent agreement for the total free energies and their components obtained from SCFT and the variational theory allows us to infer the role of different terms in driving counterion adsorption by studying the behavior of each term in the *variational theory* as a function of α and b_1 in Eqs. 5.2, 5.3 and Table 5.1. From Eq. 5.2, it is clear that the ion-pair energy (negative contribution to the free energy) favors counterion adsorption with a linear dependence on α. On the other hand, the counterion adsorption is opposed by the translational entropy of the "free" ions (see the expression for $-TS_i$ in Table 5.1). Similarly, the translational entropy of the "adsorbed" counterions drives the adsorption toward $\alpha^\star = 0.5$ to optimize this part of the entropy (cf. Eq. 5.3). Physically, it can be understood from the fact that the complete ad-

sorption or desorption of the counterions leads to the lowering of translational entropy of the "adsorbed" counterions due to the unavailability of sites or "adsorbed" counterions, respectively. Role of other contributions, i.e. the polymer-solvent interaction energies and the solvent entropy (i.e., $E_w - TS_s$), the electrostatic energy involving the "free" ions and the monomers (E_ϵ) and the conformational entropy of the chain ($-TS_p$) is minuscule in driving the counterion adsorption in a particular direction. However, these three contributions dictate the effective size of the chain (through b_1) at the equilibrium (note the non-monotonic dependence of these terms on b_1). The quantitative agreement between the first three contributions to the free energy in two formalisms explains the observed agreement in the results obtained for α^*. We must stress here that in the variational theory, b_1 and α are independent parameters, and b_1^* and α^* are intricately coupled through the electrostatic energy term, E_ϵ. This coupling is very weak in the good solvent conditions investigated here, which may not be the case in poor solvent conditions where b_1/b may be less than unity. Although a negligible effect on α, E_ϵ drives the system toward $\alpha^* = 0$, i.e., complete adsorption of counterions on the chain, which may not be an equilibrium state.

Although E_ϵ is a negligible contribution to the total free energy (less than 0.1%), the comparison reveals that the Debye-Hückel estimate for the electrostatic energy (E_ϵ) used in the variational formalism is an overestimation (as large as five times the full, non-linear Poisson-Boltzmann at low l_B/b). In other words, the Debye-Hückel approximation underestimates the degree of screening, which is in agreement with other theoretical[107] and simulation results[116]. Note that the electrostatic energy in Fig. 5.5b includes all the charged species in the system except the ion-pairs formed on the chain by the adsorbing counterions. Nevertheless, contributions due to the electrostatic energy to total free energy are almost negligible and hence, do not affect α^* significantly.

This term-by-term comparison of the free energy components explains the origin of quantitative agreement in $\alpha^\star$. We have also carried out the same comparison at higher monomer densities. It is found that an additional discrepancy arises due to the polymer-solvent interaction energy and the solvent entropy (see Fig. 5.6). The origin of this discrepancy lies in the expansion of the $(1-\rho_p)\log(1-\rho_p)$ term. which is carried up to only terms quadratic in polymer density in the variational calculations (Appendix F). The higher order terms in the expansion are ignored in the variational calculations to carry out the analysis analytically, which limits the applicability of the variational theory to sufficiently low monomer concentrations. The discrepancy clearly highlights the breakdown of this procedure at high densities and questions the use of an effective excluded volume parameter in variational calculations. However, we have not made an attempt to compute the boundary of the disagreement between the theories because $\alpha^\star$ is insensitive to this discrepancy. Also, the variational formalism predicts the polymer-solvent interaction energy and the solvent entropy to be completely independent of electrostatic interaction strength l_B/b in the high density regime, in contrast to SCFT predictions of a weak dependence on l_B/b (see Fig. 5.6). This is a result of the constraint $R_g \leq R$ used in variational calculations for mimicking the confinement effects and shows the inability of the constraint to capture the confinement effects in an appropriate fashion.

5.4 Conclusions & Future Work

In summary, we have computed the effective charge of a single flexible polyelectrolyte chain using SCFT and compared it with the results obtained from a variational theory. It is found that for all sets of parameters, the effective degree of ionization ($\alpha^\star$) computed from SCFT and the variational theory is in quantitative agreement if one-loop fluctuation corrections are ignored in the latter. The origin of this agreement lies in the fact that $\alpha^\star$ is determined as an interplay of the ion-pair energy and the

translational entropy of the "adsorbed" counterions as well as of all "free" ions. The conformational entropy of the chain, the electrostatic energy involving the "free" ions and the chain, the polymer-solvent interaction energy and the solvent entropy do not play significant roles in affecting α^*.

The comparison of different components in free energy reveals that the Debye-Hückel approximation underestimates screening effects as compared to the Poisson-Boltzmann theory. Despite the fact that there are small discrepancies in the total free energy, the effective degree of ionization (α^*) comes out to be the same in SCFT and the variational theory. This clearly supports the variational calculations to be a very useful tool for a quick, easy and transparent estimation of α^*. Density fluctuations of the "free" ions are predicted to increase the equilibrium degree of ionization in order to enhance the screening. As this latter effect is not captured by SCFT calculations within the saddle-point approximation, the variational theory is a better computational tool for computing the effective charge of a polyelectrolyte chain.

A similar comparison can be carried out for a single polyelectrolyte chain in a poor solvent by taking three body interactions into account. Another possible direction of future research is the study of competitive counterion adsorption in the presence of counterions of mixed valencies using self-consistent field theory.

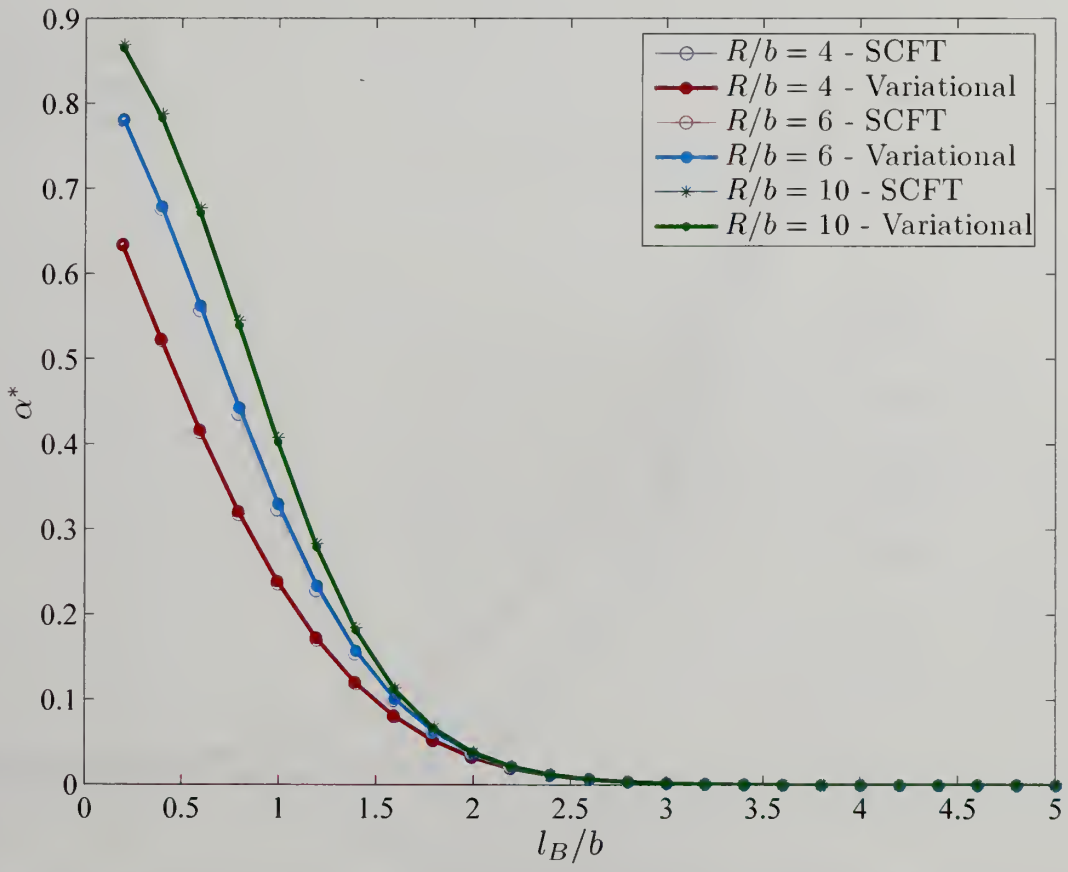

Figure 5.1. Comparison of $\alpha^\star$ computed using SCFT and the variational formalism (without one-loop corrections) for different values of R and l_B/b. $Z_p = -Z_c = -1, N = 100, c_s = 0.1M, \chi_{ps} = 0.45$ and $\delta = 3$.

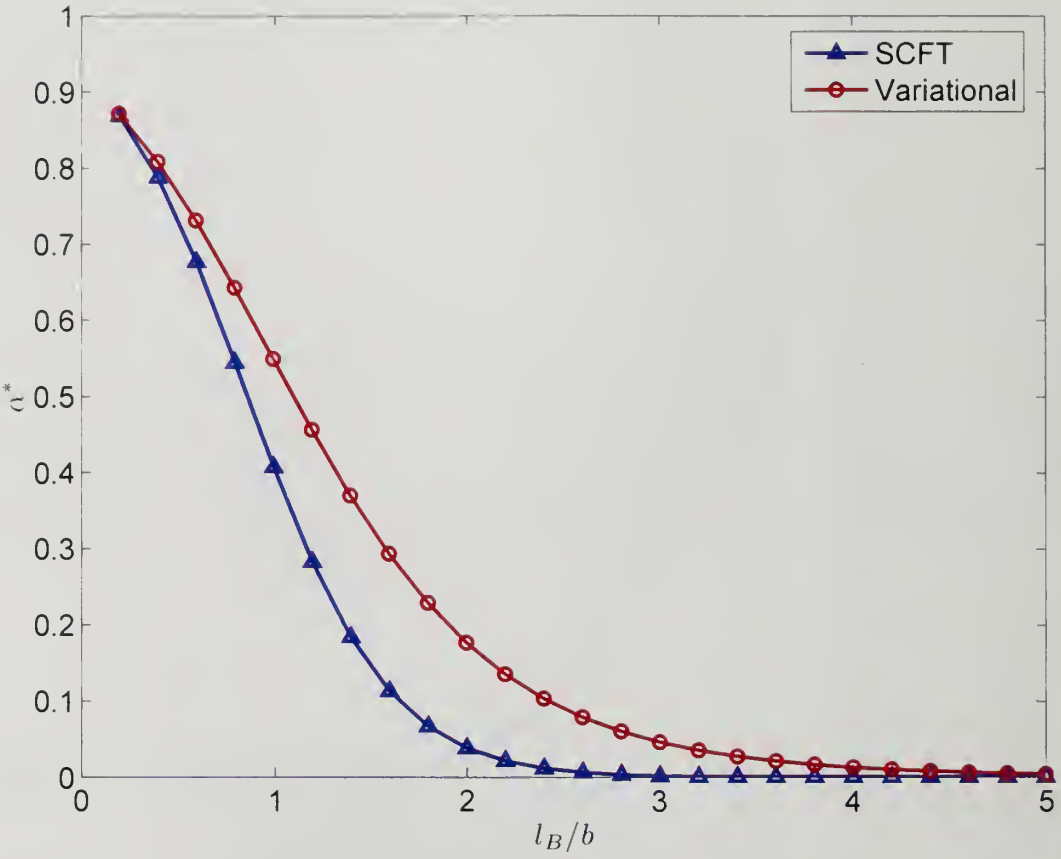

Figure 5.2. Comparison of SCFT and the variational formalism (with one-loop corrections) to illustrate the effect of correlations among small ions on the effective degree of ionization (α^*). Here, we have chosen $Z_p = -Z_c = -1, R/b = 10, N = 100, c_s = 0.1M, \lambda_{ps} = 0.45$ and $\delta = 3$. Plot for SCFT is the same as in Fig. 5.1.

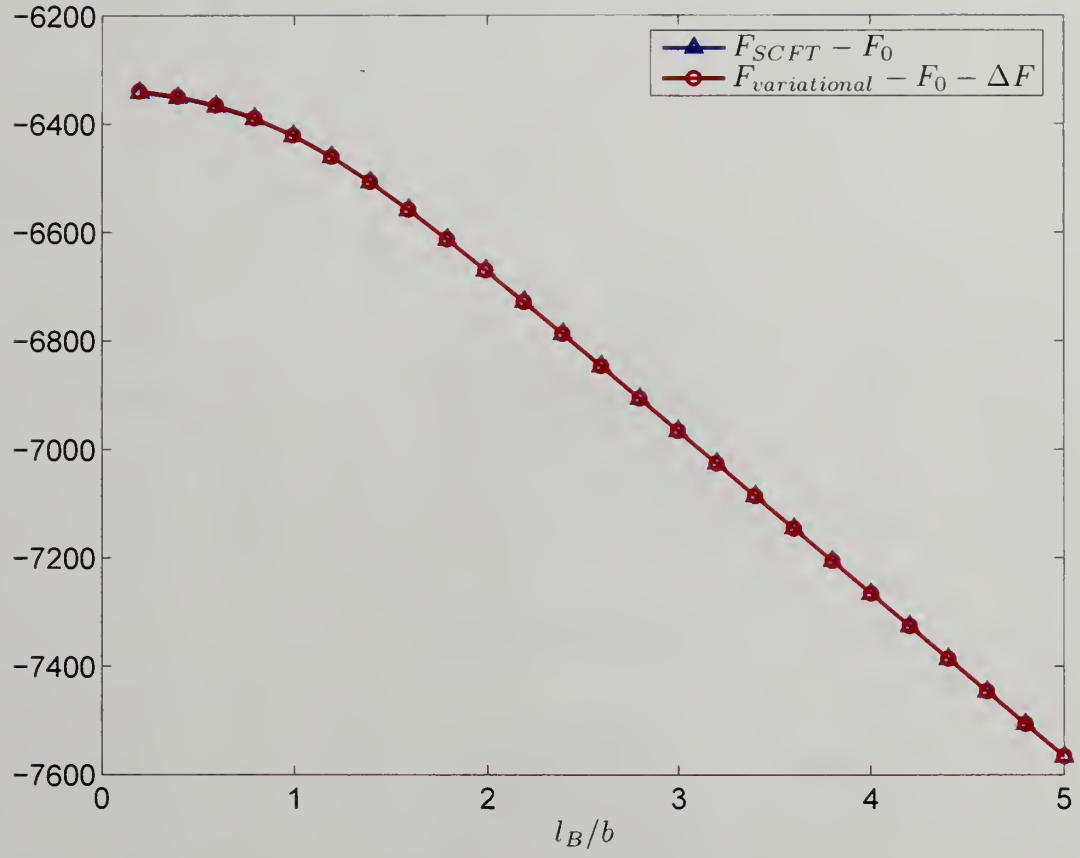

Figure 5.3. Comparison of total free energies (at equilibrium, i.e., for $\alpha = \alpha^\star$) obtained from SCFT and the variational calculations (without one-loop corrections). $Z_p = -Z_c = -1, R/b = 10, N = 100, c_s = 0.1M, \chi_{ps} = 0.45$ and $\delta = 3$.

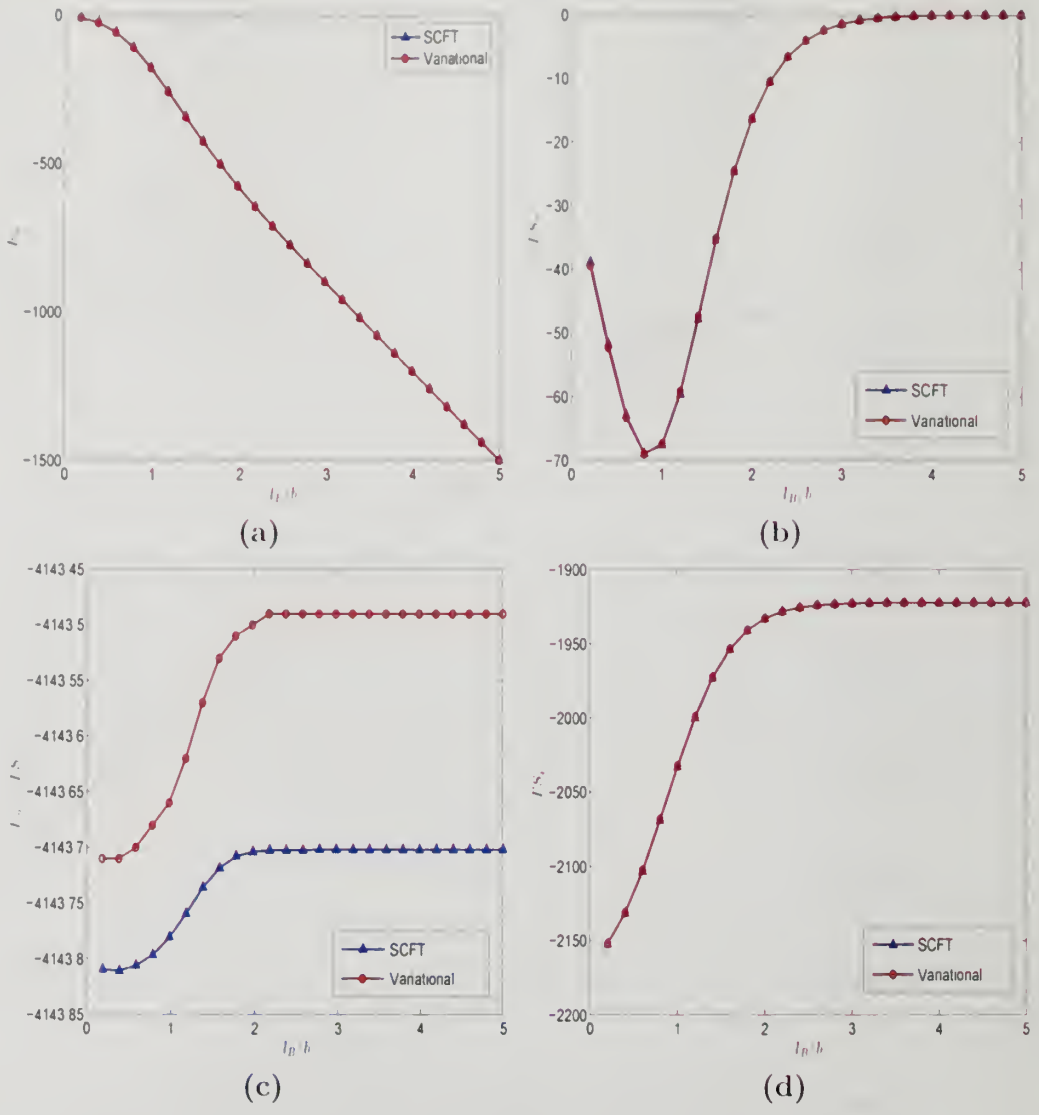

Figure 5.4. Comparison of major contributions to the free energies (presented in Fig. 5.3) obtained from SCFT and the variational formalism. (a) Ion-pair energy contributions (E_a), (b) translational entropy of the "adsorbed" counterions ($-TS_a$), (c) polymer-solvent interaction energy and solvent entropy($E_w - TS_s$); and (d) translational entropy of the "free" ions ($-TS_i$).

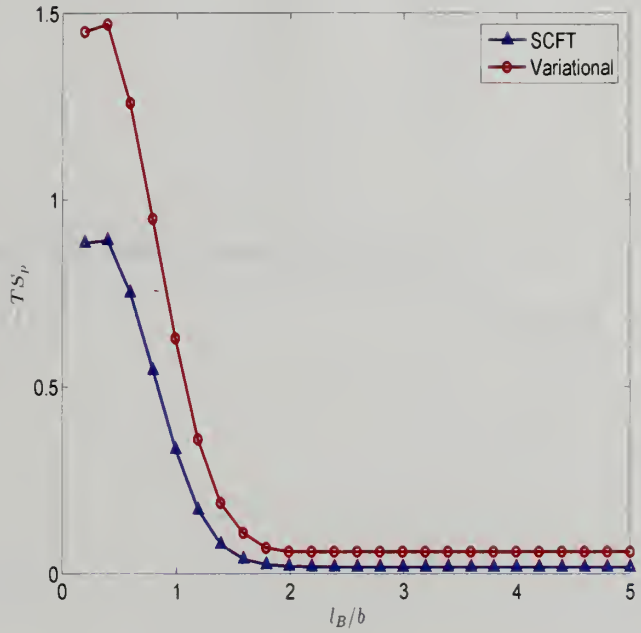

(a)

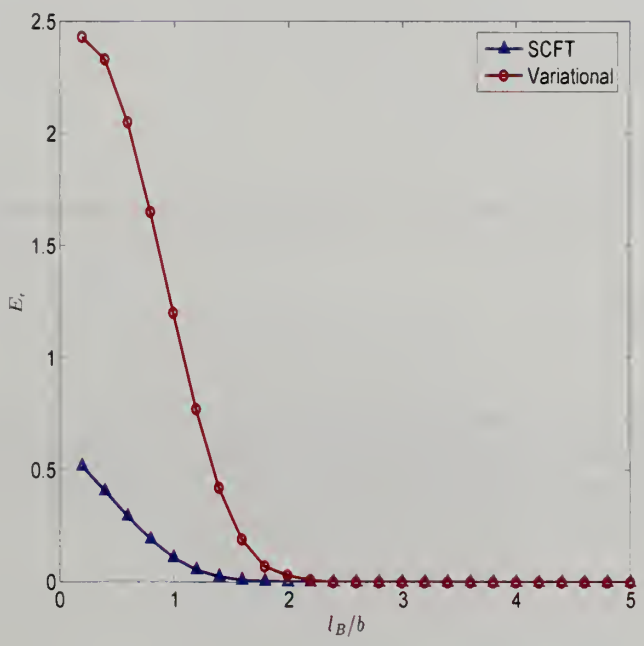

(b)

Figure 5.5. Comparison of minor contributions to the free energies (presented in Fig. 5.3). (a) Conformational entropy of the chain ($-TS_p$) and (b) electrostatic energy (E_ϵ).

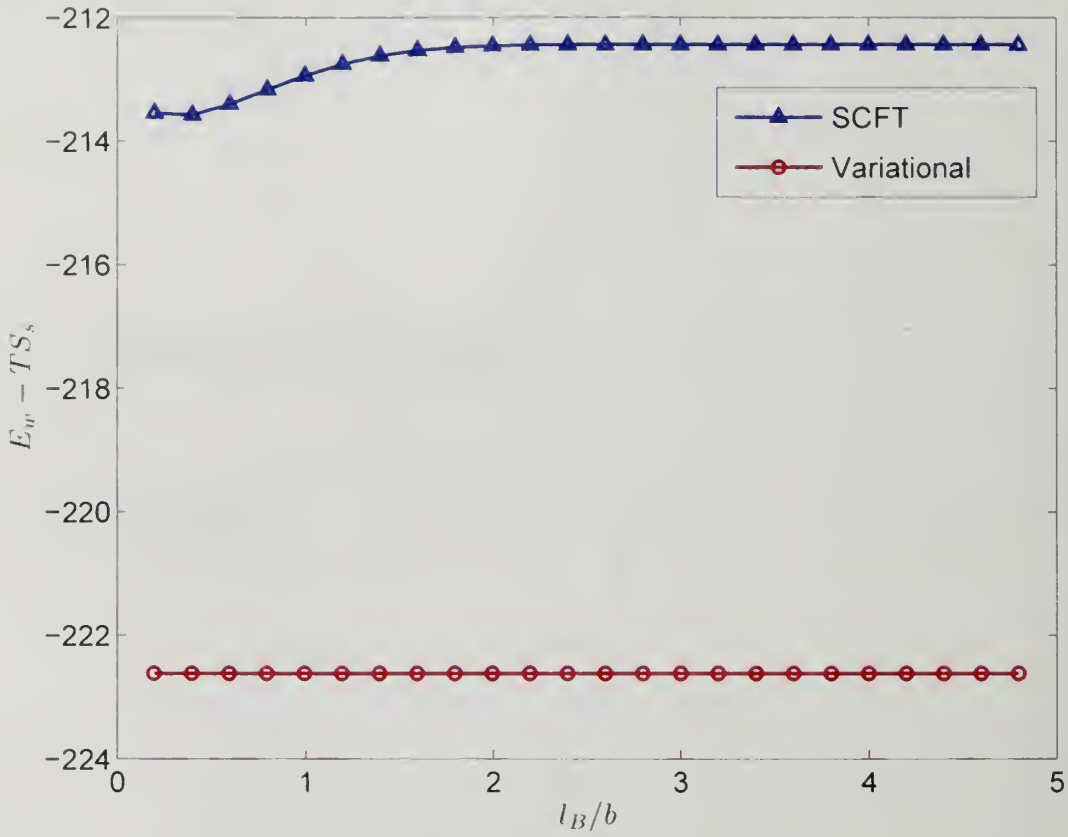

Figure 5.6. A discrepancy in the polymer-solvent interaction energy and solvent entropy contributions arise at high monomer densities. Here, we have plotted these contributions from SCFT and the variational formalism for $Z_p = -Z_c = -1$, $R/b = 4$, $N = 100$, $c_s = 0.1M$, $\chi_{ps} = 0.45$ and $\delta = 3$.

CHAPTER 6

ORIGIN OF TRANSLOCATION BARRIERS IN CHARGED SYSTEMS

6.1 Introduction

The phenomenon of translocation[61, 62, 63, 117, 118, 119, 120, 121, 122. 123, 124] of single polyelectrolyte molecules through narrow pores is ubiquitous in many biological processes[117, 118] and technology[61, 62, 119, 120, 121]. Both natural[61, 62, 119, 120] and synthetic[122] polyelectrolytes have been driven from one side of the pore to the other by an external force. The driving force is usually[61, 62, 63, 119, 120, 122] due to either an externally applied electric field or an osmotic imbalance (confinement-driven translocation[66, 67]). Independent of the nature of the driving force, the single-file translocation is envisioned as a two step process[121]. In the first step, one end of the chain arrives at the pore entrance and, in the second step, the chain is threaded through the pore from one side to the other. It has been imagined that both steps are associated with entropic barriers, with the first barrier associated with the loss of translational entropy of chain ends and the second barrier with reduction in conformational entropy of the chain.

The validity of the above conjecture for the experimentally relevant polyelectrolytes is not known. In fact, it is known[114] that the conformational entropy of a confined polyelectrolyte is only a weak contributor to the free energy where translational entropy of small ions and molecules (counterions, coions, and solvent) is dominant. Reorganization of counterion clouds around deforming polyelectrolyte chains can also contribute significantly to the free energy. Furthermore, the intrachain

electrostatic repulsion can stiffen the polymer enabling an easier access to the pore entrance. It is of fundamental interest to assess the relative magnitudes of various contributing factors to the free energy barrier associated with the translocation of a flexible polyelectrolyte molecule.

In this study, we focus on the first step in confinement driven translocation involving single flexible polyelectrolyte chain and provide a quantitative description of the free energy barriers for the chain end to find a specified location on the surface of a spherical cavity. By adopting the self-consistent-field theory (SCFT) for a flexible polyelectrolyte chain and combining with the Poisson-Boltzmann prescription for the electrolyte ions and counterions, we have computed the various energetic and entropic contributions to the free energy barrier. Since the localization of one chain end at a specific location on the surface of the cavity breaks the radial symmetry, we have solved the self-consistent coupled nonlinear differential equations in two dimensions with azimuthal symmetry. The translocation barrier for the first step is estimated by the free energy difference between "end-fixed" (one end fixed near the pore) and "free ends" (confined chain, which is free to move inside the cavity) equilibrium states of the chain. Using this approach, the free energy barriers for a Gaussian chain[69, 125] can be computed exactly and are purely entropic in nature due to lower degrees of conformational freedom in "end-fixed" state as compared with "free ends" and the absence of interactions. However, similar calculations for the excluded volume chain[68] have been carried out with in spherical symmetry and in the absence of solvent. For the case of polyelectrolyte translocation, these barriers are still unknown and the focus of this study.

6.2 Theory

We consider a single flexible polyelectrolyte chain of N Kuhn segments, each with length b in a spherical cavity of radius R filled with n_c monovalent counterions (pos-

itively charged) released by the chain in addition to n_γ ions of species $\gamma\,(=+,-)$ coming from added salt so that the whole system is globally electroneutral. Moreover, we assume that there are n_s solvent molecules (satisfying the incompressibility constraint after assuming the small ions to be pointlike) present in the cavity and for simplicity, each solvent molecule occupies a volume (v_s) same as that of the monomer (i.e. $v_s \equiv b^3$). The polyelectrolyte chain is represented as a continuous curve of length Nb and an arc length variable t is used to represent any segment along the backbone. Subscripts $p, s, c, +$ and $-$ are used to represent monomer, solvent , counterion from polyelectrolyte, positive and negative salt ions, respectively. The valency (with sign) of the charged species of type j is represented by Z_j and degree of ionization of the chain is taken to be α. Also, we consider smeared charge distribution so that each of the segments carries a charge $e\alpha Z_p$, where e is the electronic charge.

We use self-consistent field theory (SCFT) to compute the free energy of single flexible polyelectrolyte[114] in "free ends" and "end-fixed" states. Ignoring the electrostatic interactions between solvent molecules and small ions and; taking dielectric constant (ϵ) of the medium to be independent of temperature (T), the free energy (within saddle-point approximation) can be divided into enthalpic part due to excluded volume, electrostatic interactions and; entropic part due to small ions, solvent molecules and the polyelectrolyte chain. Denoting these contributions by E_w, E_e, S_i, S_s and S_p, respectively, the free energy can be written as

$$F^\star - F_0 \;=\; E_w + E_e - T(S_i + S_s + S_p). \tag{6.1}$$

where $F_0 = \frac{\rho_0}{2}\,(N w_{pp} + n_s w_{ss})$ is the self-energy contribution arising from excluded volume interactions, w_{ij} represents the strength of these interactions between species i and j. Superscript $\star$ denotes that the saddle point approximation has been used to compute the free energy. Explicit expressions for different contributions are given by

$$E_u = \chi_{ps} b^3 \int d\mathbf{r} \rho_p(\mathbf{r}) \rho_s(\mathbf{r}) + \rho_0 \int d\mathbf{r} \eta(\mathbf{r}), \tag{6.2}$$

$$E_\epsilon = \frac{1}{2} \int d\mathbf{r}\, \psi(\mathbf{r}) \rho_\epsilon(\mathbf{r}), \tag{6.3}$$

$$-TS_i = \sum_{j=c,+,-} \int d\mathbf{r}\, \rho_j(\mathbf{r}) \left\{ \ln \left[\rho_j(\mathbf{r}) \right] - 1 \right\}, \tag{6.4}$$

$$-TS_s = \int d\mathbf{r}\, \rho_s(\mathbf{r}) \left\{ \ln \left[\rho_s(\mathbf{r}) \right] - 1 \right\}. \tag{6.5}$$

$$-TS_p = -\ln Q_p - \int d\mathbf{r} \left[\left\{ Z_p \alpha \psi(\mathbf{r}) + w_p(\mathbf{r}) \right\} \rho_p(\mathbf{r}) + \rho_0 \eta(\mathbf{r}) \right]. \tag{6.6}$$

In these equations, $\rho_\beta(\mathbf{r})$ and $w_\beta(\mathbf{r})$ are respectively the macroscopic number density and the field experienced by species of type β, due to excluded volume interactions. All charged species experience electrostatic potential represented by $\psi(\mathbf{r})$ above, which is related to the local charge density $\rho_c(\mathbf{r}) = \sum_{j=c,+,-} Z_j \rho_j(\mathbf{r}) + Z_p \alpha \rho_p(\mathbf{r})$ by Poisson's equation, $\nabla^2_{\mathbf{r}} \psi(\mathbf{r}) = -4\pi l_B \rho_\epsilon(\mathbf{r})$. Note that $\psi(\mathbf{r})$ in these equations is dimensionless (in units of $k_B T/e$) and l_B is the Bjerrum length defined as $l_B = e^2/4\pi\epsilon_0\epsilon k_B T$, ϵ_0 is the permittivity of the vacuum, and ϵ is the uniform dielectric constant of the system. Moreover, χ_{ps} is the dimensionless Flory's chi parameter and $\rho_0 = (N + n_s)/\Omega \equiv 1/b^3$. Also, $\eta(\mathbf{r})$ is the Lagrange's multiplier introduced to enforce the incompressibility constraint.

At the saddle point, the macroscopic densities for the small molecules are related to the corresponding fields by the Boltzmann law, so that

$$\rho_s(\mathbf{r}) = \frac{n_s \exp\left[-w_s(\mathbf{r})\right]}{\int d\mathbf{r} \exp\left[-w_s(\mathbf{r})\right]}, \tag{6.7}$$

$$\rho_j(\mathbf{r}) = \frac{n_j \exp\left[-Z_j \psi(\mathbf{r})\right]}{\int d\mathbf{r} \exp\left[-Z_j \psi(\mathbf{r})\right]} \quad \text{for} \quad j = c, +, -. \tag{6.8}$$

The fields and densities are related to each other by the saddle point equations, given by

$$w_p(\mathbf{r}) = \chi_{ps} b^3 \rho_s(\mathbf{r}) + \eta(\mathbf{r}). \tag{6.9}$$

$$w_s(\mathbf{r}) = \chi_{ps} b^3 \rho_p(\mathbf{r}) + \eta(\mathbf{r}). \tag{6.10}$$

For the "free ends" state, the monomer density is dependent on the field by the relation

$$\rho_p(\mathbf{r}) \equiv \rho_p^f(\mathbf{r}) = \frac{\int_0^N dt\, q(\mathbf{r},t) q(\mathbf{r}, N-t)}{\int d\mathbf{r} q(\mathbf{r}, N)} \tag{6.11}$$

and for the "end-fixed" state, the relation becomes

$$\rho_p(\mathbf{r}) \equiv \rho_p^a(\mathbf{r}, \mathbf{r_a}) = \frac{\int_0^N dt\, G(\mathbf{r}, \mathbf{r_a}, t, 0) q(\mathbf{r}. N-t)}{\int d\mathbf{r} G(\mathbf{r}, \mathbf{r_a}, N, 0)}. \tag{6.12}$$

Superscript f and a depicts the free and anchored nature of the single chain. These monomer densities are related to the solvent density by incompressibility constraint, $\rho_p(\mathbf{r}) + \rho_s(\mathbf{r}) = \rho_0$.

The function $q(\mathbf{r}, t)$ is the probability of finding segment t at location $\mathbf{r}$, when starting end of the chain can be anywhere inside the spherical cavity and satisfies the modified diffusion equation

$$\frac{\partial q(\mathbf{r},t)}{\partial t} = \left[\frac{b^2}{6} \nabla_{\mathbf{r}}^2 - \{Z_p \alpha \psi(\mathbf{r}) + w_p(\mathbf{r})\}\right] q(\mathbf{r}. t), \tag{6.13}$$

along with the initial condition $q(\mathbf{r}, 0) = 1$. Similar to $q(\mathbf{r}, t)$, the Green's function, $G(\mathbf{r}, \mathbf{r_a}, t, 0)$, is the probability of finding segment t at location $\mathbf{r}$, when starting end of the chain is at $\mathbf{r_a}$. It also satisfies Eq. (6.13) but with initial condition $G(\mathbf{r}, \mathbf{r_a}. 0, 0) = \delta(\mathbf{r} - \mathbf{r_a})$, where δ represents the three dimensional delta function. The partition function of the chain (Q_p) can be written in terms of these functions. Specifically, for the "free ends" state, it is given by $Q_p \equiv Q_p^f = \int d\mathbf{r} q(\mathbf{r}, N)$ and for the "end-fixed" state, the partition function becomes $Q_p \equiv Q_p^a = \int d\mathbf{r} G(\mathbf{r}, \mathbf{r_a}, N. 0)$.

We include the effect of confinement by solving Eqs. (6.7 - 6.13) along with the Poisson's equation using Dirichlet boundary conditions for $w_\beta(\mathbf{r}), \psi(\mathbf{r}), q(\mathbf{r}. t)$ and

$G(\mathbf{r}, \mathbf{r_a}, t, 0)$. For the results presented in this letter, we have fixed one end of the chain for "end-fixed" state at $\mathbf{r_a} = [(R - 0.5)b, \pi/2, 0]$ in spherical co-ordinates .

6.3 Results

We have solved the above non-linear set of equations in two dimensions using spherical polar co-ordinates $(r, \theta = \pi/2, \phi)$ so that $r \in [0, R]$ and $\phi \in [0, 2\pi]$. Instead of solving these equations in real or Fourier space, we use split-step pseudo-spectral method[126] employing fast Fourier transform (FFT) and sine transform, which allows a faster and accurate computation of the densities and free energies. It is convenient to solve for $f(\mathbf{r}, t) = rq(\mathbf{r}, t)$ rather than solving for $q(\mathbf{r}, t)$ directly. In spherical polar co-ordinates, solution of Eq. (4.8) is obtained after expanding $f(\mathbf{r}, t) = \sum_{l=0}^{L} f_l(r, t)e^{il\phi}$ and using $\nabla^2_{\mathbf{r}} = \frac{1}{r^2}\left[\frac{\partial}{\partial r}(r^2\frac{\partial}{\partial r}) + \frac{\partial^2}{\partial \phi^2}\right]$. Writing Eq. (6.13) in terms of $f(\mathbf{r}, t)$ and using Baker-Hausdroff formula[126], the solution is given by the propagation relation

$$\begin{aligned} f(\mathbf{r}, t + dt) \simeq & \exp\left[-dt\, w(\mathbf{r})/2\right] \exp\left[dt \frac{b^2}{12} \frac{1}{r^2} \frac{\partial^2}{\partial \phi^2}\right] \exp\left[dt \frac{b^2}{6} \frac{\partial^2}{\partial r^2}\right] \\ & \exp\left[dt \frac{b^2}{12} \frac{1}{r^2} \frac{\partial^2}{\partial \phi^2}\right] \exp\left[-dt\, w(\mathbf{r})/2\right] f(\mathbf{r}, t), \end{aligned} \tag{6.14}$$

where $w(\mathbf{r}) = Z_p \alpha \psi(\mathbf{r}) + w_p(\mathbf{r})$. Also, the multiplication by r leads to $f(0, \phi, t) = 0$ for all t's so that numerical problems at $r = 0$, due to division by 0 in the Laplacian are avoided. Another major advantage of the transformation is that now, the equations are to be solved with periodic boundary conditions. So, FFT and sine transform can be used to implement the exponential of operators. Exponential of ϕ dependent operator on the right hand side of Eq. (6.14) is applied in Fourier space after taking one forward and one backward FFT. r dependent operator is applied after taking forward sine transform defined as

$$f_l(r, t) = \sum_{k=1}^{K} g_k(l, t) \sin(k\pi r/R), \tag{6.15}$$

and the corresponding inverse sine transform, so that boundary conditions for f are always satisfied during the computations. In total, each time step requires two FFTs with respect to ϕ and one sine transform with respect to r in each direction (forward and backward). The same technique has been used for solving $G(\mathbf{r}, \mathbf{r_a}, t, 0)$.

To solve Poisson's equation, $\nabla^2_{\mathbf{r}}\psi(\mathbf{r}) = -4\pi l_B \rho_e(\mathbf{r})$, we use a similar strategy. We solve for $h(\mathbf{r}) = r\psi(\mathbf{r})$, so that Poisson's equation becomes

$$\left[\frac{\partial^2}{\partial r^2} + \frac{1}{r^2}\frac{\partial^2}{\partial \phi^2}\right] h(\mathbf{r}) \;=\; -4\pi l_B r \rho_e(\mathbf{r}). \tag{6.16}$$

Now, expanding $h(\mathbf{r}) = \sum_{l=0}^{L} h_l(r) e^{il\phi}$, the equation for components h_l becomes

$$\left[\frac{\partial^2}{\partial r^2} - \frac{l^2}{r^2}\right] h_l(r) \;=\; -4\pi l_B \mathrm{FFT}_\phi \left[r\rho_e(\mathbf{r})\right]. \tag{6.17}$$

Here, the subscript ϕ means, FFT is to be taken with respect to ϕ. These sets of equations can be readily solved for the real and imaginary parts of $h_l(r)$ due to the tridiagonal nature of the finite difference equation set obtained with the constraints $h_l(0) = h_l(R) = 0$. Now, taking backward FFT with respect to ϕ, $h(\mathbf{r})$ is obtained.

Starting from an initial guess for fields, $w_p(\mathbf{r}), w_s(\mathbf{r})$ and $\psi(\mathbf{r})$, new fields and densities are computed using the method described above. Simple mixing[126] is used to obtain the new guess and the iterative process is continued until the difference in newly computed and the guessed fields is of the order of 10^{-7}. Using the converged solution for the fields and densities, free energies for the "free ends" (i.e. $F^\star \equiv F_f$) and "end-fixed" ($F^\star \equiv F_a$) state are computed. The results presented here were obtained by using $L = 32, K = 32$ and $dt = 0.1$ after optimizing the numerical algorithm for speed and accuracy.

After solving these equations, typical monomer and electrostatic potential distribution for the "free-ends" and "end-fixed" state are obtained as shown in Fig. 6.1.

It is clear that the electrostatic potential gets modulated with the monomer distribution as one end of the chain is fixed near the boundary (compare Fig. 6.1b and 6.1d). In other words, distributions of counterions and coions get changed due to the change in monomer distribution (cf. Eq. 4.6). In Fig. 6.2, we have plotted the free energy difference (or barriers) between the "end-fixed" and "free ends" state for different values of N and R. For comparison purposes, the barriers for the chains when electrostatics is switched off (i.e. self-avoiding walk chain), are also plotted. It is clear that the free energy barriers for polyelectrolytes are almost identical to those for the corresponding self-avoiding walk chain at higher monomer densities and they differ only by a small amount in lower density regime.

In order to identify the origin of these barriers for polyelectrolytes, we have plotted different energetic and entropic constituents of the barriers for one particular set of parameters in Fig. 6.3. It is found that the dominant contribution to the barriers comes from the difference in conformational entropy of the chain in the "free ends" and "end-fixed" states. Difference in solvent entropy and energy due to excluded volume interactions between different constituents plays a role, although meager, only when chain length is small and solvent is the major component in the system. Contributions due to the difference in entropy of small ions and electrostatic energy are negligible in comparison with other contributions. These results indeed support the entropic nature of the free energy barriers. Furthermore, these results are quite robust (within $1 - 2k_BT$) for a vast range of parameters involving $\alpha, l_B/b, \lambda_{ps}$ and c_s.

6.4 Conclusions & Future Work

In summary, we find the remarkable result that even though the conformational entropy of a flexible polyelectrolyte chain is a minor contributor to the chain free energy, the free energy barrier is essentially entirely due to the change in the conformational entropy of the chain, for experimentally relevant highly confined systems.

Even more remarkably, the free energy barrier for a flexible polyelectrolyte is not significantly different from that for an uncharged self-avoiding chain. This result thus enables the implementation of the various known results for the translocation of neutral polymer chains without embarking further on the more demanding simulations of polyelectrolyte translocation with long range forces. Furthermore. it is to be noted that the entropically driven free energy barrier for placing one chain end at the pore entrance is about $9 - 10k_BT$, which is within the access of energy released in one event of ATP hydrolysis[117]. Studying the effect of external forces such as applied electric field on the free energy barriers are some of the directions for future work, where the system may be far from equilibrium and hydrodynamics, entanglements play an important role. Extending these computations to include the effect of sequence heterogeneity on translocation barriers may be the focus of future work.

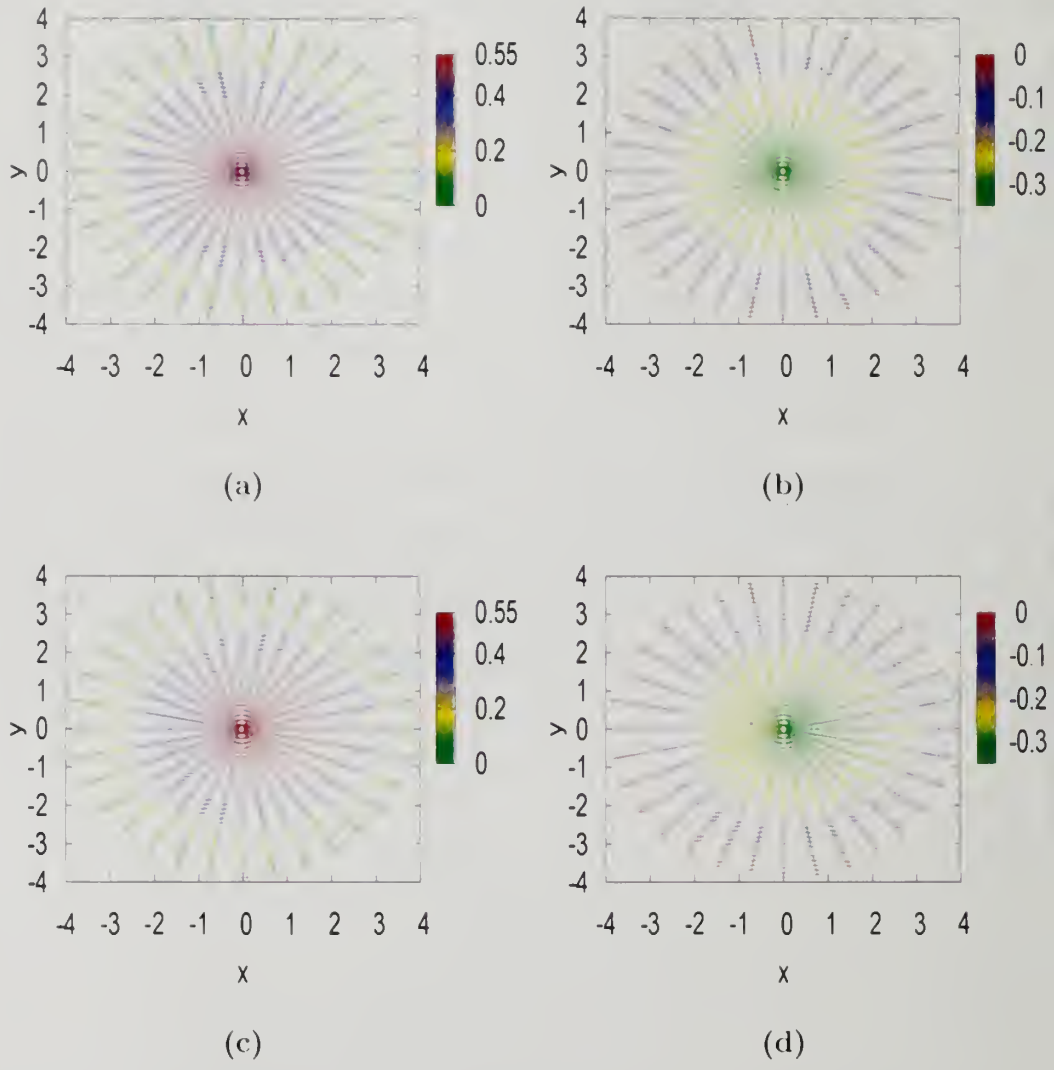

Figure 6.1. Two dimensional monomer and electrostatic potential distribution for the single flexible polyelectrolyte chain in "free-ends" [(a) and (b), respectively] and "end-fixed" state [(c) and (d), respectively]. In these plots, $l_B/b = 3, \alpha = 0.1, c_s = 0.1M, N = 50, R/b = 4$ and $\chi_{ps} = 0.45$. For plots (c) and (d), one end is anchored at $[x, y] = [(R - 0.5)b, 0]$.

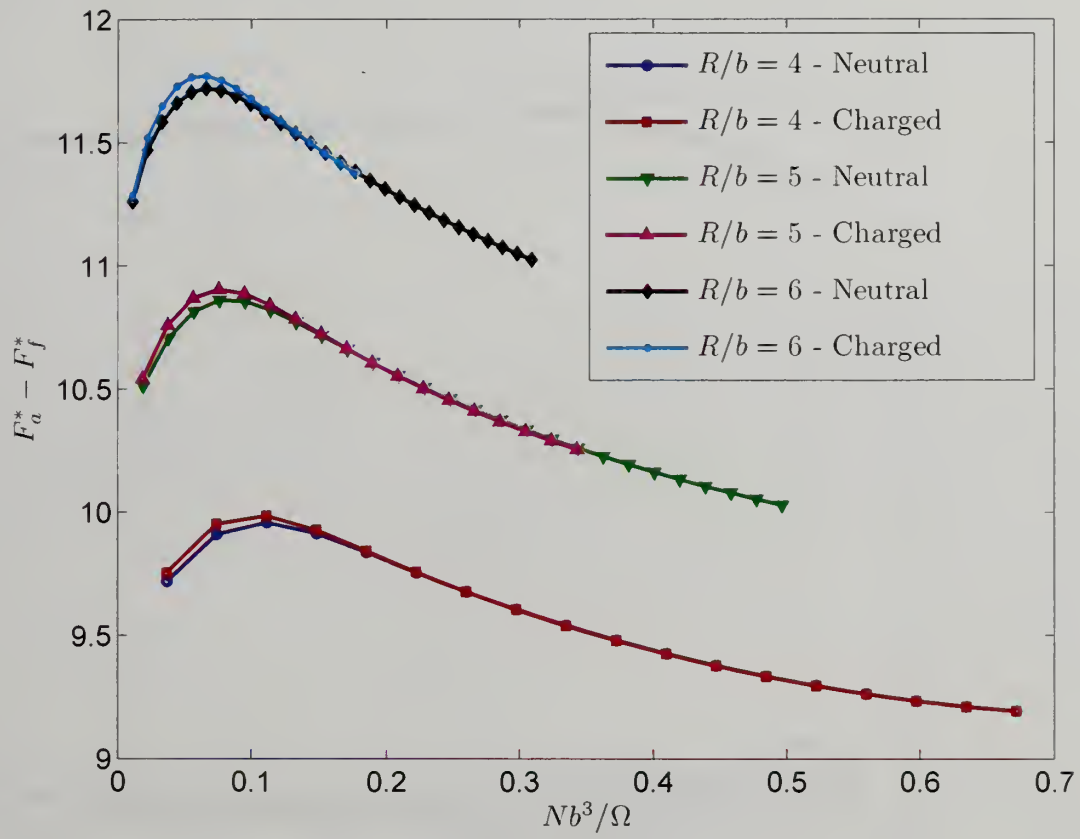

Figure 6.2. Free energy barriers for the chain end to find the hole on the surface of neutral spherical cavity - effect of R/b and N. In these plots, $l_B/b = 3, \alpha = 0.1, c_s = 0.1M$ and $\chi_{ps} = 0.45$

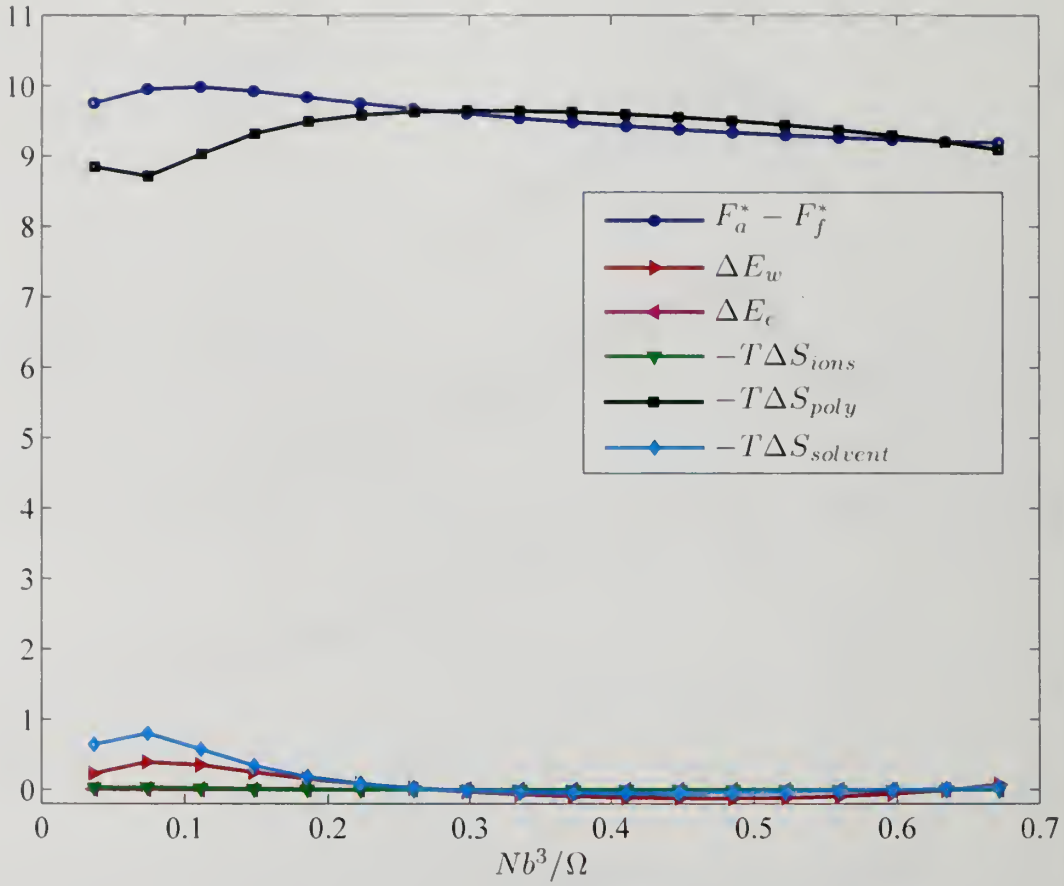

Figure 6.3. Different constituents of the free energy barriers. It is shown that the contributions due to the chain conformational entropy dominates over all other contributions. In these plots, $l_B/b = 3, \alpha = 0.1, c_s = 0.1M, R/b = 4$ and $\chi_{ps} = 0.45$ and the plot for free energy barrier is same as in Fig. 6.2.

APPENDIX A

FUNCTIONAL DERIVATIVES

Here, we present the details of the functional derivatives that need to be carried out as described in section (2.4) in Chapter 2. One very useful functional derivative rule is used extensively in these calculations according to which, for any arbitrary functional $g(\mathbf{r})$

$$\frac{\delta g(\mathbf{r})}{\delta g(\mathbf{r}')} = \delta(\mathbf{r}-\mathbf{r}'). \tag{A.1}$$

Using Eq. (A.1), functional derivatives of the functional f given in Eq. (2.35) with respect to all of the collective variables except $w_m(\mathbf{r})$ and $\psi(\mathbf{r})$ can be evaluated trivially. So, in this Appendix, we present how to evaluate $\frac{\delta f}{\delta w_m}$ and $\frac{\delta f}{\delta \psi}$.

Carrying out functional derivative of f with respect to $w_m(\mathbf{r})$ gives

$$\begin{aligned}\frac{\delta f\{w_m(\mathbf{r})\}}{\delta w_m(\mathbf{r}')} &= -i\rho_m(\mathbf{r}') - n_p\frac{\delta \ln Q_p}{\delta w_m(\mathbf{r}')} \\ &= -i\rho_m(\mathbf{r}') - \frac{n_p}{Q_p}\frac{\delta Q_p}{\delta w_m(\mathbf{r}')}.\end{aligned} \tag{A.2}$$

Note here that Q_p is the partition function of a single chain whose ends can be anywhere in space. In order to evaluate the functional derivative of Q_p, we use some

properties of the partition function of a single chain with its two ends *fixed* in space (say, G). Let's first relate these two quantities by rewriting Q_p as

$$Q_p = \int d\mathbf{r} \int d\mathbf{r}'' G(\mathbf{r}, 0, \mathbf{r}'', Nb) \tag{A.3}$$

so that

$$G(\mathbf{r}, 0, \mathbf{r}'', Nb) = \int_{\mathbf{r}}^{\mathbf{r}''} D[\mathbf{R}] \exp\left[-H\left\{\mathbf{R}(t)\right\}\right] \delta\left[\mathbf{r} - \mathbf{R}(0)\right] \delta\left[\mathbf{r}'' - \mathbf{R}(Nb)\right], \tag{A.4}$$

where

$$H = \frac{3}{2b} \int_0^{Nb} dt \left(\frac{\partial \mathbf{R}(t)}{\partial t}\right)^2 + \frac{i}{b} \sum_m \int dt \left[e Z_m \alpha_m \psi(\mathbf{R}(t)) + w_m(\mathbf{R}(t))\right]. \tag{A.5}$$

In Eq. (A.4), $G(\mathbf{r}, 0, \mathbf{r}'', Nb)$ is the partition function for a single chain with one end at $\mathbf{r} = \mathbf{R}(0)$ and the other end at $\mathbf{r}'' = \mathbf{R}(Nb)$, whose monomers experience fields $ieZ_m\alpha\psi(\mathbf{R}(t)) + iw_m(\mathbf{R}(t))$. Physically, partition function of the chain, whose ends can be anywhere in space can be obtained after integrating over all the possible positions of ends (cf. Eq. (A.3)). The function G can be shown to have properties[7, 9]

$$G(\mathbf{r}, 0, \mathbf{r}'', Nb) = \int d\mathbf{r}' G(\mathbf{r}, 0, \mathbf{r}', t) G(\mathbf{r}', t, \mathbf{r}'', Nb) \tag{A.6}$$

Using this property of G

$$\begin{aligned}
\frac{\delta Q_p}{\delta w_m(\mathbf{r}')} &= \int d\mathbf{r} \int d\mathbf{r}'' \frac{\delta G(\mathbf{r}, 0, \mathbf{r}'', Nb)}{\delta w_m(\mathbf{r}')} \\
&= -\frac{i}{b} \int d\mathbf{r} \int d\mathbf{r}'' \left[\int dt\, G(\mathbf{r}, 0, \mathbf{r}', t) G(\mathbf{r}', t, \mathbf{r}'', Nb)\right] \\
&= -\frac{i}{b} \int dt \left[\int d\mathbf{r} G(\mathbf{r}, 0, \mathbf{r}', t)\right] \left[\int d\mathbf{r}'' G(\mathbf{r}', t, \mathbf{r}'', Nb)\right]
\end{aligned}$$

$$= -\frac{i}{b}\int dt\, q(\mathbf{r}',t)q^{\star}(\mathbf{r}',Nb-t) \tag{A.7}$$

where $q(\mathbf{r}',t)$ and $q^{\star}(\mathbf{r}',Nb-t)$ are the probabilities of finding t^{th} segment at $\mathbf{r}$ starting from $t=0$ and $t=Nb$ end of the chain, respectively, which can be anywhere in the space. Mathematically, these probabilities are defined as

$$q(\mathbf{r}',t) = \int d\mathbf{r} G(\mathbf{r},0,\mathbf{r}',t). \tag{A.8}$$

$$q^{\star}(\mathbf{r}',Nb-t) = \int d\mathbf{r}'' G(\mathbf{r}',t,\mathbf{r}'',Nb). \tag{A.9}$$

Also, note that the partition function Q_p can also be written in terms of these probabilities as as

$$Q_p = \int d\mathbf{r}\int d\mathbf{r}'' G(\mathbf{r},0,\mathbf{r}'',Nb) = \int d\mathbf{r}''\left[\int d\mathbf{r} G(\mathbf{r},0,\mathbf{r}'',Nb)\right] = \int d\mathbf{r}''\, q(\mathbf{r}'',Nb) \tag{A.10}$$

or

$$Q_p = \int d\mathbf{r}\left[\int d\mathbf{r}'' G(\mathbf{r},0,\mathbf{r}'',Nb)\right] = \int d\mathbf{r}\, q^{\star}(\mathbf{r},Nb) \tag{A.11}$$

Using Eqs. (A.2, A.7 and A.10),

$$\frac{\delta f\{w_m(\mathbf{r})\}}{\delta w_m(\mathbf{r}')} = -i\rho_m(\mathbf{r}') + \frac{in_p}{b}\frac{\int dt\, q(\mathbf{r}',t)q^{\star}(\mathbf{r}',Nb-t)}{\int d\mathbf{r}\, q(\mathbf{r},Nb)}. \tag{A.12}$$

It has been shown by Edwards[1, 3] and later on by Helfand[4] that the function $G(\mathbf{r},0,\mathbf{r}',t)$ satisfies a modified diffusion equation

$$\frac{\partial G(\mathbf{r},0,\mathbf{r}',t)}{\partial t} = \left[\frac{b}{6}\nabla^2_{\mathbf{r}'} - \frac{i}{b}\{eZ_m\alpha_m\psi(\mathbf{r}') + w_m(\mathbf{r}')\}\right] G(\mathbf{r},0,\mathbf{r}',t) \tag{A.13}$$

for $t \in [0, Nb]$, subjected to the initial condition $G(\mathbf{r}, 0, \mathbf{r}', 0) = \delta(\mathbf{r} - \mathbf{r}')$ and the boundary condition $G(\mathbf{r}, 0, \mathbf{r}', t) \rightarrow 0$ as $\mid \mathbf{r} - \mathbf{r}' \mid \rightarrow \infty$. Similarly, $G(\mathbf{r}, t, \mathbf{r}', Nb)$ satisfies

$$\frac{\partial G(\mathbf{r}, t, \mathbf{r}', Nb)}{\partial t} = -\left[\frac{b}{6}\nabla_{\mathbf{r}}^2 - \frac{i}{b}\{eZ_m\alpha_m\psi(\mathbf{r}) + w_m(\mathbf{r})\}\right] G(\mathbf{r}, t, \mathbf{r}', Nb). \qquad \text{(A.14)}$$

Integrating over the position of one of the ends (cf. Eqs. (A.8 and (A.9)) in Eqs. (A.13) and (A.14), it can be shown that q and q^* satisfy the same set of modified diffusion equations with the initial conditions $q(\mathbf{r}, 0) = 1$ and $q^*(\mathbf{r}, 0) = 1$, respectively.

Using the same methodology for computing derivatives, functional derivative with respect to $\psi(\mathbf{r})$ can also be evaluated in a straightforward way.

APPENDIX B

NUMERICAL TECHNIQUES

To compute the free energy within saddle-point approximation. the coupled non-linear equations, which include second degree partial differential equations such as the modified diffusion and Poisson-Boltzmann equations are to be solved. In this Appendix, different numerical techniques used to solve these equations are presented. In general, these numerical techniques can be classified into three classes : finite-difference, spectral and pseudo-spectral methods. Finite-difference methods are straightforward to implement after approximating partial derivatives by finite difference approximation schemes. However, depending on the problem at hand, the accuracy and convergence attained using these methods may not be what is desired for the computations. In certain problems. accuracy is the main issue, sometimes even at the cost of memory. That's the reason more accurate (but difficult to implement) numerical techniques like spectral and pseudo-spectral methods have been developed. These techniques provide higher accuracy and better convergence. However, these techniques have a common drawback that they are very specialized and work for problems with specific boundary conditions. The choice of the numerical technique for a certain problem depends on the accuracy, convergence and memory issues, which appear during the implementation of different schemes.

Finite-difference methods for solving second degree partial differential equations such as Forward Time Centered Space (FTCS), Crank-Nicholson etc. are well-documented in many textbooks[9, 75]. Here, we present only the details of spectral and pseudo-spectral methods for solving the modified diffusion for *given* fields and the

Poisson-Boltzmann equation for given charge density and *space independent* dielectric constant. For a general discussion, we consider the equations of the form

$$\frac{\partial h(\mathbf{r},t)}{\partial t} = \left[\frac{b^2}{6}\,\nabla^2_{\mathbf{r}} - w(\mathbf{r})\right] h(\mathbf{r},t), \tag{B.1}$$

where $w(\mathbf{r})$ is known *a priori* along with the intial condition $h(\mathbf{r},0)$ and the equation corresponds to the time-dependent modified diffusion equation. Similarly, a general Poisson-Boltzmann equation is considered of the form

$$\nabla^2_{\mathbf{r}} \psi(\mathbf{r}) = -f\left\{\psi(\mathbf{r})\right\}, \tag{B.2}$$

when $f\left\{\psi(\mathbf{r})\right\}$ is known.

B.1 Spectral Method - Method of Basis Functions

To solve Eq. (B.1), let's approximate space dependent quantities such as $h(\mathbf{r},t)$ and $w(\mathbf{r})$ by a *finite* series in terms of orthonormal basis functions i.e., $h(\mathbf{r},t) \simeq \sum_{j=1}^{n} h_j(t) g_j(\mathbf{r})$ and $w(\mathbf{r}) \simeq \sum_{j=1}^{n} w_j g_j(\mathbf{r})$, where $g_j(\mathbf{r})$ represents the appropriate basis function of order j and n is the number of such basis functions required to correctly represent the functions $h(\mathbf{r},t)$ and $w(\mathbf{r})$. The choice of n depends on the desired accuracy for the computations. In order to solve Eq. (B.1), the basis functions must have the following properties:

(a) Basis functions,$g_j(\mathbf{r})$, must be the eigenfunctions of the Laplacian operator i.e.,

$$\nabla^2_{\mathbf{r}} g_j(\mathbf{r}) = -\frac{\lambda_j}{L^2} g_j(\mathbf{r}), \tag{B.3}$$

where $j = 2, 3, \cdots, n$, and L is the length scale describing the volume of the system, and λ_j's are the eigenvalues of the Laplacian. The first basis function ,$g_j(\mathbf{r})$, is chosen to be a constant and normally unity i.e., $g_1(\mathbf{r}) = 1$.

(b) These basis functions must be the orthonormal basis set i.e., they must satisfy $\frac{1}{\Omega}\int d\mathbf{r} g_j(\mathbf{r})g_k(\mathbf{r}) = \delta_{jk}$, Ω being the volume of the system ($\sim L^3$).

(c) These basis functions must satisfy the boundary conditions.

In this technique, the basis functions are ordered starting with $g_1(\mathbf{r}) = 1$ such that λ_j is a non-decreasing series. Also, the constraints on the fields and densities are taken care of by fixing the first term in the series, which is independent of $\mathbf{r}$. Now, the goal is to compute the coefficients $h_j(t)$ in the finite series expansion for $h(\mathbf{r}, t)$ using the initial values of these coefficients $h_j(0)$ (which comes from the known initial condition) and the known values for w_j's (due to the known values for $w(\mathbf{r})$). Using the finite series expansion and orthonormal property of the basis functions, Eq. (B.1) can be transformed into a set of equations for coefficients $h_j(t)$ as shown below.

$$\frac{\partial h_k(t)}{\partial t} = \sum_{j=1}^{n} A_{kj} h_j(t) \tag{B.4}$$

$$\text{where} \quad A_{kj} = \frac{-\lambda_k b^2}{6L^2}\delta_{kj} - \sum_{i=1}^{n} w_i \Gamma_{ijk} \tag{B.5}$$

where the function Γ_{ijk} is defined as $\Gamma_{ijk} = \frac{1}{\Omega}\int d\mathbf{r} g_i(\mathbf{r})g_j(\mathbf{r})g_k(\mathbf{r})$. Now, the equations for $h_k(t)$ in the matrix form become

$$\frac{\partial h(t)}{\partial t} = Ah(t), \tag{B.6}$$

where $h(t)$ is a column vector and A is a square matrix given by

$$h(t) = \begin{bmatrix} h_1(t) \\ h_2(t) \\ h_3(t) \\ \vdots \\ h_n(t) \end{bmatrix}, \quad A = \begin{bmatrix} A_{11} & A_{12} & \dots & A_{1n} \\ A_{21} & A_{22} & \dots & A_{2n} \\ A_{31} & A_{32} & \dots & A_{3n} \\ \vdots & \vdots & \vdots & \vdots \\ A_{n1} & A_{n2} & \dots & A_{nn} \end{bmatrix}$$

Formal solution of Eq. (B.6) is given by $h(t) = e^{At}h(0)$, where $h(0)$ is given by the initial condition for $h(\mathbf{r}, t)$. e^{At} is the exponential of the matrix At and can be calculated by diagonalizing the matrix At. Note here that t is a scalar.

Computation of exponential of a matrix is a numerically intensive job and very difficult in general. However, for real, symmetric square matrices such as A here, it can be calculated by diagonalizing the matrix after computing its eigenvalues and eigenvectors. Approach to calculate exponential of a matrix is : to compute the exponential of a matrix times a scalar, we need to solve the matrix problem $\frac{dX(t)}{dt} = AX(t)$ for a given $X(0)$, when the matrix A is diagonalizable into a diagonal matrix d. Due to the fact that A can be diagonalized, there exists a non-singular matrix P such that $P^{-1}AP = d$. Now, to solve the matrix equation for X, we change variables as

$$X(t) = PY(t) \tag{B.7}$$

$$\Rightarrow \frac{dX(t)}{dt} = AX(t) \Rightarrow \frac{dY(t)}{dt} = dY(t), \quad Y(0) = P^{-1}X(0) \tag{B.8}$$

$$\Rightarrow X(t) = P\text{diag}\left[e^{d_1 t}, e^{d_2 t}, \cdots e^{d_n t}\right] P^{-1}X(0), \tag{B.9}$$

where diag stands for a diagonal matrix. If the matrix P is made up of eigenvectors of matrix A as its columns then for symmetric, real matrices it is orthogonal i.e. $P^T = P^{-1}$, where superscripts T and -1 represent the transpose and inverse of the matrix, respectively. This means, for real, symmetric square matrices such as A here, exponential of the matrix At is given by

$$e^{At} = P\,\text{diag}\left[e^{d_1 t}, e^{d_2 t}, \cdots e^{d_n t}\right] P^T, \tag{B.10}$$

where d_j is the j^{th} eigenvalue of matrix A and P is a matrix whose columns are made up of the eigenvectors of the matrix A.

The computation of exponential of matrix is in fact the most expensive part in the numerical solution of modified diffusion equations. Also, as we can see that as the order of the matrix (n) increases, which in turn determines the accuracy of the method, the computational cost increases substantially. That is the reason, this method should be used in problems, where low values of n meet the accuracy requirements. From our experience, problems requiring $n \leq 30$ can be readily solved using this technique. The second issue with this technique is the availability of an appropriate basis set. There are only a few known orhonormal basis sets and that too depends on certain specialized geometries and specific boundary conditions. These issues make this technique very specialized.

Using this technique, solution of Poisson-Boltzmann equation as in Eq. (B.2) becomes trivial. The solution is given by $\psi_j = L^2 f_j/\lambda_j$ for $j > 1$, where f_j's are computed from the given values of $f\{\psi(\mathbf{r})\}$. First component ,ψ_1, is generally set to zero, which also fixes the unknown constant in ψ by assuring that $\int d\mathbf{r}\psi(\mathbf{r}) = 0$ in these computations.

B.2 Pseudo - Spectral Method

With the increase in the desired number of basis functions in the finite series expansion, the spectral method demands a lot of memory and becomes extremely expensive. The sets of problems, where the required number of basis functions are large can be solved by pseudo-spectral method, which optimize speed and accuracy both. Problems, where this method has shown an edge over spectral method are the ones in which one end of the polymer chains is fixed (such as in polymer brushes).

This method is based on the use of operators in solving Eq. (B.1). Within the operator formalism employed by the technique, formal solution of Eq. (B.1) is given by

$$h(\mathbf{r}, t + dt) = \exp\left[dt\left(\frac{b^2}{6}\nabla^2_{\mathbf{r}} - u(\mathbf{r})\right)\right] h(\mathbf{r}, t). \tag{B.11}$$

In Eq. (B.11), three dimensional Laplacian and $w(\mathbf{r})$ are treated as operators. Exponential of an operator has the same definition as the exponential of a number i.e., for an operator A, it can be represented as an infinite series

$$e^A = 1 + A + \frac{1}{2!}AA + \frac{1}{3!}AAA + \cdots \tag{B.12}$$

Now, the goal is to approximate the exponential of the operator on the right hand side in Eq. (B.11) by some technique. Approximation scheme must respect the fact that most of the times, the order of operation for different operators matters or in other words, operators may not commute. On the other hand, some operators do commute. As a result, for any two operators A and B, $e^{A+B} \neq e^A e^B$ unless they commute. The approximation scheme employed by the pseudo-spectral method uses the fact that if the operator on the right hand side in Eq. (B.11) can be split into two parts, then it is relatively easy to implement numerically. A powerful approximation scheme for computing the exponential of an operator by splitting into a sum of non-commuting operators uses the well-known Baker-Campbell-Hausdorff[127] formula. According to this formula, if $e^A e^B = e^C$ then

$$C = A + B + \frac{1}{2}[A, B] + \frac{1}{12}[[A, B], (B - A)] + \frac{1}{24}\left[B, A^2, B\right] + \cdots, \tag{B.13}$$

where $[x, y] = xy - yx$ is the commutator, $[x, y^2] = [[x, y], y]$ and $[x, y^2, x] = [[x, y^2], x]$.

Splitting of the operators can be quite tricky. In the case of Eq. (B.11), the splitting is motivated by the observation that it is easy to implement $\exp(w(\mathbf{r}))$ in real space (at all points on the mesh) but it is difficult to take double derivatives at all points on the mesh. This difficulty can be overcome by using the fact that the derivatives can be implemented trivially in Fourier space. So, if somehow, the Laplacian part could be split from $w(\mathbf{r})$ part then the progress can be made. This

is the motivation for splitting the operator in Eq. (B.11) into derivative and non-derivative parts by Baker-Campbell-Hausdorff formula.

For most practical purposes, a symmetric decomposition is carried out so that within an error of the order dt^3

$$\exp\left[dt\left(\frac{b^2}{6}\nabla_{\mathbf{r}}^2 - w(\mathbf{r})\right)\right] \simeq \exp\left[-\frac{dt}{2}w(\mathbf{r})\right]\exp\left[dt\frac{b^2}{6}\nabla_{\mathbf{r}}^2\right]\exp\left[-\frac{dt}{2}w(\mathbf{r})\right]. \tag{B.14}$$

So, solution of Eq. (B.1) can be approximated by

$$h(\mathbf{r}, t+dt) \simeq \exp\left[-\frac{dt}{2}w(\mathbf{r})\right]\exp\left[dt\frac{b^2}{6}\nabla_{\mathbf{r}}^2\right]\exp\left[-\frac{dt}{2}w(\mathbf{r})\right]h(\mathbf{r}, t), \tag{B.15}$$

which is correct within an error of dt^3.

Numerical implementation of Eq. (B.15) uses the fact that the rightmost operator in the exponential can be implemented as it is in real space. Let's say $g(\mathbf{r}, t)$ is the outcome of this operation, which is a function of position ($\mathbf{r}$) at some t i.e.,

$$g(\mathbf{r}, t) = \exp\left[-\frac{dt}{2}w(\mathbf{r})\right]h(\mathbf{r}, t). \tag{B.16}$$

For implementing the exponential of the Laplacian operator for systems with periodic boundary conditions, note the following (see the proof at the end of this Appendix)

$$\exp\left[dt\frac{b^2}{6}\nabla_{\mathbf{r}}^2\right]g(\mathbf{r}, t) = \mathrm{FT}^{-1}\left[\exp\left\{-dt\frac{k^2b^2}{6}\right\}\mathrm{FT}\left\{g(\mathbf{r}, t)\right\}\right], \tag{B.17}$$

where FT stands for Fourier transform and FT^{-1} stands for inverse Fourier transform, which can be carried out quite efficiently using Fast Fourier Transforms (FFT). Hence, the numerical solution of Eq. (B.1) can be obtained by using

$$h(\mathbf{r}, t+dt) \simeq \exp\left[-\frac{dt}{2}w(\mathbf{r})\right]\mathrm{FT}^{-1}\left[\exp\left\{-dt\frac{k^2b^2}{6}\right\}\mathrm{FT}\left\{\exp\left[-\frac{dt}{2}w(\mathbf{r})\right]h(\mathbf{r}, t)\right\}\right].$$

So, in pseudo-spectral method, one has to switch between real space to Fourier space back and forth. Symmetric decomposition leads to the implementation of half time step in real space and the other half in Fourier space. That's the reason this method is also known as split-step method in the literature[126].

Due to the use of Fourier Transform in the implementation of the exponential of the Laplacian operator, the technique is mainly useful for systems with periodic boundary conditions. Also, note that the technique can't be used to solve Poisson-Boltzmann equation due to time independent nature of the equation. However, the Poisson-Boltzmann equation can be solved using Fast Fourier Transforms as described in Chapter 6.

B.2.1 Proof for Equation B.17

Consider the following Fourier transform

$$\begin{aligned} \mathrm{FT}\left[\exp\left\{dt\frac{b^2}{6}\nabla_{\mathbf{r}}^2\right\}g(\mathbf{r},t)\right] &= \mathrm{FT}\left[\left\{1+dt\frac{b^2}{6}\nabla_{\mathbf{r}}^2+\frac{1}{2!}\left(dt\frac{b^2}{6}\right)^2\nabla_{\mathbf{r}}^2\nabla_{\mathbf{r}}^2+\cdots\right\}g(\mathbf{r},t)\right] \\ &= \left[1-dt\frac{k^2b^2}{6}+\frac{1}{2!}\left(dt\frac{k^2b^2}{6}\right)^2+\cdots\right]g(k,t) \\ &= \exp\left[-dt\frac{k^2b^2}{6}\right]\mathrm{FT}\left\{g(\mathbf{r},t)\right\} \end{aligned} \tag{B.19}$$

Taking inverse Fourier transform on both sides

$$\exp\left\{dt\frac{b^2}{6}\nabla_{\mathbf{r}}^2\right\}g(\mathbf{r},t) = \mathrm{FT}^{-1}\left[\exp\left\{-dt\frac{k^2b^2}{6}\right\}\mathrm{FT}\left\{g(\mathbf{r},t)\right\}\right] \tag{B.20}$$

APPENDIX C

INTEGRATION OVER POSITIONS OF SMALL IONS

Here, we present how to compute the integral over positions of small ions in diblock copolymer melts, described in section 3.2 in Chapter 3. We start from Eq. 3.1

$$\exp\left[-\frac{F}{k_BT}\right] = \Lambda \int \prod_j D[\rho_j] \int D[w_j] \int \prod_\gamma D[\rho_\gamma] \int D[w_\gamma] \int D[\eta] \exp\left[-H\right] \tag{C.1}$$

where

$$\begin{aligned} H = & \frac{\rho_0}{2} \sum_\gamma w_{\gamma\gamma} n_\gamma + \frac{1}{2} \sum_\gamma \sum_{\gamma' \neq \gamma} \chi_{\gamma\gamma'} b^3 \int d\mathbf{r} \rho_\gamma(\mathbf{r}) \rho_{\gamma'}(\mathbf{r}) + \frac{1}{2} \int d\mathbf{r} \int d\mathbf{r}' \frac{\rho_e(\mathbf{r}) \rho_e(\mathbf{r}')}{\epsilon k_B T |\mathbf{r} - \mathbf{r}'|} \\ & -i \int d\mathbf{r} \sum_\gamma w_\gamma(\mathbf{r}) \rho_\gamma(\mathbf{r}) - i \int d\mathbf{r} \sum_j w_j(\mathbf{r}) \rho_j(\mathbf{r}) \\ & -i \int d\mathbf{r}\, \eta(\mathbf{r}) \left\{ \sum_\gamma \rho_\gamma(\mathbf{r}) - \rho_0 \right\} - \ln \left[\frac{Q_p^{n_p}}{n_p!} \prod_j \frac{Q_j^{n_j}}{n_j!} \right]. \end{aligned} \tag{C.2}$$

In these equations, $j = c, +, -$ and $\gamma = A, B$. Here, $\rho_e(\mathbf{r})$ represents the charge density given by $\rho_e(\mathbf{r}) = e\left[Z_A \alpha \rho_A(\mathbf{r}) + \sum_j Z_j \rho_j(\mathbf{r})\right]$. In Eq. (C.2), the Q's are the partition functions of individual components in the presence of a field. Explicitly, for the charged-neutral diblock copolymer chain with smeared charge distribution along the charged block, single chain partition function is given by

$$Q_p = \int D[\mathbf{R}] \exp\left[-\frac{3}{2b} \int_0^{Nb} dt \left(\frac{\partial \mathbf{R}}{\partial t} \right)^2 - \frac{i}{b} \sum_{m=A,B} \int dt\, w_m(\mathbf{R}) \right], \tag{C.3}$$

where the limits of t integrals are values of contour variable t over which monomer of type m is found along the chain i.e. $t = [0, N_A b]$ and $t = [N_A b, Nb]$ for $m = A$ and $m = B$, respectively. Similarly, partition function for small ion of type $j = c, +, -$ is given by

$$Q_j = \int d\mathbf{r} \exp\left[-iw_j(\mathbf{r})\right] \tag{C.4}$$

Integrals over w_j's can't be calculated exactly. So, in order to proceed further, integrals over collective field variables for small ions i.e. $w_j(\mathbf{r})$ for $j = c, +, -$ are approximated by the maximum value of the integrand (saddle point approximation). Maximization of the integrand with respect to $w_j(\mathbf{r})$ gives

$$\rho_j(\mathbf{r}) = \frac{n_j}{Q_j} \exp\left[-iw_j(\mathbf{r})\right] \Rightarrow iw_j(\mathbf{r}) = \ln\left[\frac{n_j}{Q_j}\right] - \ln\left[\rho_j(\mathbf{r})\right] \tag{C.5}$$

Plugging w_j back into Eq. (C.2),

$$\exp\left(-\frac{F}{k_B T}\right) \simeq \Lambda \int \prod_j D[\rho_j] \int \prod_\gamma D[\rho_\gamma] \int D[w_\gamma] \int D[\eta] \exp\left[-H^*\right], \tag{C.6}$$

where

$$\begin{aligned} H^* = & \frac{\rho_0}{2} \sum_\gamma w_{\gamma\gamma} n_\gamma + \frac{1}{2} \sum_\gamma \sum_{\gamma' \neq \gamma} \chi_{\gamma\gamma'} b^3 \int d\mathbf{r} \rho_\gamma(\mathbf{r}) \rho_{\gamma'}(\mathbf{r}) + \frac{1}{2} \int d\mathbf{r} \int d\mathbf{r}' \frac{\rho_e(\mathbf{r}) \rho_e(\mathbf{r}')}{\epsilon k_B T |\mathbf{r} - \mathbf{r}'|} \\ & -i \int d\mathbf{r} \sum_\gamma w_\gamma(\mathbf{r}) \rho_\gamma(\mathbf{r}) + \int d\mathbf{r} \sum_{j=c,+,-} \rho_j(\mathbf{r}) \ln\left[\rho_j(\mathbf{r})\right] \\ & -i \int d\mathbf{r}\, \eta(\mathbf{r}) \left\{ \sum_\gamma \rho_\gamma(\mathbf{r}) - \rho_0 \right\} - \ln\left[\frac{Q_p^{n_p}}{n_p!}\right]. \end{aligned} \tag{C.7}$$

In order to calculate the integrals over small ions collective density variables $\rho_j(\mathbf{r})$ for $j = c, +, -$, we consider fluctuations of the densities about their values in the disordered phase[16]. For weak fluctuations, the entropic term $\rho_j \ln \rho_j$ can be expanded in

powers of these fluctuations. Keeping the leading terms (neglecting cubic and higher order terms), integrals over ρ_j become Gaussian and can be easily calculated. So, by writing

$$\rho_j(\mathbf{r}) = \bar{\rho}_j + \delta\rho_j(\mathbf{r}), \rho_\gamma(\mathbf{r}) = \bar{\rho}_\gamma + \delta\rho_\gamma(\mathbf{r}), \tag{C.8}$$

and using $\int d\mathbf{r}\, \delta\rho_j(\mathbf{r}) = \int d\mathbf{r}\, \delta\rho_\gamma(\mathbf{r}) = 0$ (so that $\bar{\rho}_j = n_j/\Omega$ and $\bar{\rho}_{A/B} = n_p N_{A/B}/\Omega$) in combination with the global electroneutrality in the homogeneous phase, integrals over ρ_j (i.e. small ions) become

$$\begin{aligned} I &= \int \prod_j D[\delta\rho_j] \exp\left[-\frac{1}{2}\int \frac{d^3k}{(2\pi)^3}\left\{\sum_j\sum_q \delta\rho_j(k)\left(\frac{\delta_{jq}}{\bar{\rho}_j} + V_k^{(0)} Z_j Z_q\right)\delta\rho_q(k)\right.\right. \\ &\left.\left. +2\sum_j V_k^{(0)} \alpha Z_A Z_j \delta\rho_A(k)\delta\rho_j(k)\right\}\right] \exp\left[-\frac{1}{2}\int \frac{d^3k}{(2\pi)^3} V_k^{(0)} \alpha^2 Z_A^2 \delta\rho_A^2(k)\right], \end{aligned} \tag{C.9}$$

where $V_k^{(0)} = \frac{4\pi l_B}{k^2}$, δ_{mp} is the Kronecker delta and $q = c, +, -$, respectively. By calculating the Gaussian integrals, the value of I is found to be

$$\begin{aligned} I = \frac{(2\pi)^{\frac{3}{2}}}{\sqrt{\lambda_c \lambda_+ \lambda_-}} \quad & \exp\left[-\frac{\Omega}{2}\int \frac{d^3k}{(2\pi)^3} \ln\left[1 + V_k^{(0)}\lambda_0\right]\right] \\ & \exp\left[-\frac{1}{2}\alpha^2 Z_A^2 \int \frac{d^3k}{(2\pi)^3} \frac{V_k^{(0)}}{1 + V_k^{(0)}\lambda_0} \delta\rho_A^2(k)\right] \end{aligned} \tag{C.10}$$

where $\lambda_j = \frac{\Omega}{n_j}, j = c, +, -$ and λ_0 is given by

$$\lambda_0 = \frac{1}{\Omega}\sum_{j=1,2,3} Z_j^2 n_j = \frac{\kappa^2}{4\pi l_B} \tag{C.11}$$

Now, using the relation

$$\int_0^\infty x^2 \left\{\ln\left[1 + \frac{\alpha^2}{x^2}\right] - \frac{\alpha^2}{x^2}\right\} = -\frac{\pi}{3}\alpha^3, \tag{C.12}$$

we get

$$\frac{\Omega}{2}\int\frac{d^3k}{(2\pi)^3}\ln(1+\lambda_0 V_k^{(0)}) = -\frac{\Omega}{12\pi}(4\pi l_B\lambda_0)^{3/2} + \frac{\Omega}{2}\int\frac{d^3k}{(2\pi)^3}\frac{4\pi l_B\lambda_0}{k^2} \qquad \text{(C.13)}$$

Here, the last term is divergent. But the divergence is for k being large (ultraviolet divergence) and we are interested on a length scale corresponding to small k. So, this term is neglected. Note that the same result can be obtained by employing the central limit theorem[53]. Now, electrostatic terms are decoupled from the rest of the terms and remaining treatment is the same as that done for the corresponding neutral copolymer[31].

APPENDIX D

SCFT FOR A FLEXIBLE POLYELECTROLYTE CHAIN

Here, we present a summary of the steps in obtaining the saddle point equations for a single polyelectrolyte chain in the presence of salt ions and solvent molecules (section (4.2.1) in Chapter 4). The procedure is similar to the ones presented in section 2.2.2 of Chapter 2 and the saddle-point equations obtained at the end of the analysis are similar to the ones presented in Refs. [44, 45]. As the first step, we define microscopic densities as

$$\hat{\rho}_p(\mathbf{r}) = \frac{1}{b}\int_0^{Nb} dt\, \delta(\mathbf{r}-\mathbf{R}(t)) \tag{D.1}$$

$$\hat{\rho}_j(\mathbf{r}) = \sum_{i=1}^{n_j} \delta(\mathbf{r}-\mathbf{r}_i) \quad \text{for} \quad j=s,c,+,- \tag{D.2}$$

$$\hat{\rho}_e(\mathbf{r}) = e\left[\alpha Z_p \hat{\rho}_p(\mathbf{r}) + \sum_{j=c,+,-} Z_j \hat{\rho}_j(\mathbf{r})\right], \tag{D.3}$$

where $\hat{\rho}_p(\mathbf{r}), \hat{\rho}_j(\mathbf{r})$ and $\hat{\rho}_e(\mathbf{r})$ stand for monomer, small molecules (ions and solvent molecules) and local charge density, respectively.

As the second step, we use a functional integral representation for the incompressibility constraint

$$\prod_r \delta\left(\hat{\rho}_p(\mathbf{r}) + \hat{\rho}_s(\mathbf{r}) - \rho_0\right) = \int D[w_+(\mathbf{r})] e^{-i\int d\mathbf{r} w_+(\mathbf{r})(\hat{\rho}_p(\mathbf{r})+\hat{\rho}_s(\mathbf{r})-\rho_0)}, \tag{D.4}$$

where $w_+(\mathbf{r})$ is the well-known pressure field which enforces the incompressibility constraint at all points in the system and $i=\sqrt{-1}$.

As the third step, dimensionless Flory's chi parameter is introduced to club together the three excluded volume parameters so that

$$\chi_{ps} b^3 = w_{ps} - \frac{w_{pp} + w_{ss}}{2}. \tag{D.5}$$

Note that the clubbing of excluded volume parameters has been possible because of the incompressibility constraint so that only one independent parameter appears in the theory. Otherwise, there would have been three independent parameters.

Following these three steps, the partition function $Z = \exp[-F/k_B T]$ for a single polyelectrolyte chain in the presence of solvent and salt molecules becomes

$$\begin{aligned} Z = & \frac{1}{\prod_j n_j!} \int D[\mathbf{R}] \int \prod_j \prod_{m=1}^{n_j} d\mathbf{r}_m \int D[w_+(\mathbf{r})] \quad \exp\left\{ -\frac{3}{2b} \int_0^{Nb} dt \left(\frac{\partial \mathbf{R}(t)}{\partial t} \right)^2 \right. \\ & -i \int d\mathbf{r} w_+(\mathbf{r}) \left(\hat{\rho}_p(\mathbf{r}) + \hat{\rho}_s(\mathbf{r}) - \rho_0 \right) - \chi_{ps} b^3 \int d\mathbf{r} \hat{\rho}_p(\mathbf{r}) \hat{\rho}_s(\mathbf{r}) \\ & \left. -\frac{1}{2} \int d\mathbf{r} \int d\mathbf{r}' \frac{\hat{\rho}_e(\mathbf{r}) \hat{\rho}_e(\mathbf{r}')}{\epsilon k_B T |\mathbf{r} - \mathbf{r}'|} \right\} \quad \exp\left\{ -\frac{\rho_0}{2} \left(N w_{pp} + n_s w_{ss} \right) \right\}. \end{aligned} \tag{D.6}$$

So far, we have written the partition function in terms of the local densities. Now, we want to write this partition function in terms of the order parameter of the system. There are many different choices we can make for the order parameter[31, 9]. However, in this study, we follow the method as described in ref. [9] to introduce the order parameter. As the fourth step, we define

$$\hat{\rho}_+(\mathbf{r}) = \hat{\rho}_p(\mathbf{r}) + \hat{\rho}_s(\mathbf{r}) = \rho_0 \tag{D.7}$$

$$\hat{\rho}_-(\mathbf{r}) = \hat{\rho}_p(\mathbf{r}) - \hat{\rho}_s(\mathbf{r}), \tag{D.8}$$

where $\hat{\rho}_-(\mathbf{r})$ is the order parameter for the inhomogeneous system.

As the fifth step, to go from densities to fields, we use the Hubbard-Stratonovich transformation for short range excluded volume interactions as well as long range electrostatic interactions, so that

$$\exp\left(\frac{\chi_{ps}b^3}{4}\int d\mathbf{r}\hat{\rho}_-^2(\mathbf{r})\right) = \int\frac{D[w_-(\mathbf{r})]}{\mu_-}\exp\left[\int d\mathbf{r}\left\{w_-(\mathbf{r})\hat{\rho}_-(\mathbf{r})-\frac{1}{\chi_{ps}b^3}w_-^2(\mathbf{r})\right\}\right], \tag{D.9}$$

$$\exp\left(-\frac{1}{2}\int d\mathbf{r}\int d\mathbf{r}'\frac{\hat{\rho}_e(\mathbf{r})\hat{\rho}_e(\mathbf{r}')}{\epsilon k_BT|\mathbf{r}-\mathbf{r}'|}\right) = \int\frac{D[\psi(\mathbf{r})]}{\mu_\psi}\exp\left[-\int d\mathbf{r}\left\{i\psi(\mathbf{r})\frac{\hat{\rho}_\epsilon(\mathbf{r})}{e} -\frac{\psi(\mathbf{r})}{8\pi l_B}\nabla_{\mathbf{r}}^2\psi(\mathbf{r})\right\}\right], \tag{D.10}$$

where

$$\mu_- = \int D[w_-(\mathbf{r})]\exp\left[-\frac{1}{\chi_{ps}b^3}\int d\mathbf{r}w_-^2(\mathbf{r})\right] \tag{D.11}$$

$$\mu_\psi = \int D[\psi(\mathbf{r})]\exp\left[\frac{1}{8\pi l_B}\int d\mathbf{r}\psi(\mathbf{r})\nabla_{\mathbf{r}}^2\psi(\mathbf{r})\right]. \tag{D.12}$$

Note that, $w_+(\mathbf{r}), w_-(\mathbf{r})$ and $\psi(\mathbf{r})$ are the *real* fields, which can be envisioned as chemical potential fields[28]. Now, taking these two steps, Eq. (D.6) becomes

$$\exp\left(-\frac{F}{k_BT}\right) = \frac{1}{\mu_-\mu_\psi}\int D[w_+(\mathbf{r})]\int D[w_-(\mathbf{r})]\int D[\psi(\mathbf{r})]\quad\exp\left[-f\left\{w_+,w_-,\psi\right\}\right], \tag{D.13}$$

where

$$f\left\{w_+,w_-,\psi\right\} = \frac{1}{\chi_{ps}b^3}\int d\mathbf{r}w_-^2(\mathbf{r})-i\rho_0\int d\mathbf{r}w_+(\mathbf{r})-\ln Q_p-\sum_{j=s,c,+,-}n_j\ln Q_j -\frac{1}{8\pi l_B}\int d\mathbf{r}\psi(\mathbf{r})\nabla_{\mathbf{r}}^2\psi(\mathbf{r})+\frac{\rho_0}{2}\left(Nw_{pp}+n_sw_{ss}+\frac{\chi_{ps}b^3}{2}\Omega\rho_0\right)$$

$$+ \sum_{j=s,c,+,-} \ln n_j!, \tag{D.14}$$

$$Q_p = \int D[\mathbf{R}] \exp\left[-\frac{1}{b}\int_0^{Nb} dt \left\{\frac{3}{2}\left(\frac{\partial \mathbf{R}}{\partial t}\right)^2 + iw_+\{\mathbf{R}\} - w_-\{\mathbf{R}\} + iZ_p\alpha\psi\{\mathbf{R}\}\right\}\right], \tag{D.15}$$

$$Q_s = \int d\mathbf{r} \quad \exp\left[-\{iw_+(\mathbf{r}) + w_-(\mathbf{r})\}\right], \tag{D.16}$$

$$Q_j = \int d\mathbf{r} \quad \exp\left[-iZ_j\psi(\mathbf{r})\right] \quad \text{for} \quad j = c, +, -. \tag{D.17}$$

The functional integrations over real fields are to be carried out by contour integration techniques and are almost impossible to compute exactly. However, if the number of small molecules is large then we can compute the integrals in the numerator by steepest descent technique, using the knowledge that the integral along the constant phase (imaginary part of the integrand) contour is dominated by the local minima of the integrand[9] (note that the functional integrals in the denominator are divergent and ignored at the level of saddle point approximation). So, we approximate the functional integrals in the numerator by the value of the integrand at the local minima (where the phase comes out to be zero) so that the final approximated integral is real ($= f\left\{w_+^*, w_-^*, \psi^*\right\}$). However, the saddle point values for w_+ $(= w_+^*)$ and $\psi (= \psi^*)$ come out to be purely imaginary in contrast to $w_-(= w_-^*)$, which is real.

Also, it should be noted that the densities remain unchanged with the shift in fields by an arbitrary constant. So, we write $iw_+(\mathbf{r}) - \frac{1}{2}\chi_{ps}b^3\rho_0 = iw_+(\mathbf{r})$ to get rid of the constant in saddle point equations. Now, deriving local minima equations for the integrand in Eq. (D.14) with respect to w_+, w_- and ψ, and using notation $iw_+(\mathbf{r}) - w_-(\mathbf{r}) \rightarrow \phi_p(\mathbf{r})$, $iw_+(\mathbf{r}) + w_-(\mathbf{r}) \rightarrow \phi_s(\mathbf{r})$, $i\psi(\mathbf{r}) \rightarrow \psi(\mathbf{r})$, $iw_+(\mathbf{r}) \rightarrow \eta(\mathbf{r})$, Eqs.

(4.1- 4.7) are obtained. Using these saddle point equations and employing Stirling's approximation for $\ln n!$, we obtain Eq. (4.12).

APPENDIX E

FLUCTUATION CORRECTIONS FOR A CONFINED CHAIN

Here, we provide details for one loop treatment of the fluctuations[7] for a confined polyelectrolyte chain in spherical cavities. We expand the integrand f in Eq. (D.13) up to second degree terms in w_+, w_- and v around their respective saddle point values. For convenience in writing the expansion, we introduce a dummy functional variable $\zeta_p(\mathbf{r})$, where $p = 1, 2, 3$ correspond to w_+, w_- and v, respectively. In this notation, the expression for free energy becomes (cf. Eq. (D.13))

$$\exp\left(-\frac{F-F^\star}{k_BT}\right) = \frac{1}{\mu_- - \mu_v}\int\prod_{p=1}^{3} D[\zeta_p(\mathbf{r})] \exp\left[-\frac{1}{2}\int d\mathbf{r}\int d\mathbf{r}'\sum_{m=1}^{3}\sum_{p=1}^{3} K_{mp}(\mathbf{r},\mathbf{r}')\Delta\zeta_m(\mathbf{r})\Delta\zeta_p(\mathbf{r}')\right], \tag{E.1}$$

where

$$K_{mp}(\mathbf{r},\mathbf{r}') = \frac{\delta^2 f\{\zeta_1,\zeta_2,\zeta_3\}}{\delta\zeta_m(\mathbf{r})\delta\zeta_p(\mathbf{r}')}\,|_{\zeta_1^\star,\zeta_2^\star,\zeta_3^\star}\,. \tag{E.2}$$

and $\Delta\zeta_m(\mathbf{r}) = \zeta_m(\mathbf{r}) - \zeta_m^\star(\mathbf{r})$. In the expansion, linear terms in fields vanish because of the saddle point condition. K_{mp} can be computed in a straightforward way and are presented here for completeness

$$K_{11}(\mathbf{r},\mathbf{r}') = A(\mathbf{r},\mathbf{r}') + B_s(\mathbf{r},\mathbf{r}') \tag{E.3}$$

$$K_{22}(\mathbf{r},\mathbf{r}') = C(\mathbf{r},\mathbf{r}') - A(\mathbf{r},\mathbf{r}') - B_s(\mathbf{r},\mathbf{r}') \tag{E.4}$$

$$K_{33}(\mathbf{r},\mathbf{r}') = -\frac{1}{4\pi l_B}\nabla_{\mathbf{r}}^2\,\delta(\mathbf{r}-\mathbf{r}') + Z_p^2\alpha^2 A(\mathbf{r},\mathbf{r}') + \sum_{j=c,+,-} Z_j^2 B_j(\mathbf{r},\mathbf{r}') \quad \text{(E.5)}$$

$$K_{12}(\mathbf{r},\mathbf{r}') = K_{21}(\mathbf{r},\mathbf{r}') = i\left[A(\mathbf{r},\mathbf{r}') - B_s(\mathbf{r},\mathbf{r}')\right] \quad \text{(E.6)}$$

$$K_{13}(\mathbf{r},\mathbf{r}') = K_{31}(\mathbf{r},\mathbf{r}') = Z_p\alpha A(\mathbf{r},\mathbf{r}') \quad \text{(E.7)}$$

$$K_{23}(\mathbf{r},\mathbf{r}') = K_{32}(\mathbf{r},\mathbf{r}') = iZ_p\alpha A(\mathbf{r},\mathbf{r}') \quad \text{(E.8)}$$

where

$$A(\mathbf{r},\mathbf{r}') = -\rho_p(\mathbf{r})\rho_p(\mathbf{r}') + g(\mathbf{r},\mathbf{r}') \quad \text{(E.9)}$$

$$g(\mathbf{r},\mathbf{r}') = \left[\int_0^N dt' \int_0^{t'} dt q(\mathbf{r},t)G(\mathbf{r},\mathbf{r}',t,t')q(\mathbf{r}',N-t') + \int_0^N dt \int_0^t dt' q(\mathbf{r}',t')G(\mathbf{r}',\mathbf{r},t',t)q(\mathbf{r},N-t)\right]\frac{1}{\int d\mathbf{r}\, q(\mathbf{r},N)} \quad \text{(E.10)}$$

$$B_j(\mathbf{r},\mathbf{r}') = -\frac{1}{n_j}\rho_j(\mathbf{r})\rho_j(\mathbf{r}') + \rho_j(\mathbf{r})\delta(\mathbf{r}-\mathbf{r}') \quad \text{for} \quad j = s,c,+,- \quad \text{(E.11)}$$

$$C(\mathbf{r},\mathbf{r}') = \frac{2}{\chi_{ps}b^3}\delta(\mathbf{r}-\mathbf{r}'). \quad \text{(E.12)}$$

In the case of confined chain within a spherical cavity, where electrostatic potential and monomer density are zero at the boundary (Dirichlet boundary conditions), the functional integral over ζ_p can be carried out in Eq. (E.1) by expanding all vectorial quantities in terms of spherical harmonics (Y_{lm}) and spherical Bessel functions (j_l). For an arbitrary function $h(\mathbf{r},\mathbf{r}')$ this means

$$h(\mathbf{r},\mathbf{r}') = \sum_{k=1}^{\infty}\sum_{l=0}^{\infty}\sum_{m=-l}^{l} h_{kl}d_{kl}(r)d_{kl}(r')Y_{lm}(\theta,\phi)Y_{lm}^{\star}(\theta',\phi') \quad \text{(E.13)}$$

$$d_{kl}(r) = \sqrt{\frac{2}{3}}\frac{j_l(\nu_{kl}r/R)}{|j_{l+1}(\nu_{kl})|}, \quad \text{(E.14)}$$

where ν_{kl} is k^{th} zero of the spherical Bessel function of order l (i.e. $j_l(\nu_{kl}) = 0$). Similarly, we expand $\zeta_p(\mathbf{r})$ as

$$\zeta_p(\mathbf{r}) = \sum_{k=1}^{\infty}\sum_{l=0}^{\infty}\sum_{m=-l}^{l}\zeta_{pk}d_{kl}(r)Y_{lm}(\theta,\phi). \tag{E.15}$$

Now, using orthogonal properties of spherical Bessel and spherical harmonics, the functional integrals can be computed. After some lengthy algebra,

$$\begin{aligned}\frac{F}{k_BT} &= \frac{F^*}{k_BT} + \frac{1}{2}\sum_{k=1}^{\infty}\sum_{l=0}^{\infty}(2l+1)\ln\left(A_{kl} + B_{s,kl} - 4\sum_{u=1}^{\infty}\sum_{v=1}^{\infty}A_{ku}C^{-1}_{uv}B_{s,vl}\right)\\ &+ \frac{1}{2}\sum_{k=1}^{\infty}\sum_{l=0}^{\infty}(2l+1)\ln\left(1 + \frac{4\pi l_B R^2}{\nu_{kl}^2}\sum_{j=c,+,-}Z_j^2 B_{j,kl}\right)\\ &+ \frac{1}{2}\sum_{k=1}^{\infty}\sum_{l=0}^{\infty}(2l+1)\ln\left(1 + Z_p^2\alpha^2\frac{A_{kl} - \sum_{u=1}^{\infty}\sum_{v=1}^{\infty}A_{ku}L^{-1}_{uv}A_{vl}}{\frac{\nu_{kl}^2}{4\pi l_B R^2} + \sum_{j=c,+,-}Z_j^2 B_{j,kl}}\right).\end{aligned} \tag{E.16}$$

In the above equation, the second term on the r.h.s. represents the contribution of correlations arising due to excluded volume interactions between monomers (neutral polymer contribution), the third term arises as a result of small-ions density fluctuations and the last term correctly represents the correlation energy of charges along the backbone of the chain.

Also, $L(\mathbf{r},\mathbf{r}')$ is given by

$$\begin{aligned}L(\mathbf{r},\mathbf{r}') &= A(\mathbf{r},\mathbf{r}') + B(\mathbf{r},\mathbf{r}')\\ &+4\int d\mathbf{r}''\int d\mathbf{r}'''B(\mathbf{r},\mathbf{r}'')\left(C-4B\right)^{-1}(\mathbf{r}'',\mathbf{r}''')B(\mathbf{r}''',\mathbf{r}').\end{aligned} \tag{E.17}$$

Furthermore, C^{-1}_{kl} and L^{-1}_{kl} correspond to the coefficients in the spherical harmonics expansion for the inverse operator of $C(\mathbf{r},\mathbf{r}')$ and $L(\mathbf{r},\mathbf{r}')$, respectively. Inverse operator for any arbitrary functional $h(\mathbf{r},\mathbf{r}')$ is defined by

$$\int d\mathbf{r}'h(\mathbf{r},\mathbf{r}')h^{-1}(\mathbf{r}',\mathbf{r}'') = \delta(\mathbf{r}-\mathbf{r}''), \tag{E.18}$$

which gives $\sum_{u=1}^{\infty}h_{ku}h^{-1}_{ul} = \delta_{kl}$, where δ_{kl} is Kronecker delta.

Unfortunately, computation of the coefficients involved in Eq. (E.16) requires three dimensional calculations for the densities and it is very hard to compute the sums exactly, which diverge in general. To gain an insight into the problem, we have identified one particular case, where we can evaluate the first two terms analytically.

If the number of small molecules (solvent and small ions) is large, then operators $B_j(\mathbf{r},\mathbf{r}')$ become diagonal and also, number densities ($\rho_j(\mathbf{r})$) show a weak dependence on $\mathbf{r}$. Similarly, if degree of polymerization N is large (strictly if $N \to \infty$), then monomer density becomes independent of $\mathbf{r}$ except near the surface of the cavity characterized by the width of the depletion zone, which can be neglected. If both of these conditions are satisfied, then suppressing position dependence of densities, we get

$$\begin{aligned}
&\frac{1}{2}\sum_{k=1}^{\infty}\sum_{l=0}^{\infty}(2l+1)\ln\left(A_{kl}+B_{s,kl}-4\sum_{u=1}^{\infty}\sum_{v=1}^{\infty}A_{ku}C_{uv}^{-1}B_{s,vl}\right)\\
&=\frac{1}{2}\sum_{k=1}^{\infty}\sum_{l=0}^{\infty}(2l+1)\ln\left(1-\bar{\rho}_p\right)+\frac{1}{2}\sum_{k=1}^{\infty}\sum_{l=0}^{\infty}(2l+1)\ln\left(1+w_r b^3 A_{kl}\right). \qquad \text{(E.19)}
\end{aligned}$$

where $\bar{\rho}_p = \frac{Nb^3}{\Omega}$ and $w_r = \frac{1}{1-\bar{\rho}_p} - 2\chi_{ps}$ is the renormalized excluded volume interaction parameter. For constant monomer density (while working in the limit $N \to \infty$), $A(\mathbf{r},\mathbf{r}')$ satisfies

$$\nabla^2_{\mathbf{r}} A(\mathbf{r},\mathbf{r}') = -\frac{12N}{b^2\Omega}\delta(\mathbf{r}-\mathbf{r}') \qquad \text{(E.20)}$$

so that $b^3 A_{kl} = 12NbR^2/(\nu_{kl}^2\Omega)$. Neglecting the correlation energy of the charges along the backbone of the chain (the last term on r.h.s. of Eq. (E.16)) and an ultraviolet divergent sum in Eq. (E.19) (first term on r.h.s. of the equation), Eq. (4.34) is obtained.

APPENDIX F

COMPARISON OF SCFT AND VARIATIONAL THEORY

Here, we present a brief description of SCFT for a single flexible polyelectrolyte chain having a fixed degree of ionization (= α) in the presence of salt ions and solvent molecules. We start from the partition function using Edward's Hamiltonian, written as

$$
\begin{aligned}
Z = & \frac{\exp\left[-(E_a + F_0)/k_BT\right]}{\mu \prod_j n_j!} \int D[\mathbf{R}] \int \prod_j \prod_{m=1}^{n_j} d\mathbf{r}_m \quad \left[\exp\left\{-\frac{3}{2b}\int_0^{Nb} dt \left(\frac{\partial \mathbf{R}(t)}{\partial t}\right)^2 \right.\right. \\
& \left. - \chi_{ps} b^3 \int d\mathbf{r} \hat{\rho}_p(\mathbf{r}) \hat{\rho}_s(\mathbf{r}) - \frac{1}{2}\int d\mathbf{r} \int d\mathbf{r}' \frac{\hat{\rho}_c(\mathbf{r})\hat{\rho}_c(\mathbf{r}')}{4\pi\epsilon_0 \epsilon k_B T |\mathbf{r} - \mathbf{r}'|}\right\} \\
& \left. \prod_{\mathbf{r}} \delta\left(\hat{\rho}_p(\mathbf{r}) + \hat{\rho}_s(\mathbf{r}) - \rho_0\right) \delta\left(\frac{1}{b}\int_0^{Nb} dt\, y(t) - \alpha N e\right)\right]_y ,
\end{aligned}
\tag{F.1}
$$

where $\mathbf{R}(t)$ represents the position vector for the t^{th} segment and subscripts $j = s, c, +, -$. In Eq. (F.1) k_BT is the Boltzmann constant times absolute temperature. In writing the interaction energies between the polyelectrolyte segments and small ions, we have taken the small ions to be point charges so that they have zero excluded volume, and hence, interactions are purely electrostatic in nature. As we consider the "permuted" charge distribution, the partition function has an additional sum over all possible locations of the "adsorbed" ions on the backbone, which appears as an average over the parameter y in Eq. (F.1). We define the average over y as $[\cdots]_y = \int dy [\cdots] g(y)$, where $g(y) = \alpha\delta(y(t) - 1) + (1 - \alpha)\delta(y(t))$.

In the above equation, the microscopic densities are defined as

$$
\hat{\rho}_p(\mathbf{r}) = \frac{1}{b}\int_0^{Nb} dt\, \delta(\mathbf{r} - \mathbf{R}(t)), \tag{F.2}
$$

$$\hat{\rho}_j(\mathbf{r}) = \sum_{i=1}^{n_j} \delta(\mathbf{r} - \mathbf{r}_i) \quad \text{for} \quad j = s, c, +, -, \tag{F.3}$$

$$\hat{\rho}_e(\mathbf{r}) = e\left[\frac{1}{b}\int_0^{Nb} dt\, Z_p y(t)\delta(\mathbf{r} - \mathbf{R}(t)) + \sum_{j=c,+,-} Z_j \hat{\rho}_j(\mathbf{r})\right], \tag{F.4}$$

where $\hat{\rho}_p(\mathbf{r}), \hat{\rho}_j(\mathbf{r})$ and $\hat{\rho}_e(\mathbf{r})$ stand for the monomers, small molecules (both ions and solvent molecules) and the local charge density, respectively. The Dirac delta functions involving microscopic densities enforce the incompressibility condition at all points in the system (ρ_0 being the total number density of the system). The delta function involving y is a constraint that for all the charge distributions to be considered for one particular value of α, the net charge on the chain must be a constant ($= \alpha Ne$). Taking different charge distributions of the chain for the same net charge ($= \alpha Ne$) and a particular chain conformation to be degenerate, the partition function is divided by the number of ways (μ) the "adsorbed" counterions can be distributed along the chain. If M out of total N sites on the backbone are occupied at any particular instance, then μ is given by $\mu = N!/(M!(N-M)!)$ so that $1 - \alpha = M/N$.

The dimensionless Flory parameter for chemical mismatch, χ_{ps}, is given by $\chi_{ps} b^3 = w_{ps} - (w_{pp} + w_{ss})/2$, where w_{pp}, w_{ss}, and w_{ps} are the excluded volume parameters, which characterize the short range excluded volume interactions of type monomer-monomer, solvent-solvent and monomer-solvent, respectively. F_0 and E_a are the self-energy and ion-pair energy contributions, respectively, given by

$$\frac{F_0}{k_B T} = N w_{pp} + n_s w_{ss}, \tag{F.5}$$

$$\frac{E_a}{k_B T} = -(1-\alpha) N \delta l_B / b, \tag{F.6}$$

where $\delta = \epsilon b/\epsilon_l d$, ϵ_l and d being the local dielectric constant and the dipole length, respectively, is used to characterize the formation of an ion-pair on the backbone due to "adsorbed" counterion.

Now, using the methods of collective variables and the Hubbard-Stratonovich transformation[9, 114] for the electrostatic part in Eq. (F.1), the partition function ($= \exp(-F/k_BT)$) can be written as integrals over the collective densities and corresponding fields so that Eq. (F.1) becomes

$$\exp\left(-\frac{F-F_0}{k_BT}\right) = \int D[w_p]D[\rho_p]D[\psi]D[\eta]du D[w_s]D[\rho_s]\left[\exp\left\{-\frac{H_{scf}}{k_BT}\right\}\right]_y \quad \text{(F.7)}$$

Here, w_p, w_s are the fields experienced by the monomers and solvent, respectively, and ρ_p, ρ_s represent their respective collective densities. All charged species (excluding the ion-pairs formed due to adsorption of counterions) experience a field ψ (which is equivalent to the electrostatic potential). η and u are Lagrange's multipliers corresponding to, respectively, the incompressibility and net charge constraints in the partition function. We must stress here that this procedure is equivalent to introducing collective fields and densities for small ions instead of using the Hubbard-Stratonovich transformation for the electrostatics part.

Within SCFT, the functional integrals over the fields and the densities are approximated by the value of the integrand at the extremum (also known as the saddle-point approximation). Extremizing the integrand leads to a number of non-linear equations for the fields and the densities. The saddle point approximation with respect to u gives equations similar to a "smeared" charge distribution, where every monomer has a charge ($= \alpha e$). The extremization with respect to $\psi, w_p, \rho_p, \eta, w_s$, and ρ_s, leads to the saddle point specified by Eqs. (5.4 - 5.6, 5.8 - 5.11). Using these saddle point equations and employing the Stirling's approximation for $\ln n!$, we obtain the approximated free energy, i.e., $F - F_0 \simeq H^{\star}_{scf}$, as presented in section 5.2.1 after taking $k_BT = 1$. The superscript $\star$ represents the saddle point estimate of the free energy.

Similarly, we can obtain the variational free energy as presented in Ref. [85] in the absence of ion-pair correlations. In Ref.[85], it has been assumed that the counterions from the polyelectrolyte are indistinguishable from the counterions from the salt. So, we start from a partition function similar to Eq. (F.1) with the solvent, counterions (from the polyelectrolyte and the salt), coions and the chain as distinguishable species. After using collective variables, the partition function can be written as

$$Z = \frac{1}{\mu}\exp\left[-\frac{E_a+F_0}{k_BT}\right]\int D[w_p]D[\rho_p]D[\eta]\prod_j D[\rho_j]D[w_j]\exp\left\{-\frac{h}{k_BT}\right\}, \quad \text{(F.8)}$$

where $j = s, c, -$ and, where the integral over u has already been evaluated by the saddle point method so that the functional h corresponds to a single chain with a "smeared" charge distribution. Here, we have introduced collective fields and densities for small ions instead of using the Hubbard-Stratonovich transformation for the electrostatic part (as already pointed out). This is the analog of Eq. (F.7) in SCFT. Now, evaluating the path integrals over w_j by the saddle point method, Eq. (F.8) can be written in terms of the densities ρ_j. Functional integrals over η and ρ_s can be carried out in a trivial way. To carry out functional integrals over small ion densities, i.e. the $\rho_j \log \rho_j$ terms, which emerge after integrations over fields w_j, are expanded up to the quadratic terms after writing $\rho_j(\mathbf{r}) = n_j/\Omega + \delta\rho_j(\mathbf{r})$ so that $\int d\mathbf{r}\delta\rho_j(\mathbf{r}) = 0$, and the resulting integrals are Gaussian. This procedure also gives one-loop corrections to the free energy coming from the small ions density fluctuations ($\Delta F/k_BT$). Now, expanding the $(1-\rho_p)\log(1-\rho_p)$ term up to the quadratic terms in ρ_p, the problem of carrying out the functional integrals over w_p and ρ_p is equivalent to a single chain problem whose monomers interact with each other via a renormalized excluded volume parameter and an electrostatic potential. The renormalized excluded volume parameter comes out to be $w = 1 - 2\chi_{ps}$ and the electrostatic potential comes out to be the Debye-Hückel potential, where the inverse Debye length (κ) depends on the "free" ions only. Eventually, Eq. (F.8) becomes

$$Z = \frac{1}{\mu}\exp\left[-\frac{F_0 + E_a - TS_t + \Delta F}{k_B T}\right]\int D[w_p]D[\rho_p]\exp\left\{-\frac{H_{var}}{k_B T}\right\}, \quad \text{(F.9)}$$

where $-TS_t$ is the translational entropy of the "free" ions as presented in Table 3.1 for the variational theory. Now, writing the Hamiltonian of a single polyelectrolyte chain using an effective excluded parameter (w) and the Debye-Hückel potential[85], the functional integrals over w_p and ρ_p can be computed using the variational technique developed by Muthukumar[50]. Taking $k_B T = 1$, the results are presented in section 5.2.2.

BIBLIOGRAPHY

[1] S. F. Edwards, Proc. Phys. Soc. London **85**, 613 (1965).

[2] S. F. Edwards, J. Phys. A : Math. Gen. **8**, 1670 (1975).

[3] M. Doi and S.F. Edwards, *The Theory of Polymer Dynamics* (Clarendon Press, Oxford, 1986).

[4] E. Helfand, J. Chem. Phys. **62**, 999 (1975).

[5] J. Hubbard, Phys. Rev. Lett. **3**, 77 (1959).

[6] P . G. de Gennes,*Scaling Concepts in Polymer Physics* (Cornell University Press, Ithaca and London, 1979).

[7] K.F. Freed, *Renormalization Group Theory of Macromolecules* (Wiley, New York, 1987).

[8] G . J. Fleer, M.A.Cohen Stuart, J.M.H.M. Scheutjens, T. Cosgrove and B. Vincent, *Polymers at Interfaces* (Chapman & Hall, London, 1993).

[9] G.H. Fredrickson, *The Equilibrium Theory of Inhomogeneous Polymers* (Oxford University Press, New York, 2006).

[10] D.S. Falk, Phys. Rev. **118**, 105 (1960).

[11] G.D. Mahan, *Many-Particle Physics* (Springer, 3rd Ed., 2000).

[12] I. Borukhov, D. Andelman and H. Orland, *Eur Phys. J. B* **5**, 869 (1998).

[13] J.P. Hansen and I.R. McDonald, *Theory of Simple Liquids* (Elsevier Academic Press, San Diego, CA, 1996).

[14] A.R. Khokhlov, J.Phys.A: Math. Gen. **13**, 979 (1980).

[15] V.Yu. Borue and I.Ya. Erukhimovich, Macromolecules **21**, 3240 (1988).

[16] J.F. Marko and Y. Rabin , Macromolecules **24**, 2134 (1991); *ibid.* **25**, 1503 (1992).

[17] M. Benmouna, T.A. Vilgis and J. François, Makromol. Chem.,Theory Simul. **1**, 3 (1992).

[18] M. Benmouna and Y. Bouayed, Macromolecules **25**, 5318 (1992).

[19] E.E. Dormidontova, I. Ya. Erukhimovich and A.R. Khokhlov, Macromol. Theory and Simul. **3**, 661 (1994).

[20] G.A. Carri and M. Muthukumar, J. Chem. Phys. **111**, 1765 (1999).

[21] K. Ghosh, G.A. Carri and M. Muthukumar, J. Chem. Phys. **116**, 5299 (2002).

[22] K. Nishida, K. Kaji and T. Kanaya, J. Chem. Phys. **114**, 8671 (2001).

[23] K. Nishida, K. Kaji and T. Kanaya, J. Chem. Phys. **115**, 8217 (2001).

[24] K. Yu and A. Eisenberg, Macromolecules **31**, 3509 (1998).

[25] S.A. Jenekhe and X.L. Chen, Science **279**, 1903 (1998).

[26] X.L. Chen and S.A. Jenekhe, Langmuir **15**, 8007 (1999).

[27] T. Nakanishi, S. Fukushima, K. Okamoto, M. Suzuki, Y. Matsumara, M. Yokoyama, T. Okano, Y. Sakurai and K. Kataoka, J. Control. Release **74**, 295 (2001).

[28] E. Helfand, Macromolecules **8**, 552 (1975); *ibid.* **9**, 879 (1976);*ibid.* **11**, 960 (1978); *ibid.* **13**, 994 (1980).

[29] L. Leibler, Macromolecules **13**, 1602 (1980).

[30] A.N. Semenov, Zh. Eksp. Teor. Fiz. **88**, 1242 (1985); Macromolecules **22**, 2849 (1989).

[31] T. Ohta and K. Kawasaki , Macromolecules **19**, 2621 (1986); *ibid.* **21**, 2972 (1988); *ibid.* **23**, 2413 (1990).

[32] J. Melenkevitz and M. Muthukumar, Macromolecules **24**, 4199 (1991).

[33] R.L. Lescanec and M. Muthukumar, Macromolecules **26**, 3908 (1993).

[34] M.W. Matsen and M. Schick, Phys. Rev. Lett. **72**, 2660 (1994); M.W. Matsen and F.S. Bates, Macromolecules **29**, 1091 (1996); M.W. Matsen, J. Phys.: Condens. Matter **14**, R21 (2002).

[35] G.H. Fredrickson and E. Helfand, J. Chem. Phys. **87**, 697 (1987).

[36] M. Olvera de la Cruz. Phys. Rev. Lett. **67**, 85 (1991).

[37] M. Muthukumar, Macromolecules **26**, 5259 (1993).

[38] E.B. Zhulina and O.V. Borisov , Macromolecules **35**, 9191(2002); O.V. Borisov and E.B. Zhulina , *ibid.* **35**, 4472(2002); *ibid.* **36**, 10029(2003).

[39] N. Dan and M. Tirrell, Macromolecules **26**, 4310 (1993).

[40] N.P. Shusharina, I.A. Nyrkova, and A.R. Khokhlov, Macromolecules **29**, 3167 (1996).

[41] I.A. Nyrkova and A.N. Semenov, Faraday Discuss. **128**, 113(2005).

[42] A.V. Kyrylyuk and J.G.E.M. Fraaije, J. Chem. Phys. **121**, 2806(2004).

[43] A.V. Kyrylyuk and J.G.E.M. Fraaije, J. Chem. Phys. **121**, 9166(2004).

[44] A. Shi and J Noolandi, Macromol. Theory Simul. **8**, 214 (1999).

[45] Q. Wang, T. Taniguchi and G.H. Fredrickson, J. Phys. Chem. B **108**, 6733 (2004); *ibid.* **109**, 9855 (2005).

[46] M. Muthukumar, Macromolecules, **35**, 9142 (2002).

[47] There are few misprints in Ref.[29]. Corrections are:
(1) Equation (V-33) should read

$$\gamma_n = [3a_n + 1 + 2(3a_n + 1)^{1/2}]/3(a_n - 1)$$

(2) Equation (C-6) should read

$$\begin{aligned} g_4(f,h) &= \{1 - \exp[-(1-f)x]\}\{1 + \exp(-hfx)/(h-1) \\ &\quad -h\exp(-fx)/(h-1)\}/hx^3 \end{aligned}$$

(3) In Appendix C, functions $g_i(f,h)$ and $f_i(f,h)$ where $i = 2,3,4$, are defined and these functions have special cases for $h = 0,1,3,4$. In fact, these functions differ from general expressions(like Eq. (C-4)) only for $h = 0,1$ and for all other values of h, general expressions are true. So, the equations like (C-4a) and (C-4b) are valid *only* for $h = 0$ and $h = 1$, respectively.

[48] K. Almdal, J. H. Rosedale, F. Bates, G. D. Wignall and G. H. Fredrickson, Phys. Rev. Lett. **65**, 1112 (1990).

[49] J. D. Vavasour and M. D. Whitmore, Macromolecules **25**, 5477 (1992); M.W. Matsen and F.S. Bates, J. Polym. Sci. B: Polym. Phys. **35**, 945 (1997);

[50] M. Muthukumar, J. Chem. Phys. **86**, 7230 (1987).

[51] C.J.F. Böttcher, *Theory of Electric Polarization* (Elsevier, Amsterdam, 1973).

[52] P.G. de Gennes, P. Pincus, R.M. Velasco and F. Brochard, J. de Phys. **37**, 1461 (1976).

[53] M. Muthukumar , J. Chem. Phys., **105**, 5183 (1996).

[54] K.K. Mahdi, M. de la Cruz, Macromolecules **33**, 7649 (2000).

[55] C. Holm, J.F. Joanny, K. Kremer, R.R. Netz, P. Reineker, C. Seidel, T.A. Vilgis, and R.G. Winkler, Advances in Polymer Science **166**, 67 (2004).

[56] L. Zhang and A. Eisenberg, Science **268**, 1728 (1995); L. Zhang and A. Eisenberg, Macromolecules **29**, 8805 (1996).

[57] V.M. Prabhu, M. Muthukumar, G.D. Wignall, and Y.B. Melnichenko, J. Chem. Phys. **119**, 4085 (2003).

[58] S. Forster, V. Abetz, and A.H.E. Muller, Advances in Polymer Science **166**, 173 (2004).

[59] D.A. McQuarie, *Statistical Mechanics* (University Science Books, Sausalito, California, 20 00).

[60] R.T. Fraley, S.L. Dellaporta, and D. Papahadjopoulos, Proc. Nat. Acad. Sci. **79**,1859 (1982).

[61] J. J. Kasianowicz, E. Brandin, D. Branton, and D. W. Deamer, Proc. Nat. Acad. Sci. **93**, 13770 (1996).

[62] M. Akeson, D. Branton, J. J. Kasianowicz, E. Brandin, and D. W. Deamer, Biophys. J. **77**, 3227 (1999).

[63] R.J. Murphy and M. Muthukumar, J. Chem. Phys. **126**, 051101 (2007).

[64] Y. Chen and M. Muthukumar, Phys. Rev. B **33**, 6187 (1986).

[65] A.Y. Grosberg and A. R. Khokhlov, *Statistical Physics of Macromolecules* (American Institute of Physics, New York, 1994).

[66] A. Cacciuto and E. Luijten, Nano Lett. **6**, 901 (2006).

[67] A. Cacciuto and E. Luijten, Phys. Rev. Lett. **96**, 238104 (2006).

[68] C. Y. Kong and M. Muthukumar, J. Chem. Phys. **120**, 3460 (2004).

[69] W. Sung and P. J. Park, Phys. Rev. Lett. **77**, 783 (1996).

[70] M. Muthukumar, J. Chem. Phys. **118**, 5174 (2003).

[71] A. Torres and G. Téllez, J. Stat. Phys. **118**, 735 (2005).

[72] M. Muthukumar and S.F. Edwards, J. Chem. Phys. **76**, 2720 (1982).

[73] J. des Cloizeaux and G. Jannink, *Polymers in Solution* (Clarendon Press, Oxford, 1990).

[74] R. A. Marcus, J. Chem. Phys. **23**, 1057 (1955).

[75] W.H. Press, S.A. Teukolsky, W.T. Vetterling and B. P. Flannery, *Numerical Recipes in C* (Cambridge University Press , New York, 1992).

[76] M. Muthukumar and J. S. Ho, Macromolecules 22, 965 (1989).

[77] R. Podgornik, J. Phys. Chem. **97**, 3927 (1993).

[78] I.S. Gradshteyn and I.M. Ryzhik , *Tables of Integrals, Series, and Products* (Academic Press,San Diego, 2000).

[79] S. Tsonchev, R. D. Coalson, and A. Duncan, Phys. Rev. E **60**, 4257 (1999).

[80] E.J.W. Verwey and J.T.G.Overbeek, *Theory of The Stability of Lyophobic Colloids* (Dover Publications, Inc., New York, 1999).

[81] M. Beer, M. Schmidt, and M. Muthukumar, Macromolecules **30**, 8375 (1997).

[82] M. Muthukumar and B. G. Nickel, J. Chem. Phys. **86**, 460 (1987).

[83] J.R. Naughton and M.W. Matsen, Macromolecules **35**, 5688 (2002); M.W. Matsen, J. Chem. Phys. **106**, 7781 (1997).

[84] J.N. Israelachvili, *Intermolecular and Surface Forces* (Academic Press, London. 1991).

[85] M. Muthukumar, J. Chem. Phys. **120**, 9343 (2004).

[86] J.T.G. Overbeek, Colloids Surf. **51**, 61 (1990).

[87] J.Wang, R. Kumar and M. Muthukumar, (unpublished).

[88] S.A. Rice and M. Nagasawa, *Polyelectrolyte Solutions* (Academic Press, London, 1961).

[89] G. S. Manning, J. Chem. Phys. **51**, 924 (1969), .

[90] H. Dautzenberg, W. Jaeger and J. Kotz, *Polyelectrolytes: Formation, Characterization and Application*(Hanser Publishers,New York, 1994).

[91] N. Volk, D. Vollmer, M. Schmidt, W. Oppermann and K. Huber, Adv. Poly. Sci. **166**, 29 (2004).

[92] M.J. Stevens and K. Kremer, J. Chem. Phys. **103**, 1669 (1995).

[93] R. G. Winkler, M. Gold, and P. Reineker, Phys. Rev. Lett. **80**, 3731 (1998).

[94] S. Liu and M. Muthukumar, J. Chem. Phys. **116**, 9975 (2002).

[95] S. Liu, K. Ghosh, and M. Muthukumar, J. Chem. Phys. **119**, 1813 (2003).

[96] Q. Liao, A.V. Dobrynin, and M. Rubinstein, Macromolecules **36**, 3399 (2003).

[97] Q. Liao, A.V. Dobrynin, and M. Rubinstein, Macromolecules **39**, 1920 (2006).

[98] P.Y. Hsiao and E. Luijten, Phys. Rev. Lett. **97**, 148301-1 (2006).

[99] R.W. Chang and A. Yethiraj, Macromolecules **39**, 821 (2006).

[100] F. Bordi, C. Cametti, J.S. Tan, D.C. Boris, W.E. Krause, N. Plucktaveesak, and R.H. Colby, Macromolecules **35**, 7031 (2002).

[101] R. Schweins, J. Hollmann, and K. Huber, Polymer **44**, 7131 (2003).

[102] V.M. Prabhu, E.J. Amis, D.P. Bossev, and N. Rosov, J. Chem. Phys. **121**, 4424 (2004).

[103] A. Popov and D.A. Hoagland, J. Polym. Sci. Pol. Phys. **42**, 3616 (2004).

[104] W. Essafi, F. Lafuma, D. Baigl, and C.E. Williams, Europhys. Lett. **71**, 938 (2005).

[105] V.M. Prabhu, Curr. Opin. Colloid In. **10**, 2 (2005).

[106] P. González-Mozuelos and M. Olvera de la cruz, J. Chem. Phys. **103**, 3145 (1995).

[107] D. Stigter, Biophys. J. **69**, 380 (1995).

[108] N. V. Brilliantov, D.V. Kuznetsov, and R. Klein, Phys. Rev. Lett. **81**, 1433 (1998).

[109] H. Schiessel and P. Pincus, Macromolecules **31**, 7953 (1998).

[110] P.S. Kuhn and M.C. Barbosa, Physica A **357**, 142 (2005).

[111] T. B. Liverpool and K.K. Muller-Nedebock, J. Phys.-Condens. Mat. **18**, L135 (2006).

[112] A.Y. Grosberg, T.T. Nguyen, and B.I. Shklovskii, Reviews of Modern Physics **74**, 329 (2002).

[113] A. Kundagrami and M. Muthukumar, J. Chem. Phys. **128**, 244901 (2008).

[114] R. Kumar and M. Muthukumar, J. Chem. Phys. **128**, 184902 (2008).

[115] M. Muthukumar, J. Chem. Phys. **118**, 5174 (2003).

[116] M.J. Stevens and K. Kremer, J. Phys. II **6**, 1607 (1996).

[117] B. Alberts *et al.*, *Molecular Biology of the Cell* (Garland Science, New York,NY, 2002).

[118] R. Dalbey and G. Heijne, *Protein Targetting, Transport, and Translocation* (Academic Press, San Diego, CA, 2002).

[119] A. Meller *et al.*, Proc. Natl. Acad. Sci. U.S.A. **97**, 1079 (2000).

[120] R. M. M. Smeets *et al.*, Nano Letters **6**, 89 (2006).

[121] M. Muthukumar, Annu. Rev. Bioph. Biom. **36**, 435 (2007).

[122] L. Brun *et al.*, Phys. Rev. Lett. **100**, 4 (2008); G. Oukhaled *et al.*, Euro. Phys. Lett. **82**, 5 (2008).

[123] E. A. DiMarzio, and A. J. Mandell, J. Chem. Phys. **107**, 5510 (1997); T. Ambjornsson *et al.*, J. Chem. Phys. **117**, 4063 (2002).

[124] J. Chuang, Y. Kantor, and M. Kardar, Phys. Rev. E **65**, 011802 (2001).

[125] M. Muthukumar, J. Chem. Phys. **111**, 10371 (1999).

[126] M. R. Hermann, and J. A. Fleck, Phys. Rev. A **38**, 6000 (1988); G. Tzeremes, K.O. Rasmussen, T. Lookman, and A. Saxena, Phys. Rev. E **65**, 041806 (2002).

[127] G.H. Weiss and A.A. Maradudin, J. Math. Phys. **3**, 771 (1962).